PB87-141479

Stochastic Prediction of Dispersive Contaminant Transport

Massachusetts Inst. of Tech., Cambridge

Prepared for

Robert S. Kerr Environmental Research Lab.
Ada, OK

Dec 86

U.S. Department of Commerce
National Technical Information Service
NTIS

PB87-141479

EPA/600/2-86/114
December 1986

STOCHASTIC PREDICTION OF DISPERSIVE CONTAMINANT TRANSPORT

by

Efstratios G. Vomvoris and Lynn W. Gelhar
Massachusetts Institute of Technology
Cambridge, Massachusetts 02139

Cooperative Agreement
CR-811135-01-2

Project Officer

Joseph F. Keely
Applications and Assistance Branch
Robert S. Kerr Environmental Research Laboratory
Ada, Oklahoma 74820

ROBERT S. KERR ENVIRONMENTAL RESEARCH LABORATORY
OFFICE OF RESEARCH AND DEVELOPMENT
U.S. ENVIRONMENTAL PROTECTION AGENCY
ADA, OK 74820

REPRODUCED BY
U.S. DEPARTMENT OF COMMERCE
NATIONAL TECHNICAL
INFORMATION SERVICE
SPRINGFIELD, VA. 22161

TECHNICAL REPORT DATA
(Please read Instructions on the reverse before completing)

1. REPORT NO.	2.	3. RECIPIENT'S ACCESSION NO.
EPA/600/2-86/114		PB87 141479/AS

4. TITLE AND SUBTITLE	5. REPORT DATE
STOCHASTIC PREDICTION OF DISPERSIVE CONTAMINANT TRANSPORT	December 1986
	6. PERFORMING ORGANIZATION CODE

7. AUTHOR(S)	8. PERFORMING ORGANIZATION REPORT NO.
Efstratios G. Vomvoris and Lynn W. Gelhar	

9. PERFORMING ORGANIZATION NAME AND ADDRESS	10. PROGRAM ELEMENT NO.
Massachusetts Institute of Technology Department of Civil Engineering Cambridge, Massachusetts 02139	CBPC1A
	11. CONTRACT/GRANT NO.
	CR-811135

12. SPONSORING AGENCY NAME AND ADDRESS	13. TYPE OF REPORT AND PERIOD COVERED
Robert S. Kerr Environmental Research Lab. - Ada, OK Office of Research and Development U.S. Environmental Protection Agency Ada, Oklahoma 74820	Final (09/01/83 - 04/30/86)
	14. SPONSORING AGENCY CODE
	EPA/600/15

15. SUPPLEMENTARY NOTES

16. ABSTRACT

The objective of this research agreement was to develop mathematical models to quantify the concentration variability observed in field measurements of concentration plumes. The concentration variability is attributed mainly to spatial heterogeneity of the hydraulic conductivity field. Since there is limited information about actual distributions of hydraulic conductivity in a given site, the log-hydraulic conductivity is modeled as a three-dimensional anisotropic stationary random process. It is shown that the concentration variance, which measures the intensity of the variations, is proportional to the mean concentration gradient and to the variance and correlation scales of the log-hydraulic conductivity; it is inversely proportional to the local dispersivity values. The main contribution to the concentration variability results from the coefficients corresponding to the longitudinal mean concentration gradients. Analysis of a portion of the data from the Canadian Forces Base, Borden, Ontario, shows the applicability of the developed results in field situations. Simple analytical examples demonstrate the way to use the results in a predictive context.

17. KEY WORDS AND DOCUMENT ANALYSIS

a. DESCRIPTORS	b. IDENTIFIERS/OPEN ENDED TERMS	c. COSATI Field/Group

18. DISTRIBUTION STATEMENT	19. SECURITY CLASS *(This Report)*	21. NO. OF PAGES
RELEASE TO PUBLIC.	UNCLASSIFIED	104
	20. SECURITY CLASS *(This page)*	22. PRICE
	UNCLASSIFIED	

EPA Form 2220-1 (Rev. 4-77) PREVIOUS EDITION IS OBSOLETE

DISCLAIMER

"The information in this document has been funded wholly or in part by the United States Environmental Protection Agency under Cooperative Agreement CR-811135-01-2 to the Massachusetts Institute of Technology. It has been subjected to the Agency's peer and administrative review, and it has been approved for publication as an EPA document."

Mention of trade names or commercial products does not constitute endorsement or recommendation for use.

FOREWORD

EPA is charged by Congress to protect the Nation's land, air and water systems. Under a mandate of national environmental laws focused on air and water quality, solid waste management and the control of toxic substances, pesticides, noise and radiation, the Agency strives to formulate and implement actions which lead to a compatible balance between human activities and the ability of natural systems to support and nurture life.

The Robert S. Kerr Environmental Research Laboratory is the Agency's center of expertise for investigation of the soil and subsurface environment. Personnel at the Laboratory are responsible for management of research programs to: (a) determine the fate, transport and transformation rates of pollutants in the soil, the unsaturated and the saturated zones of the subsurface environment; (b) define the processes to be used in characterizing the soil and subsurface environment as a receptor of pollutants; (c) develop techniques for predicting the effect of pollutants on ground water, soil, and indigenous organisms; and (d) define and demonstrate the applicability and limitations of using natural processes, indigenous to the soil and subsurface environment, for the protection of this resource.

This report contributes to that knowledge which is essential in order for EPA to establish and enforce pollution control standards, predict the extent of existing contamination, and to develop ways to restore the environment, when contaminated, in a reasonable and cost-effective manner.

Clinton W. Hall

Clinton W. Hall
Director
Robert S. Kerr Environmental
Research Laboratory

CONTENTS

	Page
Abstract	vi
Figures	vii
Tables	ix
Symbols	x
Section	
1. Introduction	1
2. Conclusions	3
3. Recommendations	4
4. Natural Variability and the Stochastic Approach	5
5. Analysis of Concentration Variability	15
6. Application Examples	38
7. Field Data Analysis: The CFB Borden Site	47
8. Discussion of Results	67
References	69
Appendices	
A. The Mathematics of the Approximate Analytical Evaluations	74
B. The Integration Over Wave-Number	84
C. Transformation to Polar Coordinates	88
D. Mean Concentrations Fitted at the Borden Site Data	91

Preceding page blank

ABSTRACT

The objective of this research agreement was to develop mathematical models in order to quantify the concentration variability observed in field measurements of concentration plumes.

The concentration variability is attributed mainly to the spatial heterogeneity of the hydraulic conductivity field. Since there is limited information about the actual distribution of the hydraulic conductivity in a given site, the log-hydraulic conductivity is modeled as a three-dimensional anisotropic stationary random process. It is characterized by its mean and its covariance function or spectrum. Implementing Darcy's equation and the convective-dispersive equation at the local scale, relationships among the concentration variations and characteristic parameters of the porous medium are found. Approximate analytical expressions are also developed.

It is shown that the concentration variance, which measures the intensity of the variations, is proportional to the mean concentration gradient and to the variance and correlation scales of the log-hydraulic conductivity; it is inversely proportional to the local dispersivity values. The main contribution to the concentration variability results from the coefficients corresponding to the longitudinal mean concentration gradients.

There is a very high correlation in the concentration values along the direction of the flow, which is still under investigation. The orientation of the hydraulic conductivity principal axes does not have a significant effect on the concentration variance values.

Analysis of a portion of the data from the CFB Borden site shows the applicability of the developed results in field situations. Simple analytical examples demonstrate the way to use the results in a predictive context.

This report was submitted in fulfillment of Cooperative Agreement No. CR-811135-01-2 by the Massachusetts Institute of Technology under the sponsorship of the U.S. Environmental Protection Agency. This report covers a period from September 1, 1983 to April 30, 1986, and work was completed as of April 8, 1986.

FIGURES

Number		Page
4.1	(a) Hydraulic conductivity data from laboratory cores from a borehole in the Mt. Simon aquifer Illinois (Bakr, 1976)	6
	(b) Hydraulic conductivity profile from a core in the CFB Borden site, Canada (Sudicky, 1985b)	6
4.2	Concentration measurements from the Borden site. (a) Depth averaged data (b) Vertical profiles (Freyberg et al. 1983 and personal communication)	8
4.3	Schematic graph of a stationary one dimensional covariance function of ℓnK showing the correlation scale λ	10
4.4	Schematic graph and comparison of the measured, predicted with field scale dispersion and predicted with laboratory scale dispersion concentration profiles .	10
5.1	Coordinate systems for the case $x_2 = x_2'$; the dashed elipse represents schematically the e^{-1} level of the correlation function	18
5.2	Comparison of sample autocorrelation function (crosses) for hydraulic conductivity (from grain-size analysis) with theoretical autocorrelation function (solid line) (From the CRNL, Ontario experiment, Moltyaner, 1985) . . .	24
5.3	Comparison of the exponential correlation function and the "hole-type" correlation function	25
5.4	Comparison of the variance for an anisotropic aquifer (correlation scales ℓ_1, ℓ_2, ℓ_3) and an equivalent isotropic (correlation scale $\ell = (\ell_1\ell_2\ell_3)^{1/3}$)	29
5.5	Comparison of the approximate analytical expressions and the numerical results for the T_{ij} coefficients . . . . (a) $T_{11}(\cdot)$ along the x direction for different ε (b) $T_{22}(\cdot)$ along the x direction (c) $T_{22}(\cdot)$ along the y direction	30
5.6	Test of the validity of the approximate result for the variance T_{11} (1, 1, ε, 1;0) with respect to the ε values	32
6.1	Normalized mean concentration and standard deviation at x = 50 m, z = 0 m	39
6.2	Isoconcentration lines and standard deviations at z = 0 m	41

Number		Page
6.3	Correlation function for a point at y = z = 0 m . . . . . (a) Correlation along x (b) Correlation along lines in the x-y plane at various angles with x (c) Lag-correlation contours in the x-y plane	42
6.4	Normalized concentration and one standard deviation interval along a longitudinal section (line coordinates y = z = 0)	44
6.5	Normalized concentration and one standard deviation interval along a vertical section (line coordinates $x = x_c$ - center of mass of plume, y = 0)	45
6.6	Normalized concentration and two standard deviation interval along another vertical section (line coordinates $x = x_c - 5$ m, z = 1 m)	46
7.1	Instrumentation, location of cores and hydraulic head distribution on August 10, 1984 (solid line) and November 15, 1984 (---) at the tracer-test site (after Sudicky 1985b). The circled samplers show the locations of the wells used in this analysis. V denotes the well used for the vertical section analysis	48
7.2	Isoconcentration contours at depth z = -5.31 m from the Borden site data (original data from D. Freyberg, personal communication)	49
7.3	Schematic presentation of the methods used for the estimation of the mean concentrations	58
7.4	The measured, fitted and plus-minus one standard deviation concentration profiles along the longitudinal section at z = -5.31 m	59
7.5	The mean concentration curves fitted at the wells on the longitudinal section (c in the vertical vs. z)	60
7.6	The measured, fitted and plus-minus one standard deviation concentration profiles along the vertical section at (x,y) = (38.3, 16.08)	64
7.7	The values plotted in Fig. 7.6 shown in a semi-logarthmic plot	65
C.1	Schematic graph of the coordinate transformation geometry . .	90

TABLES

Number		Page
5.1	Approximate analytical results for the concentration covariance	27
5.2	Effect of the stratification orientation on the concentration variance	34
7.1	Existing information on the Borden site parameters	48
7.2	Effect of the input parameters on effective hydraulic conductivity	53
7.3	Effect of the input parameters on the macrodispersivities	55
7.4	Parameters used in the variance estimation	56
7.5	Concentration gradients in the vertical section at (x,y) = (38.3m., 16.08m.)	56
7.6	Estimation of the range of variations in the longitudinal section	62
7.7	Estimation of the range of variations in the vertical section	63
D.1	Parameters used to fit mean concentrations at the wells	91

LIST OF SYMBOLS

A	auxiliary variable defined in Eq. (5.27)
A_{11}, A_{22}, A_{33}	macrodispersivities along axes x, y, and z
B	auxiliary variable defined in Eq. (5.27)
c	concentration of the transported solute (volumetric)
$dZ_f(\underline{k})$	Fourier-Stieltjes wave amplitude of the random process $f(\underline{x})$
$E[\cdot]$	expectation operator
E_{ij}	local bulk dispersion coefficient tensor
E	coefficient defined in Eq. (A.1)
F	mean of log-hydraulic conductivity
$f(\underline{x})$	perturbation of log-hydraulic conductivity field and generic symbol for a random field in Section 4.
G_j	mean concentration gradient along x_j; $G_j = -\partial\overline{c}/\partial x_j$
g_{ij}	coefficients used in the evaluation of $\overline{K}_{ij}$; defined in Eq. (7.11)
J_i	hydraulic gradient in direction x_i
K	hydraulic conductivity
K_ℓ	defined from $\exp[E(\ln K)]$
$\overline{K}_{ij}$	effective hydraulic conductivities
$K(t)$	auxiliary variable defined in Eq. (5.16)
$\underline{k}$	the three-dimensional wave number vector; (k_1, k_2, k_3)
ℓ_i	characteristic correlation scales of the hole type exponential covariance function

$m(\underline{x})$	mean of a random field
m	rate of mass injection
M	total mass injected
n	porosity
q_i	specific discharge in the x_i direction
$R_{ff}(\underline{x}_1, \underline{x}_2)$	covariance function of the random field ($f(\underline{x})$
$S_{ff}(\underline{x}_1, \underline{x}_2)$	spectrum of the random field ($f(\underline{x})$
T_{jp}	nondimensional coefficients used in the evaluation of the concentration covariance; defined in Eq. (5.33)
T'_{jp}	dimensional coefficients used in the evaluation of the concentration covariance; defined in Eq. (5.33)
V	mean pore velocity
$\underline{x}$	$(x_1, x_2, x_3) = (x, y, z)$ coordinate vector and coordinate axes in the three-dimensional space
x_c	location of center of mass of a plume
α_L, α_T	longitudinal and transverse local dispersivities
β	coefficient defined in Eq. (A.1)
γ	flow factor = $q/K_\ell J_1$
$\gamma(\underline{x}_1, \underline{x}_2)$	semi-variogram of a random process
δ_{ij}	Kronecker delta, equals 1 if $i = j$
ε	defined from α_L/ℓ_3
z	defined in Eq. (A.1)
θ	auxiliary variable defined in Eq. (5.16)
κ	ratio of transverse to longitudinal local dispersivity
λ	correlation scale of the negative exponential covariance function

ρ_1, ρ_2	aspect ratios of the covariance of the ℓnK defined in Eq. (5.33c)
$\rho_{gg}(\underline{x}_1, \underline{x}_2)$	correlation function of the random process $g(\underline{x})$
σ_g^2	the variance of a random field $g(\underline{x})$
ψ	rotation angle of the concentration plume with respect to the mean flow direction
-	(overbar) mean of a random field
'	(prime) perturbation of a random field

SECTION 1

INTRODUCTION

Field observations of solute transport in groundwater indicate that dispersivities are scale dependent and can range over many orders of magnitude. This discrepancy between the laboratory and field experience has been attributed mainly to the spatial variation of the flow properties of the natural porous earth materials. Therefore, over the last decade a substantial portion of the research in the area of subsurface hydrology has focused on understanding the effects of the spatial heterogeneity of natural formations on flow and solute transport.

Continuously expanding computer capabilities have facilitated the use of deterministic numerical models with parameters which may be spatially variable over a grid and have, in principle, made it possible to obtain solutions that previously could be described only qualitatively. However, such solutions are limited to the specific application and are unable to generate relationships valid over a broad range of problems. More importantly, in order for a numerical model to reproduce the actual detail of a given field situation, it must have sufficient grid resolution to represent the velocity field producing the mass transport and information about the controlling parameters, such as hydraulic conductivity and porosity, at each grid point. While the former may be practical for small idealized flow systems (say over tens of meters), the number of nodes required to resolve the actual three-dimensional heterogeneity at a more practical field scale (say 1 km) can easily exceed the capacity of even the largest supercomputers. Furthermore, the actual measurement of the required parameters with that degree of resolution is a totally impractical task.

It is the lack of information about the spatial distribution of the controlling parameters that has led to modeling them as realizations of random fields. A random field can be viewed as a generalization of the random variable concept. Before measuring the value of a random variable the only information known is a range for its possible values (defined by its mean and variance). In a random field it is further assumed that there is a correlation in space among the different values, so that knowledge of the value at one location carries information about the possible values for the hydraulic conductivity at different locations in such a way that they fall into the prespecified ranges (defined by the mean and the variance) and have the appropriate correlation in space (defined by the correlation function). This approach is coined the stochastic approach. The fundamental assumption is that for each one realization the classical laws of flow and mass transport hold at some representative scale.

In the stochastic approach, the mean or expected value behavior of the concentration field is found to be equivalent to the classical dispersive transport equation. The theory also predicts the resulting field-scale dispersion coefficients in terms of the statistical characteristics of the hydraulic conductivity variability. However, the mean concentration represents the average behavior of the ensemble rather than the actual realization of the aquifer. Therefore, a classical transport model will simulate a smoothed approximation of an actual field simulation; the actual concentration will vary around the smooth mean. In order to realistically present the results of model simulations, it is necessary to understand and quantify this error in classical models.

The stochastic approach can be used to quantify the variation around the mean concentration. The main focus of this research is the development of the theory to describe such variability. The degree of variability will be characterized by the concentration variance. It will be shown that the concentration variance depends on measurable or determinable quantities characterizing the aquifer material, such as the correlation scales and the variance of the log-hydraulic conductivity, the inclination of the stratification, and the local dispersivity values. It also depends on the mean concentration gradient which, through the macrodispersivities, represents the overall effect of the aquifer heterogeneity on the mass transport. Section 6 shows how the mean concentration gradient can be estimated in a predictive context with numerical or analytical models. Section 7 demonstrates how it can be estimated through a simple curve fitting with existing plume measurements, by the analysis of the field data from the Borden site in Canada.

The stochastic approach is complementary to classical deterministic modeling. The predicted concentration variance can be used as a realistic and physically-based calibration target for the large-scale numerical models. Furthermore, one can use any classical numerical or analytical model that reproduces the general characteristics of the contamination event and, in addition, obtain a measure of the expected variability around the model results. Finally, knowledge of the possible deviations of the actual plume from the predicted one can improve substantially the design of monitoring schemes.

The present study is focusing on quantifying the variation of the concentration measurements or model predictions, in heterogeneous porous formations. Examples demonstrate the practical application of these results.

SECTION 2

CONCLUSIONS

The concentration variability resulting from the heterogeneity of the natural aquifers can be quantified using stochastic analysis in terms of measurable or determinable properties of the hydraulic conductivity field. It can be expressed mathematically as the sum of the products of the concentration gradients weighted by appropriate coefficients, which depend on the variance and the correlation scales of the log-hydraulic conductivity, the local dispersivity values and the orientation of the stratification. The dominant coefficient corresponds to the gradient along the mean flow and is inversely proportional to the local dispersivity and proportional to the correlation scales.

The effects of the orientation of the stratification in a preliminary analysis appear to be less important, but further investigation is required for definitive conclusions. The structure of the concentration covariance for the particular spectrum used results in a singular effect, namely, high correlations along the mean flow direction.

Approximate analytical results have been developed that establish the role of the key parameters.

The preliminary analysis of field data from the Borden site shows that the results of the proposed theory can be applied in practical situations and produce consistent confidence intervals for the anticipated concentration variability.

SECTION 3

RECOMMENDATIONS

A local relationship that quantifies the concentration variability anticipated in mass transport in heterogeneous aquifers has been found. The relationship involves the gradient of the mean concentration, the correlation scales of the log hydraulic conductivity field and the local dispersivity values. As shown in Section 7, it can be readily used and produce quite tight confidence intervals for the concentration values, even with crude estimation of the mean concentration field.

The obtained concentration standard deviation can be implemented for the calibration of numerical models. The discretization inherent in the numerical models induces a smoothing or averaging of the true concentration field and makes it impossible to reproduce the measured values. The estimated standard deviation of the concentration can be used as a measure of the acceptable deviation of the numerical model results from the measured values.

The preliminary application of the results to a field site was very encouraging. Further analysis is needed to explore the full three-dimensional nature of the controlled plume and to follow its movement and its response to the orientation of the stratification. Important issues such as spatial averaging of the concentration field introduced by the sampling technique and its associated filtering properties need to be addressed.

The developed theory established the basic relationships among the aquifer characteristics, the flow parameters and the concentration variance. However, the effects of unsteady concentration input, initial conditions, flow reversal, and unknown history of injection need to be investigated. The singular behavior of the concentration covariance along the mean flow direction requires additional investigation before accepted as a valid descriptor of the physical system.

Finally the issue of the mean concentration field, central to the theme of all stochastic theories, should be investigated. Methods to enhance the ability to identify or estimate the mean concentration need to be developed.

SECTION 4

NATURAL VARIABILITY AND THE STOCHASTIC APPROACH

THE THEORETICAL FRAMEWORK

The conventional approach in groundwater modeling is to treat an aquifer as an idealized homogeneous formation with a constant value for each physical parameter so that the idealized aquifer behaves like the actual formation. In cases where there is predictable heterogeneity one might divide the aquifer into a number of homogeneous zones, each with a different equivalent value for any used parameter. The simple case of known anisotropy can be treated incorporating suitable coordinate transformations.

However, the actual heterogeneity in a formation which would conventionally be treated as homogeneous can be very pronounced. Figure 4.1 illustrates this variability for the hydraulic conductivity which is considered the most important flow property of an earth porous material. Note that the quantity plotted is the logarithm of the hydraulic conductivity. The observed spatial variation is well documented in the literature; "... the jigs and jags of every electric log, the spread of measurements from every sampling program, and common sense geological reasoning attest to this fact." (Freeze, 1975). The intensity of the variability of hydraulic conductivity can be characterized by the estimated variance of the natural logarithm of the hydraulic conductivity and which may be as high as 13 for some rocks (Freeze, 1975).

In addition, due to the underlying depositional process, the hydraulic conductivity field will typically exhibit some spatial structure. Oftentimes this structure manifests itself as layers or lenses and reflects directional dependence or anisotropy.

In a practical sense variability of the porous formation results in variations of the flow field and the head distributions around the ones predicted for homogeneous systems. It is further propagated to the distribution of the concentration since the latter is directly affected by the flow field. Figure 4.2 presents actual concentration data from the field scale experiment at the Borden site. Notice that intense variation of the measured values is observed for the vertical sections and an even substantial one for the depth averaged data, Figure 4.2a.

The fundamental question that emerges is how can these effects be modeled. If it is assumed that a complete knowledge of the hydraulic conductivity process is available, the existing and continuously expanding computer capabilities that permit the implementation of numerical models with parameters spatially variable across the grid, can produce the required solutions. However, at the current level of computing capabilities the allowed resolution of the input field is not fine enough to capture the anticipated effects. Furthermore, such solutions will be case specific and unable to establish general relationships among the key parameters valid over a broad range of problems. But the "Achille's heel" of the sophisticated numerical modeling of the spatial heterogeneity is that for all practical

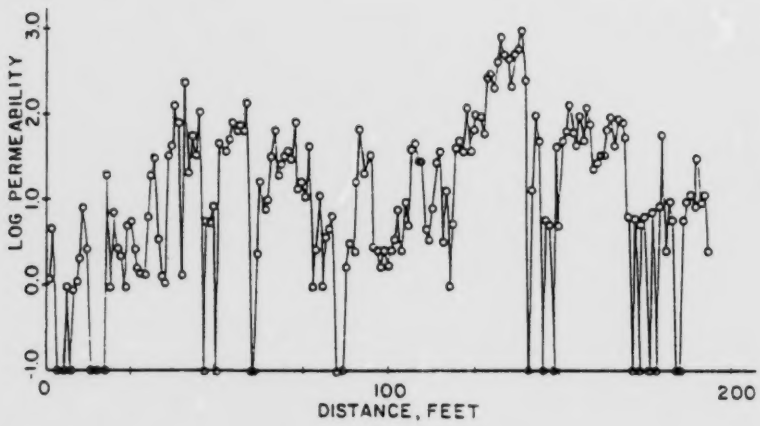

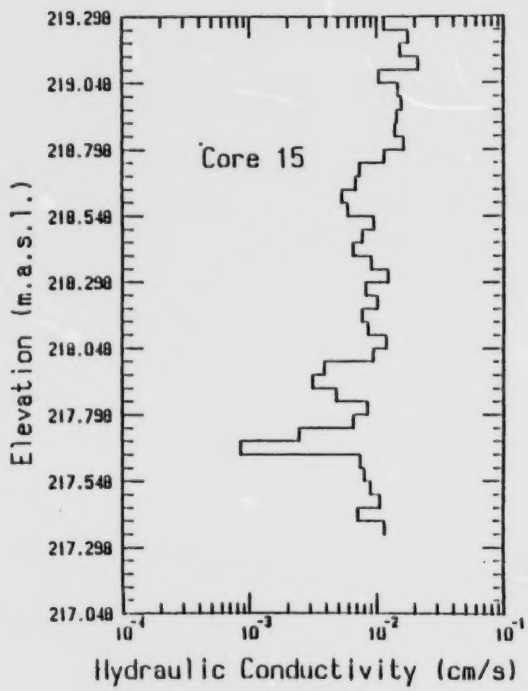

Figure 4.1 (a) Hydraulic conductivity data from laboratory cores from a borehole in the Mt. Simon aquifer, Illinois (Bakr, 1976)
(b) Hydraulic conductivity profile from a core in the CFB Borden site, Canada (Sudicky, 1985b)

purposes it is impossible to acquire all the detailed data required to adequately represent the actual variation of the parameters.

The lack of information about the controlling parameters, in addition to the need for analytical and general relationships, has led to modeling the appropriate parameters of the porous medium as realizations of random fields. The fundamental assumption is that for each one realization, and usually we have only one in groundwater related problems, the classical laws of flow and mass transport hold at some representative scale.

The concept of a random field or spatial stochastic process is a generalization of a random variable. If $\underline{x}$ represents a point in the three-dimensional space and $f(\underline{x})$ a random variable corresponding to that point $\underline{x}$, the set of random variables $\{f(\underline{x}_1), f(\underline{x}_2), \ldots f(\underline{x}_k), \ldots\}$ where $\underline{x}_1, \underline{x}_2, \ldots \underline{x}_k$, are the coordinate vectors of points 1,2, ... k, is called a random field and is simply written as $f(\underline{x})$.

As a random variable is completely characterized by its probability density function, for the complete probabilistic characterization of a random field $f(\underline{x})$ one would need to determine the joint probability density function of any set $f(\underline{x}_1), f(\underline{x}_2), \ldots f(\underline{x}_n)$ for any n and for $\underline{x}_1, \underline{x}_2, \ldots \underline{x}_n$ arbitrary points in the spatial domain of interest. In most applications the entire spatial law can neither be identified from finite data nor is required; the first two moments of the distribution suffice to characterize the random fields in a number of problems. The first two moments are,

- the mean function or first-order moment of the random field

$$E[f(\underline{x})] = m(\underline{x}) \tag{4.1}$$

  where $E[\cdot]$ denotes mathematical expectation
- the covariance function or second-order moment,

$$R_{ff}(\underline{x}_1,\underline{x}_2) = E\{[f(\underline{x}_1) - m(\underline{x}_1)]\,[f(\underline{x}_2) - m(\underline{x}_2)]\} \tag{4.2}$$

The zero lag covariance, when $\underline{x}_1 = \underline{x}_2$, is the variance, denoted as σ_f^2. Another representation of a second-moment is the variogram (Journel and Huijbregts, 1978) introduced in the field of geostatistics, and defined as,

$$2\gamma(\underline{x}_1,\underline{x}_2) = E\{[f(\underline{x}_1) - f(\underline{x}_2)]^2\} \tag{4.3}$$

Note that Eq. (4.1) and Eq. (4.2) is a generalization of the concepts of mean and variance of a random variable. Eq. (4.2) incorporates the information about the spatial structure of the process. It defines the correlation between two points of the field located at x_1 and x_2, if it is normalized by the variance.

The mean and the covariance can in general depend on the location $\underline{x}$, as can be seen in Eqs. (4.1) and (4.2). When the mean and covariance are independent of $\underline{x}$, the process is said to be (second order) stationary or statistically homogeneous:

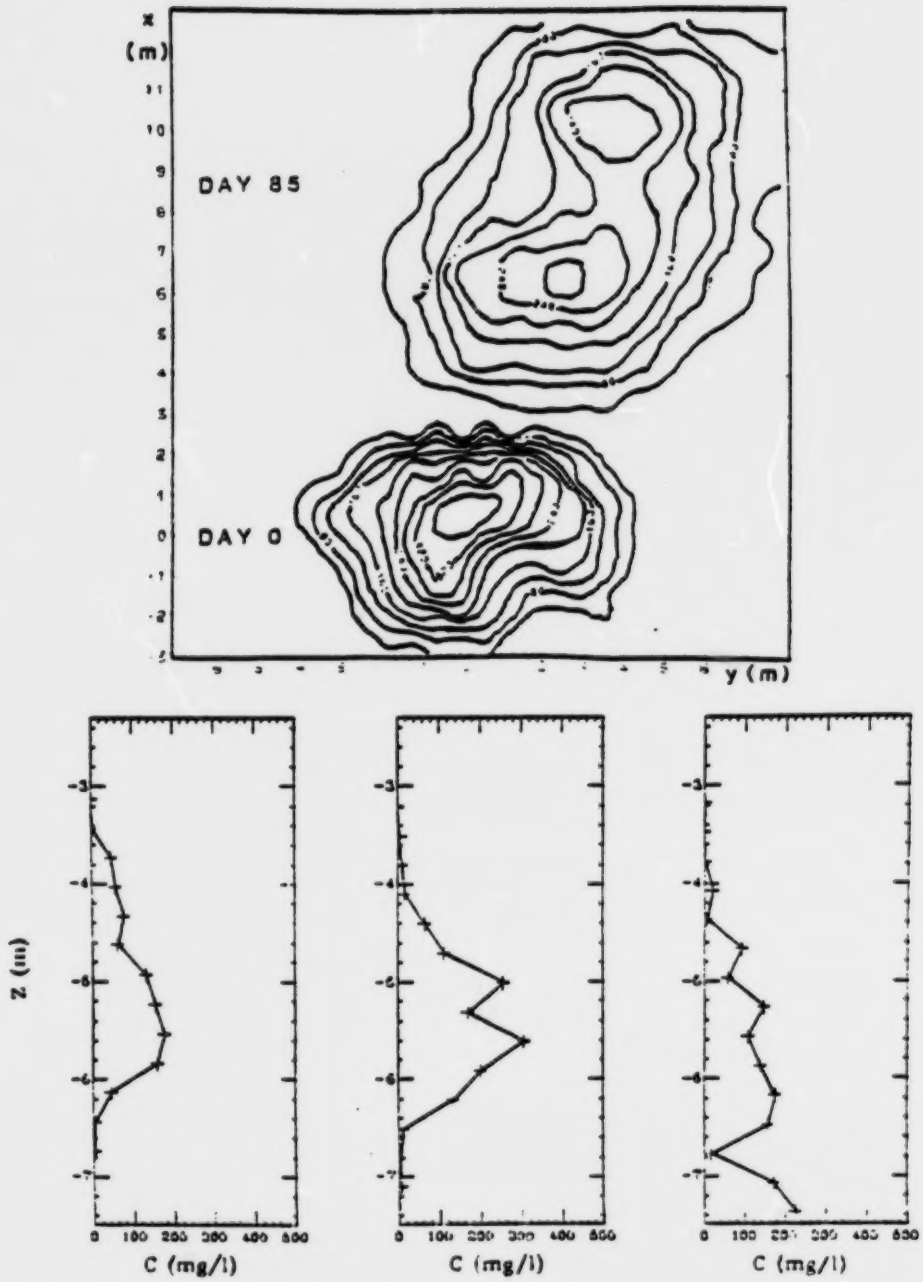

Figure 4.2 Concentration measurements from the Borden site. (a) Depth averaged data, (b) Vertical profiles (Freyberg et al, 1983 and personal communication)

$$E\{f(x)\} = m$$

$$R_{ff}(x_1, x_2) = R_{ff}(x_1 - x_2) \tag{4.4}$$

If the field is said to be isotropic, the same correlation exists for points that are separated by the same distance regardless of their orientation in space, i.e.,

$$R_{ff}(\underline{x}_1 - \underline{x}_2) = R_{ff}(|\underline{x}_1 - \underline{x}_2|) \tag{4.5}$$

Figure 4.3 illustrates graphically a one-dimensional stationary covariance function. One characteristic length scale is the separation distance at which the correlation decreases to the e^{-1} level, designated as the correlation scale. In the general stationary case the covariance can always be expressed in terms of the spectral density function or spectrum as follows,

$$R_{ff}(\underline{\xi}) = \iiint_{-\infty}^{\infty} e^{+i\underline{k}\cdot\underline{\xi}} S_{ff}(\underline{k})\, d\underline{k} \tag{4.6}$$

where the spectral density function can be expressed as,

$$S_{ff}(\underline{k}) = \frac{1}{(2\pi)^3} \iiint_{-\infty}^{\infty} e^{-i\underline{k}\cdot\underline{\xi}} R_{ff}(\underline{\xi}) d\underline{\xi} \tag{4.7}$$

and $\underline{k}$ is the three-dimensional wave number vector. The Fourier transform pair in Eqs. (4.6) and (4.7) implies that knowledge of only one of the two, spectrum or covariance, is sufficient. They both carry the same information, but it is displayed differently. The covariance function has a physical meaning that is easier to grasp: how two actual values of the process under consideration, a certain distance apart are expected to be correlated. The meaning of the spectrum is more abstract: if one could decompose a whole set of statistically similar processes in trigonometric waves and make a histogram of the encountered wave-length, that would be the spectrum. It gives the distribution of the variance over the wave-number domain.

If a process is statistically homogeneous, it will always have a spectrum, and then it is possible to take advantage of the representation theorem [Lumley and Panofsky, (1962), Gelhar (1984)],

$$f(\underline{x}) = \iiint_{-\infty}^{\infty} e^{i\underline{k}\cdot\underline{x}}\, dZ_f(\underline{k})$$

$$E\{dZ_f(\underline{k})\, dZ_f^*(\underline{k}')\} = S_{ff}(\underline{k})d\underline{k} \quad , \text{ if } \underline{k} = \underline{k}'$$

$$= 0 \quad , \text{ if } \underline{k} \neq \underline{k}' \tag{4.8}$$

where $dZ_f(\underline{k})$ is the Fourier-Stieltjes wave amplitude of the process $f(\underline{x})$. This theorem essentially states that the process $f(\underline{x})$ is composed of a sum of uncorrelated or orthogonal increments in the wave number domain. Furthermore, the representation in Eq. (4.8) is unique and provides a convenient formalism for treating differential equations involving stationary variables.

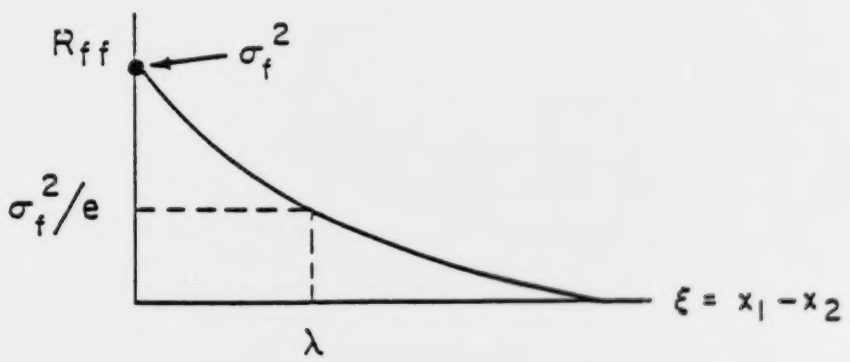

Figure 4.3 Schematic graph of a stationary one dimensional covariance function of ℓnK showing the correlation scale λ

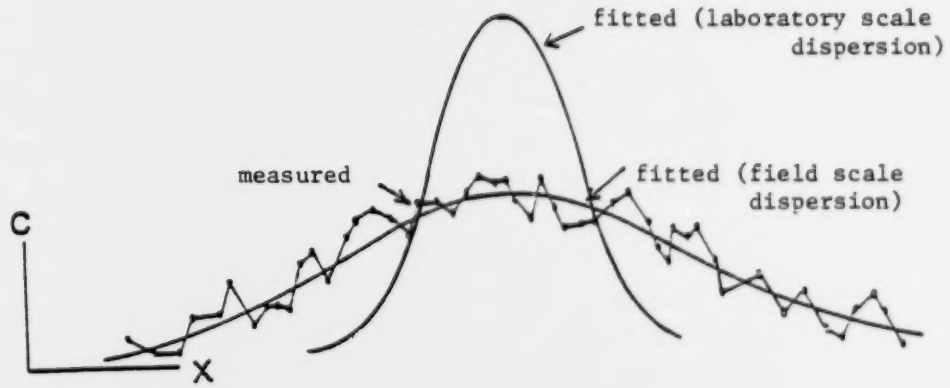

Figure 4.4 Schematic graph and comparison of the measured, predicted with field scale dispersion and predicted with laboratory scale dispersion concentration profiles

The spectral methodology will be adopted in the current work. The characteristic random fields are decomposed in a known mean function, $\bar{g}$, and a zero-mean stationary perturbation, g',

$$g(\underline{x}) = \bar{g}(\underline{x}) + g'(\underline{x}) \tag{4.9}$$

Utilizing the representation theorem in the differential equations relating the various fields, one can relate the spectrum of the dependent variable to the spectrum of the input processes.

Following the traditional deterministic approach, the aquifer is modeled as a continuum and the accepted expressions for the mass conservation, the solute conservation and Darcy's equation are assumed to hold at the local scale.

REVIEW OF RELATED WORK

Groundwater Flow

Historically the problem treated initially in a probabilistic framework was that of groundwater flow. The approaches developed can be briefly summarized into the following categories:

Monte Carlo Simulations--

Realizations of sets of aquifer properties are generated through a model, and the direct problem is deterministically solved for each realization. From the statistical analysis of these solutions, stochastic characteristics of the head and flow fields can be inferred. Freeze (1975) in his pioneering paper treated the problem of one-dimensional saturated flow in finite domain where the head at the boundaries was specified. Spatial variation but not spatial structure was the main limitation. The latter was introduced later in the work of Smith and Freeze (1979a, 1979b), where the nearest neighbor model generator was used to generate one- and two-dimensional fields.

Perturbation or Linearization Models--

This was the most widely used theoretical approach. The stochastic differential equations are solved using "small" pertubations theory or Taylor expansions in the space or frequency domain. Gelhar (1984) presents a good review of the spectral methodology which has been used in a series of papers, namely, Gelhar (1974, 1977), Bakr et al. (1978), Gutjar et al. (1978), and Mizell et al. (1980). In the aforementioned works head variances and covariances are obtained for the cases of one-, two- and three-dimensional flow in confined and unconfined aquifers. Comparable results are obtained in Gutjahr and Gelhar (1981), Dagan (1982a), Vomvoris (1982), Kitanidis and Vomvoris (1983), Hoeksema and Kitanidis (1984), and McLaughlin (1985) using first order analysis in the space domain. The advantage of the latter approach is that it can be applied in bounded domains, while the spectral method is tailored for infinite stationary domains. Note that all the results, regardless of the method used, show that the one- and two-dimensional cases provide erroneously large variances, due to the unrealistically limited number of paths that are offered to the flow system.

Composite Media Analysis--

This approach was followed by Dagan (1979) and follows closely the self-consistent method described in Beran (1968). The hydraulic conductivity field was represented as a collection of homogeneous blocks with random radii arranged at random locations. A similar method, that of the embedding matrix was presented in Chirlin and Dagan (1980).

Solute Transport in Groundwater

In the late seventies, the probabilistic framework was extended to include the solute transport problem where the heterogeneity of the natural formations is believed to be more influential. An apparent influence is on the dispersivity values corresponding to field scale plumes where an increase of two or three orders of magnitude with respect to the anticipated laboratory measured values was observed. A critical analysis of existing field observations of solute transport has revealed that dispersivities are scale dependent, Gelhar et al. (1985). Furthermore, concentration measurements exhibit significant fluctuations around the values predicted from analytical or numerical solutions. The review by Anderson (1979) suggests that the dispersivities used in numerical models are little more than fitting parameters and as such lack a sound physical basis.

The central questions that the related research has focused on are:

- What are the governing equations for large-scale mass transport in a heterogeneous aquifer?
- How do the different scales affect the characteristic parameters of what seems to be the same phenomenon?

A typical situation is depicted in Figure 4.4. The two smooth curves correspond to numerical or analytical solutions predicted with laboratory scale dispersivities and fitted field scale dispersivities. The actual measurements exhibit significant fluctuations around the values predicted by the models. The current work therefore attempts to answer the following question:

- How can the concentration variability around the predicted solutions be quantified?

The first attempt to show the effects of spatial heterogeneity was through Monte Carlo simulations [Schwartz (1977), and Smith and Schwartz (1980)]. From a numerical analysis point of view, the solution of the mass transport equation is by far more difficult than the solution of the flow equation. Instabilities in the algorithm are very frequent and numerical dispersion of the same order of magnitude as the physical dispersion may occur (Ababou et al. 1985). No quantitative conclusions were drawn from the Monte Carlo simulations.

Gelhar et al (1979) quantified for the first time the relationships among field scale or macro-dispersivities and characteristic measures of the hydraulic conductivity field. The physical situation examined was that of macrodispersion in a stratified aquifer, and the method used was spectral analysis and Fourier-Stieltjes representation. The authors developed the governing equations near and far away from the source, demonstrated the transition in the dispersivity until it reached its asymptotic value and showed the skewness of the concentration distribution near the injection vs.

the symmetric Gaussian concentration distribution at points far downstream. Some further aspects of the stratified case were discussed in Matheron and de Marsily (1980). In a subsequent paper, Gelhar and Axness (1983) treated the general three-dimensional case of macrodispersion in aquifers. That work focused on the asymptotic dispersivity coefficient from the simple case of isotropic media to the most general one of statistically anisotropic media with arbitrary orientation of the stratification. The results produced numerical values of the expected order of magnitude and compared favorably with the scarce existing field data.

Dagan (1984) produced similar results for the macrodispersivity following a Lagrangian approach which considers displacement of particles in random velocity field generated from a random hydraulic conductivity field. This analysis for the case of a statistically isotropic medium yields results for the asymptotic dispersion coefficient which are equivalent to those of Gelhar and Axness (1983).

A detailed quantitative testing of the macrodispersivity prediction has not been completed yet [Gelhar, 1985], but a number of carefully designed field experiments are now underway [Freyberg et al. (1983), LeBlanc (1985), and Betson et al. (1985)]. Hufschmied (1985) has shown that macrodispersivities calculated from measurements of the heterogeneity of hydraulic conductivity field are consistent with those estimated for a cold-water plume in an aquifer in Switzerland. Encouraging comparisons are also shown in Sudicky (1985b).

The issue of concentration variation has not been yet widely recognized. Gelhar et al. (1981) developed the concentration variance for the stratified case in answering a comment on their 1979 paper. They found that the concentration variance is proportional to the variance of the log hydraulic conductivity, the square of the mean concentration gradient, the fourth power of the correlation scale of the hydraulic conductivity and inversely proportional to the square of the local transverse dispersivity. The assumption of perfect layering is very restrictive and thus these results are primarily of qualitative significance in demonstrating the factors which influence the concentration variability. These results do indicate that significant variations of concentration are to be expected across the layers even after very large mean transport distances.

Gelhar and Gutjahr (1982) have developed the equation for the concentration variance for one-dimensional transport of a solute undergoing radioactive decay. They have considered transport in a stream tube with varying cross-section, thus incorporating the influence of a three-dimensional flow variation. The results relate the concentration variance to statistical parameters of the longitudinal velocity field. Dependence of the concentration variance on the square of the mean concentration gradient and the square of the correlation scale of the velocity is observed. Due to the one-dimensional structure of the problem, analytical solutions for the concentration perturbations can be obtained which could be used in a finite domain. The radioactive decay results in a finite concentration variance even when local mixing is eliminated by setting the local dispersivity value equal to zero.

Gutjahr et al. (1985) developed similar results following a slightly different methodology. They treated the same problem with emphasis on the development of equivalent macrodispersivity values. Their result for the concentration variance is still under investigation.

Dagan (1982b, 1984) is the only other available work focusing on the calculation of the concentration variance. His approach follows closely the theory of diffusion by continuous movements [Taylor (1921)] referred to above as the Lagrangian method. In a qualitative sense, Dagan's results are similar to the ones found in this research work. One of the assumptions made was that the effects of local dispersivity can be neglected when calculating the mean motion of the plume. It is thus believed that Dagan's results are applicable in a region near the source of pollution where the convective component of the hydrodynamic dispersion is predominant. In contrast, the results in this study correspond to the far field downstream region. From the analyses of the mean concentration, it is indicated that the local dispersivity does not have an important effect on the macrodispersivity values. The opposite effect is observed when examining the concentration variance. A final point is that the approach of Dagan is performed for statistically homogeneous, isotropic media, while the current work is based on the more realistic case of anisotropic hydraulic conductivity fields.

SECTION 5

ANALYSIS OF CONCENTRATION VARIABILITY

THE GOVERNING EQUATIONS

The general equation describing transport of an ideal nonreactive conservative solute in a saturated, rigid porous medium is, [Gelhar and Axness (1983)]:

$$n \frac{\partial c}{\partial t} + q_i \frac{\partial c}{\partial x_i} = \frac{\partial}{\partial x_i} E_{ij} \frac{\partial c}{\partial x_j} \tag{5.1}$$

where, n = porosity
q_i = specific discharge in the x_i direction
c = concentration of the transported solute
E_{ij} = local bulk dispersion coefficient tensor.

The dispersivity values in E_{ij} will be assumed constant at the scale at which Eq. (5.1) is valid. Eq. (5.1) incorporates the conservation of mass equation for a homogeneous fluid,

$$\frac{\partial}{\partial x_i} q_i = 0 \tag{5.2}$$

The fields of log hydraulic conductivity, specific discharge and concentration will be decomposed into a mean and a small perturbation about the mean. Therefore,

$$\begin{aligned} &\ell nK = f = F + f' && \text{(log hydraulic conductivity)} \\ &q_i = \overline{q}_i + q_i' && i = 1, 2, 3 \text{ (specific discharge)} \\ &c = \overline{c} + c' && \text{(concentration)} \end{aligned} \tag{5.3}$$

The log hydraulic conductivity perturbation field, f', is assumed to be a statistically homogeneous random field with zero mean and known covariance function. Note that through the Darcy equation, the specific discharge and the hydraulic conductivity are directly related, [Gelhar and Axness (1983)]. The concentration perturbation, c', becomes a random field also and substituting Eq. (5.3) into Eq. (5.1) the equations for the mean concentration, $\overline{c}$, and perturbation, c', can be found. Without loss of generality, we can align the x_1 axis along the mean flow, which renders

$$q = \overline{q}_1 \neq 0 \ , \ \overline{q}_2 = \overline{q}_3 = 0 \tag{5.4}$$

The local dispersion tensor may then be approximated in the form

$$[E_{ij}] = \begin{bmatrix} \alpha_L q & 0 & 0 \\ 0 & \alpha_T q & 0 \\ 0 & 0 & \alpha_T q \end{bmatrix} \tag{5.5}$$

where α_L and α_T are the local longitudinal and transverse dispersivities. Eq. (5.4) and Eq. (5.5) can simplify the equations for the mean concentration and perturbation to:

$$n \frac{\partial \bar{c}}{\partial t} + q \frac{\partial \bar{c}}{\partial x_1} + \overline{q_i' \frac{\partial c'}{\partial x_i}} = q \alpha_L \frac{\partial^2 \bar{c}}{\partial x_1^2} + q \alpha_T \left(\frac{\partial^2 \bar{c}}{\partial x_2^2} + \frac{\partial^2 \bar{c}}{\partial x_3^2}\right) \qquad (5.6)$$

$$n \frac{\partial c'}{\partial t} + q_i' \frac{\partial \bar{c}}{\partial x_i} + q \frac{\partial c'}{\partial x_1} - q \alpha_L \frac{\partial^2 c'}{\partial x_1^2} - q \alpha_T \left(\frac{\partial^2 c'}{\partial x_2^2} + \frac{\partial^2 c'}{\partial x_3^2}\right) \qquad (5.7)$$

$$= \overline{q_i' \frac{\partial c'}{\partial x_i}} - q_i' \frac{\partial c'}{\partial x_i} \simeq 0$$

The zero mean term on the right hand side of Eq. (5.7) is of second order in perturbations and is assumed to be negligible compared to the first order terms on the left side.

In Gelhar and Axness (1983) Eq. (5.6) and Eq. (5.7) are used to calculate an expression for the macrodispersivity tensor A_{ij}. It is shown that far away from the source, the mean concentration satisfies the classical transport equation with constant macrodispersivities. In the current work, the attention focuses on Eq. (5.7). It will be assumed that the mean concentration field is known.

The effects of the velocity field variations on the local dispersion were addressed in Naff (1978). He retained the actual velocity field in Eq. (5.5) and found that the effects of the velocity variations on the macrodispersivities were of second order. An extension of his analysis to study these effects on the concentration variability showed that they were negligible in this case also. Consequently, Eq. (5.5) is considered a valid representation of the local dispersion effects, at the current level of approximation.

SPECTRAL SOLUTIONS

The equation for the concentration perturbation, Eq. (5.7), can be easily solved if it is assumed that the concentration perturbation field is statistically homogeneous. Invoking the Fourier-Stieltjes representation theorem [Lumley and Panofsky (1962)] one can find relations between the spectra of the concentration and log hydraulic conductivity. The simple case of a steady concentration field will be investigated first.

Steady State Concentration Field

The perturbed quantities are represented as,

$$c' = \int_{-\infty}^{\infty} \exp(i\underline{k}\cdot\underline{x}) dZ_c(\underline{k}); \quad q_i' = \int_{-\infty}^{\infty} \exp(i\underline{k}\cdot\underline{x}) dZ_{q_i}(\underline{k}) \qquad (5.8)$$

where $\underline{k}=(k_1,k_2,k_3)$ is the wave number vector, $\underline{x}=(x_1,x_2,x_3)$ is the position

vector, and the integration is over three-dimensional wave number space. Combining eq. (5.8) and eq. (5.7) and invoking the uniqueness of the spectral representation

$$[ik_1+\alpha_L k_1^2+\alpha_T(k_2^2+k_3^2)]qdZ_c=G_j dZ_{q_j} \tag{5.9}$$

where $G_j = -\frac{\partial \bar{c}}{\partial x_j}$, the mean concentration gradient, is taken to be locally constant.

The complex conjugate Fourier amplitude of $dZ_{c^*}^*$, namely dZ_c, can be easily found from Eq. (5.9). Taking expectation of $dZ_c dZ_c^*$ results in the following spectral relationship:

$$S_{cc}(\underline{k}) = \frac{1}{q^2} \frac{G_j G_\ell \, S_{q_j q_\ell}(\underline{k})}{k_1^2 + [\alpha_L k_1^2 + \alpha_T (k_2^2+k_3^2)]^2} \tag{5.10}$$

where $S_{cc}(\underline{k})$ = the three-dimensional spectrum of the concentration perturbation,
$S_{q_j q_\ell}(\underline{k})$ = the three-dimensional spectrum of the specific discharges along the axes x_j and x_ℓ (j, ℓ = 1,2,3).

The final step is to establish the relationship between $S_{q_j q_\ell}(\underline{k})$ and $S_{ff}(\underline{k})$, the spectrum of the log-hydraulic conductivity field. In the general case, one expects aquifers to exhibit three-dimensional anisotropic heterogeneity with the mean flow arbitrarily oriented with respect to the stratification. The coordinate systems might look then as in Figure (5.1) where it can be observed that the mean hydraulic gradient vector does not coincide with the direction of the mean flow. The covariance function has its principal axes at the primed system. Using the Darcy equation for a locally isotropic medium, Gelhar and Axness (1983) showed that the specific discharge spectra can be expressed in terms of the log-conductivity spectrum as

$$S_{q_j q_\ell}(\underline{k}) = K_\ell J_m J_n \left(\delta_{jm} - \frac{k_j k_m}{k^2}\right)\left(\delta_{\ell n} - \frac{k_\ell k_n}{k^2}\right) S_{ff}(\underline{k}) \tag{5.11a}$$

where j,ℓ,m,n = 1,2,3. (Note that summation over m and n is implied.)
A simplified case corresponds to statistically isotropic ℓnK field, for which the specific discharge spectrum becomes,

$$S_{q_j q_\ell}(\underline{k}) = \frac{q^2}{\gamma^2}\left(\delta_{j1} - \frac{k_1 k_j}{k^2}\right)\left(\delta_{\ell 1} - \frac{k_1 k_\ell}{k^2}\right) S_{ff}(\underline{k}) \tag{5.11b}$$

where $\gamma = q/K_\ell J_1$, and J_1 is the hydraulic gradient in the x_1 direction.

The covariance function of the concentration field can be computed combining Eq. (5.10) and Eq. (5.11),

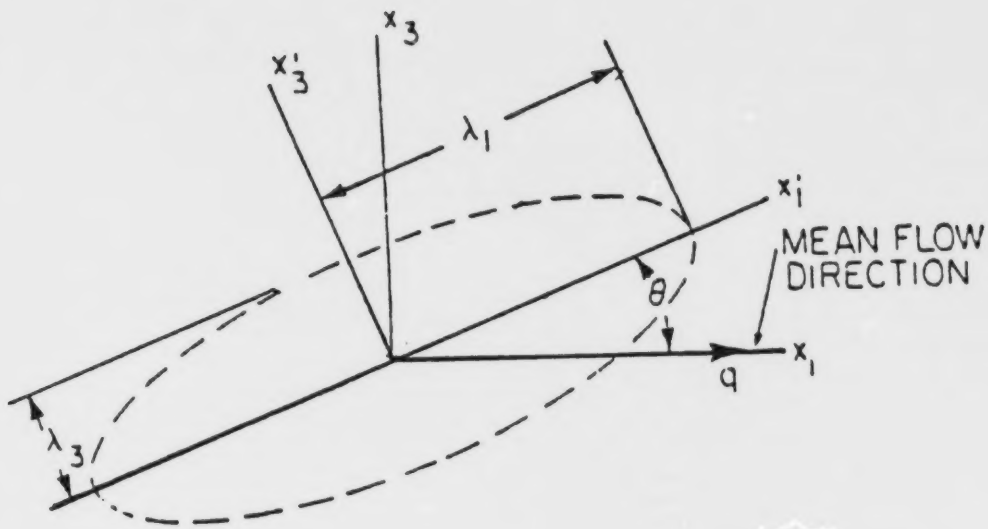

Figure 5.1 Coordinate systems for the case $x_2 = x_2'$; the dashed elipse represents schematically the e^{-1} level of the correlation function

$$R_{cc}(\underline{\xi}) = \int_{-\infty}^{\infty} \exp\left(i\underline{k}\cdot\underline{\xi}\right) S_{cc}(\underline{k})d\underline{k} \tag{5.12}$$

where $R_{cc}(\underline{\xi})$ is the covariance function of the concentration field, at lag $\underline{\xi}$. The variance is found by taking $\underline{\xi} = 0$,

$$\sigma_c^2 = R_{cc}(0) = \int_{\infty}^{\infty} S_{cc}(\underline{k})d\underline{k} \tag{5.13}$$

Unsteady Concentration Field

The concentration perturbation field, $c'(\underline{x},t)$, is, in general, time varying. Again it will be assumed that the concentration field is locally stationary (statistically homogeneous) since the time-invariant hydraulic conductivity field is spatially homogeneous. This assumption is expected to be particularly valid away from the source. Because the unsteady mean concentration solution will be expressed in terms of a moving coordinate system, ξ_i ($\xi_1 = x_1 - qt/n$, $\xi_2 = x_2$, $\xi_3 = x_3$), it is appropriate to express the perturbation transport equation (Eq. (5.7)) in that system as

$$\left.\frac{\partial c'}{\partial t}\right|_{\underline{\xi}} + q_i' \frac{\partial \bar{c}}{\partial \xi_i} = \alpha_L q \frac{\partial^2 c'}{\partial \xi_1^2} + \alpha_T q \left(\frac{\partial^2 c'}{\partial \xi_2^2} + \frac{\partial^2 c'}{\partial \xi_3^2}\right) \tag{5.7a}$$

where $c'(\underline{\xi},t)$, i.e., $\underline{\xi}$ and t and are the independent variables. The flow field is steady in the fixed coordinate system so that q_1' in (5.7a) is represented by

$$q_i'(\underline{x}) = \int_{-\infty}^{\infty} e^{i\underline{k}\cdot\underline{x}}\, dZ_{q_i}(\underline{k}) \tag{5.14a}$$

but the time varying $c'(\underline{\xi},t)$ will be represented as

$$\begin{aligned} c'(\underline{x},t) &= \int_{-\infty}^{\infty} e^{i\underline{k}\cdot\underline{x}}\, dZ_c(\underline{k};t,x_i) \\ &= \int_{-\infty}^{\infty} \exp\left[i(k_1\xi_1 + qt/n) + k_2\xi_2 + k_3\xi_3)\right] dZ_c(\underline{k};t,\xi_i) \\ &= c'(\xi_i,t) \end{aligned} \tag{5.14b}$$

Note that dZ_c is considered to vary slowly in space so that the dependence on ξ_i is only parametric. It should be mentioned parenthetically that the introduction of the moving coordinate system is the more natural system to use, but, of course, from a mathematical point of view the two systems are equivalent. The moving system is introduced in order to take advantage of the fact that in the moving system, the concentration field will vary slowly in time.

Using Eqs. (5.11a) and (5.14b) in (5.7a) along with the uniqueness of the representation theorem,

$$\eta \frac{\partial}{\partial t}\Big|_{\underline{\xi}} dZ_c(\underline{k};\, t) - G_j dZ_{q_j}(\underline{k}) + iqk_1\, dZ_c(\underline{k};t)$$

$$= -q\left[\alpha_L k_1^2 + \alpha_T(k_2^2 + k_3^2)\right] dZ_c(\underline{k};t) \qquad (5.15)$$

Denoting,

$$dZ_c(\underline{k};\, t) = p$$

$$\theta = \frac{q}{n}\left[ik_1 + \alpha_L k_1^2 + \alpha_T (k_2^2 + k_3^2)\right] \qquad (5.16)$$

$$K(t) = \frac{1}{n} G_j dZq_j(\underline{k})$$

Eq. (5.15) can be simply written as

$$\frac{\partial p}{\partial t}\Big|_{\underline{\xi}} + \theta p = K \qquad (5.17)$$

With initial condition $c'(\underline{x},0) = 0$, or in the wave number domain $dZ_c(k,0) = 0 = p(0)$, Eq. (5.17) can be solved. The solution is,

$$p = e^{-\theta t} \int_o^t K(\tau)\, e^{\theta\tau}\, d\tau \qquad (5.18)$$

$$p = e^{-\theta t} \frac{1}{n} dZ_{q_j}(\underline{k}) \int_o^t e^{\theta\tau}\, G_j(\underline{\xi},\tau)\, d\tau \qquad (5.19)$$

The integral in this last equation can not be evaluated analytically (G_j's are complicated functions which are unknown in the sense that they depend on the solution of the concentration perturbation). Because of the exponential term in Eq. (5.19), the main contribution will, for large θ, come from the region near the upper limit, $\tau = t$. Therefore, $G_j(\underline{\xi};\tau)$ is expanded around the value at $\tau = t$. The expansion leads to,

$$G_j(\underline{\xi},\tau) = G_j(\xi,\tau) + \frac{\partial G_j}{\partial \tau}\Big|_{\tau=t} (\tau - t) + \ldots \qquad (5.20)$$

where it is implied that the time derivative is in the moving coordinate system $\frac{\partial}{\partial t}\Big|_{\xi}$. This expansion also has the important advantage that it allows the mean transport equation to be approximated in the form of the classical advection-dispersion equation; otherwise the governing equation will be known in the form of an integro-differential equation wherein the macrodispersive flux is dependent on the mean concentration gradient at earlier times. This feature is discussed by Gelhar (1986). Here because the goal is to develop results which can make use of mean solutions based on the classical transport equation, this analytical approximation will be explored in detail. Keeping only second-order derivatives and combining Eqs. (5.19) and (5.20):

$$p \simeq \frac{1}{n} dZ_{q_j} \int_o^t e^{-\theta(t-\tau)} \left[G_j(\underline{\xi},t) + \frac{\partial G_j}{\partial \tau} \Big|_{\tau=t} (\tau - t) \right] d\tau \tag{5.21}$$

A change of variables, $u=t-\tau$, and the limit for $t \to \infty$, gives.

$$p \simeq \frac{1}{n} dZ_{q_j} \int_{-\infty}^{\infty} e^{-\theta u} \left[G_j(\underline{\xi},t) - u \frac{\partial G_j}{\partial t} \Big|_{\xi} (\xi,t) \right] du \tag{5.22}$$

Consequently, $dZ_c(\underline{k},t)$ has an approximate analytical expression. From this point and on the procedure of the previous section can be followed. Integrating Eq. (5.22) the complex amplitude is given from,

$$dZ_c(\underline{k},t) = \frac{1}{n} dZ_{q_j} \left[G_j(\underline{\xi},t) \frac{1}{\theta} - \frac{\partial G_j}{\partial t} \Big|_{\xi} \frac{1}{\theta^2} \right] \tag{5.23}$$

with complex conjugate,

$$dZ_c^*(\underline{k},t) = \frac{1}{n} dZ_{q_j}^* \left[G_j(\underline{\xi},t) \frac{1}{\theta^*} - \frac{\partial G_j}{\partial t} \Big|_{\xi} \frac{1}{\theta^{*2}} \right] \tag{5.24}$$

The spectrum of $c'(x,t)$ is found by multiplying the complex conjugate amplitudes and taking expectations. Recall,

$$\begin{aligned} E\left[dZ_c(\underline{k};t)\, dZ_c^*(\underline{k};t) \right] &= S_{cc}(\underline{k},t)\, d\underline{k}; \\ E\left[dZ_{q_j}(\underline{k})\, dZ_{q_\ell}^*(\underline{k}) \right] &= S_{q_j q_\ell}(\underline{k}) d\underline{k} \end{aligned} \tag{5.25}$$

This operation leads to the following expression

$$\begin{aligned} S_{cc}(\underline{k},t) = \frac{1}{n} S_{q_j q_\ell} \Big[& G_j G_\ell \frac{1}{\theta} \frac{1}{\theta^*} - \frac{\partial G_j}{\partial t} G_\ell \frac{1}{\theta^2} \frac{1}{\theta^*} - \frac{\partial G_\ell}{\partial t} G_j \frac{1}{\theta^{*2}} \frac{1}{\theta} \\ & + \frac{\partial G_j}{\partial t} \frac{\partial G_\ell}{\partial t} \frac{1}{\theta^2} \frac{1}{\theta^{*2}} \Big] \end{aligned} \tag{5.26}$$

where summation over all the values of j and ℓ is implied. To simplify notation further denote

$$A = \frac{q}{n} k_1$$

$$B = \frac{q}{n} [\alpha_L k_1^2 + \alpha_T (k_2^2 + k_3^2)] \tag{5.27}$$

$$\theta = B + iA$$

$$\theta^* = B - iA$$

$$\theta\theta^* = B^2 + A^2 \tag{5.28}$$

$$\theta^2 = B^2 - A^2 + 2iAB$$

$$\theta^{*2} = B^2 - A^2 - 2iAB$$

Thus, Eq. (5.26) can be written as,

$$S_{cc}(\underline{k}, t) = \frac{1}{n^2} S_{q_j q_\ell} \frac{1}{A^2 + B^2} \left[G_j G_\ell + \frac{\partial G_j}{\partial t}\Big|_{\underline{\xi}} \frac{\partial G_\ell}{\partial t}\Big|_{\underline{\xi}} \frac{1}{A^2 + B^2} \right.$$

$$\left. - \frac{\partial G_j}{\partial t}\Big|_{\underline{\xi}} G_\ell \frac{1}{B + iA} - \frac{\partial G_\ell}{\partial t}\Big|_{\underline{\xi}} G_j \frac{1}{B - iA} \right] \tag{5.29}$$

The relationship between $S_{q_j q_\ell}$ and S_{ff} is presented in the previous section (Eq. 5.11a)). Note that the inclusion of the time variation has introduced three additional terms in the concentration spectrum, as can be seen by the comparison of Eq. (5.24) with Eq. (5.10). This implies that the "zero" order behavior of the unsteady case solution will be determined from the steady state. The results will be different only in the region where the concentration gradients change rapidly, i.e., near the peak concentration.

THE LOG-HYDRAULIC CONDUCTIVITY SPECTRUM

The intuitive notion for a covariance function structure dictates that it should have its maximum at zero lag and decay, in some way, as the lag increases dropping to zero at some distance. A simple model that captures such an image is a negative exponential. It has been used extensively and appears to be consistent with the available data [(Bakr (1976) Sudicky (1985a)]. However within the statistical limitation of field data, other forms of the covariance can be equally acceptable. Occasionally, the mathematical structure of the models used to describe the physical behavior require a stronger assumption about the covariance behavior. Bakr et al. (1978), Gutjahr and Gelhar (1981), Vomvoris (1982) have used different covariance models, which still show a decay with distance but, in one sense, reinforce the periodic or stationary nature of

the modeled process. The simplest of these latter models is the so-called "hole type" covariance function (Bakr et al, 1978). Its main characteristic, besides the negative exponential decay, is the negative correlation after a certain lag. In the wave number domain this characteristic corresponds to a zero value of the spectrum at $\underline{k} = 0$, i.e., zero integral scale. Moltyaner (1985, p. 363-22, 23) has observed such negative correlations in field data (Figure 5.2). In turbulence, where similar mathematical analysis has been used, a popular spectrum is the following [Hinze (1975), Aldama (1985)].

$$S(k) \sim k^4 \exp\left(-\frac{1}{2}a^2k^2\right) \tag{5.30}$$

which also has zero integral scale.

For the concentration covariance a similar zero integral scale log hydraulic conductivity covariance has to be used. It can be seen from Eq. (5.10) that for $k_2 = k_3 = 0$, the k_1 in the denominator will cause the integral to blow up at $k_1 = 0$, when one integrates from $-\infty$ to $+\infty$. This behavior can be avoided if $S_{q_i q_\ell}(0,0,0) = 0$, or, from Eq. (5.11), $S_{ff}(\underline{0}) = 0$, which is the zero-integral requirement postulated.

A simple hole-type, three-dimensional covariance is the following:

$$R_{ff}(\underline{\xi}) = \sigma_f^2 \left(1 - \frac{1}{3}s\right)e^{-s}, \qquad s^2 = \frac{\xi_i^2}{\ell_i^2} \tag{5.31}$$

$$S_{ff}(\underline{k}) = \frac{4}{3}\sigma_f^2 \frac{\ell_1\ell_2\ell_3}{\pi^2} \frac{k_i^2\ell_i^2}{(1 + k_i^2\ell_i^2)^3} \tag{5.32}$$

The ℓ_i's are some characteristic scales of the hole exponential covariance that can be uniquely related to the e^{-1} correlation scale. The notation λ will be reserved for the negative exponential covariance function correlation scale.

Figure (5.3) compares the hole type with the exponential, $R(\xi) = \sigma_f^2 \exp(-\xi/\lambda)$, when they have the same e^{-1} value for the same distance ξ. The two covariance functions are practically indistinguishable.

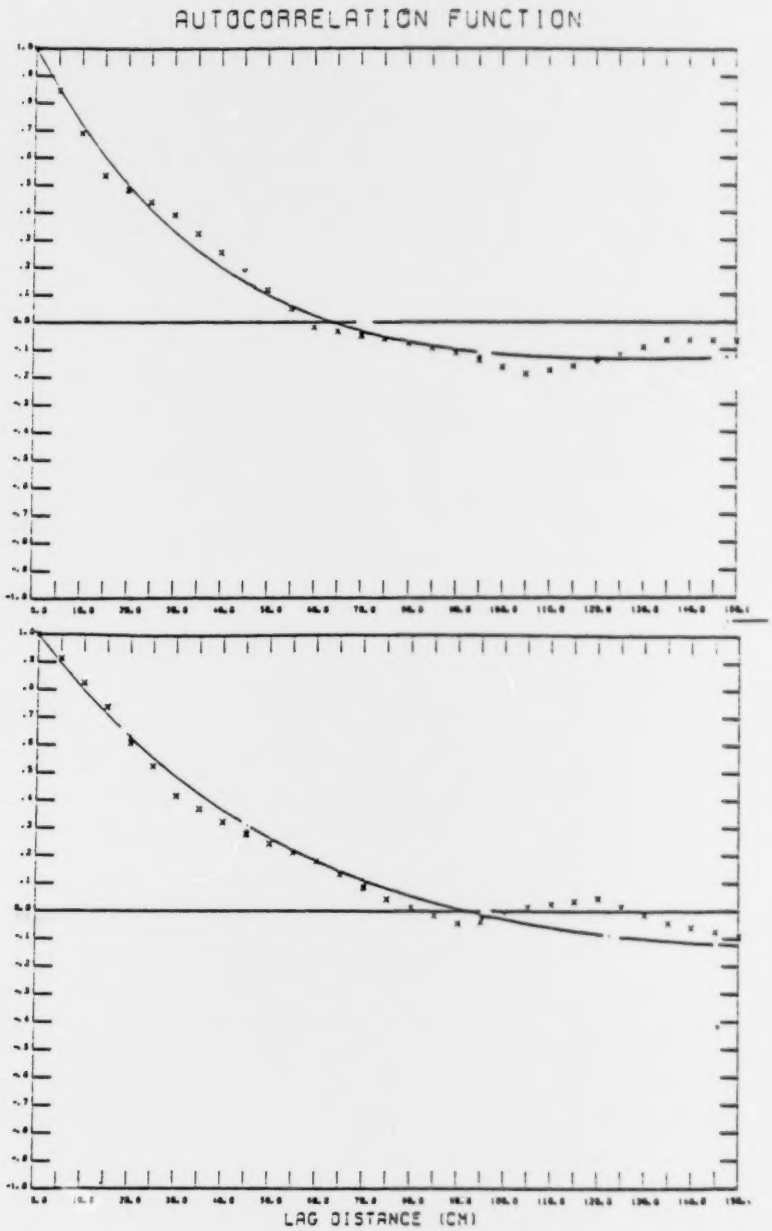

Figure 5.2 Comparison of sample autocorrelation function (crosses) for hydraulic conductivity (from grain-size analysis) with theoretical autocorrelation function (solid line). (From the CRNL, Ontario experiment, Moltyaner, 1985)

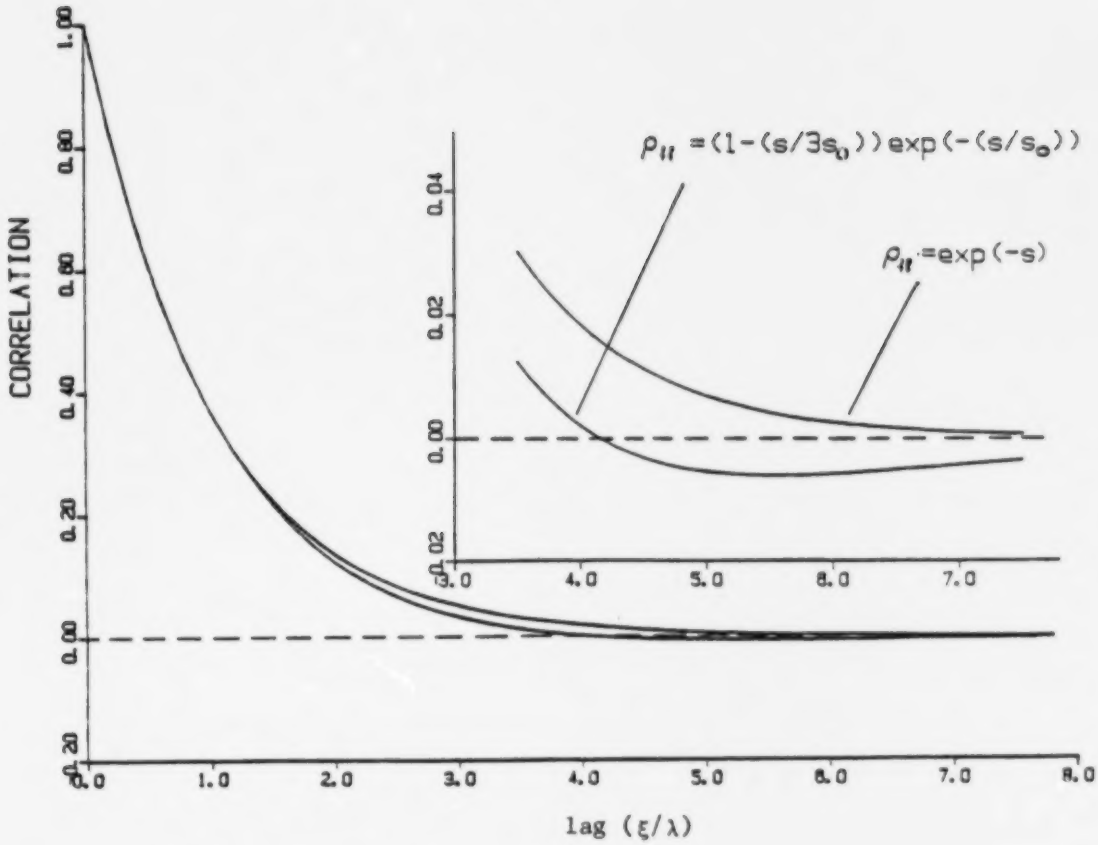

Figure 5.3 Comparison of the exponential correlation function and the hole exponential correlation function

APPROXIMATE ANALYTICAL ESTIMATIONS

The covariance function of the concentration field involves the evaluation of the three-dimensional integral in Eq. (5.12), which, for the general case, can not be performed in an analytical fashion. However, for some simple situations, approximate analytical expressions can be found. These expressions, although not directly applicable in all practical situations, reveal the structure of the concentration covariance and the influence of the various parameters.

The covariance function in Eq. (5.12) can be written as:

$$R_{cc}(\underline{\xi}) = T'_{jp}(\ell_1,\ell_2,\ell_3,\alpha_L,\alpha_T,\phi,\theta,\underline{\xi})\, G_j G_p \tag{5.33a}$$

where, the Einstein's notation for repeated indices is used and

$$T'_{jp}(\ell_1,\ell_2,\ell_3,\alpha_L,\alpha_T,\phi,\theta,\underline{\xi}) = \frac{K_\ell^2}{q^2} \int_{-\infty}^{\infty} \exp(-i\underline{k}\cdot\underline{\xi}) \frac{S_{ff}(\underline{k})}{k_1^2 + [\alpha_L k_1^2 + \alpha_T(k_2^2 + k_3^2)]^2}$$

$$\cdot \{ J_m J_n \left(\delta_{jm} - \frac{k_j k_m}{k^2}\right) \left(\delta_{pn} - \frac{k_\ell k_n}{k^2}\right) d\underline{k} \} \tag{5.33b}$$

where the $S_{ff}(\underline{k})$ has the form of Eq. (5.32) and j, p, m, n can take the values 1,2,3.

One can further convert the integral in Eq. (5.33b) to a function of non-dimensional variables (Appendix B) so that Eq. (5.33a) becomes

$$R_{cc}(\underline{\xi}) = T_{jp}(\rho_1,\rho_2,\varepsilon,\kappa,\phi,\theta,\underline{\xi})\, \sigma_f^2\, \ell_3^2\, G_j G_p \tag{5.33c}$$

where $\rho_1 = \ell_3/\ell_1$, $\rho_2 = \ell_3/\ell_2$, $\varepsilon = \alpha_L/\ell_3$, $\kappa = \alpha_T/\alpha_L$

For the following cases it will be assumed that the major principal axis of the hydraulic conductivity coincides with the mean flow.

The approximate analytical solutions are summarized in Table 5.1. Appendix A presents the details of their evaluation. In all cases advantage is taken of the almost singular behavior of the integrand around $k_1 = 0$.

The results in Table 5.1 demonstrate the following:

(i) The concentration variance is inversely proportional to the local dispersivity value. This is a physically intuitive behavior since the smaller the local dispersivity the less the capacity of the medium to attenuate developing tongues of fast moving solute. Gelhar et al. (1979) and Matheron and de Marsily (1980) have described similar phenomena.

Table 5.1

APPROXIMATE ANALYTICAL SOLUTIONS

Case	T_{11} ($\varepsilon \to o$)	T_{22} ($\varepsilon = 0$)	T_{33} ($\varepsilon = 0$)
1. Isotropic ℓnK σ_c^2	$\frac{1}{\gamma^2}\ \frac{2}{3}\ \frac{1}{\kappa\varepsilon}$	$\frac{1}{\gamma^2}\ \frac{1}{9}$	$= T_{22}$
2. Anisotropic ℓnK σ_c^2	$\frac{1}{\gamma^2}\ \frac{2}{3}\ \frac{1}{\kappa\varepsilon}\ \frac{1}{\rho_1}\ \frac{1}{\rho_2}$	$\frac{1}{\gamma^2}\ \frac{1}{6}\left[\frac{1}{2\rho_1^2} + \frac{1}{R^2} + \left(\frac{1}{2} + \frac{1}{R^2}\right) \cdot \frac{1}{R}\ \ell n \frac{R + 2R^2}{R - 2R^2}\right]$ *	$= T_{22}$
3. Isotropic ℓnK a. $R_{cc}(\xi,0,0)$	$\frac{1}{\gamma^2}\ \frac{2}{3}\ \frac{1}{\kappa\varepsilon} \cdot \left[1-\beta-\beta^2 e^{\beta} Ei(-\beta)\right]$	$\frac{1}{\gamma^2}\ \frac{4}{3}\left[\frac{2}{\zeta^3} - e^{-\zeta}\left(\frac{2}{\zeta^3} + \frac{2}{\zeta^2} + \frac{1}{\zeta} + \frac{1}{4}\right)\right]$	$= T_{22}(\xi,0,0)$
b. $R_{cc}(0,\xi,0)$	$\frac{1}{\gamma^2}\ \frac{1}{\kappa\varepsilon}\ \frac{1}{3}\ \zeta^2 K_2(\zeta)$	$\frac{1}{\gamma^2}\ \frac{1}{3}\ \frac{1}{\zeta^3}\left[e^{-\zeta}(16 + 16\zeta + 8\zeta^2 + 3\zeta^3 + \zeta^4) - 16\right]$	$= T_{22}(\xi,0,0)$
c. $R_{cc}(0,0,\xi)$	$= T_{11}(0,\xi,0)$	$= T_{22}(\xi,0,0)$	$= T_{22}(0,\xi,0)$

$\rho_1 = \frac{\ell_3}{\ell_1}$, $\rho_2 = \frac{\ell_3}{\ell_2}$, $\varepsilon = \frac{\alpha_L}{\ell_3}$, $\kappa = \frac{\alpha_T}{\alpha_L}$, $R^2 = 1 - \rho_1^2$, $\beta = \frac{\alpha_T \xi}{\ell^2}$, $\zeta = \frac{\xi}{\ell}$,

Ei(-x) = Exponential Integral, $K_2(\cdot)$ = Modified Bessel function of 2nd order, *$\rho_2 = 1$.

(ii) The concentration variance is proportional to the product of the correlation scales of the hydraulic conductivities. Higher correlation scales imply that solute trapped in a more permeable layer tends to stay there longer, since the formation persists for larger scales. Consequently a randomly located measuring probe would have higher chances for a "hit or miss" output.

Vomvoris and Gelhar (1985) presented a comparison of the variances of two different media, an anisotropic and an isotropic one, having the same product of correlation scales (Figure 5.4). The favorable comparison of the two results indicated the option, for variance calculations, of replacing an anisotropic medium by an equivalent statistically isotropic one with correlation scale equal to the geometric mean of the anisotropic correlation scales.

(iii) The concentration covariance along the direction of the mean flow has very high correlation scales (Figure 5.5). This singular behavior is still under investigation.

THE NUMERICAL CALCULATION

The equation for the concentration covariance, Eq. (5.12), cannot be evaluated analytically for a general combination of the input parameters. A direct three-dimensional numerical evaluation, unless very carefully designed, can produce unreliable results due to the irregular behavior of the integrand. A reduction to a two-dimensional integral can be accomplished if one converts Eq. (5.12) to spherical coordinates and integrates over wave number u. Appendix B presents the details of the above integration. The result is, Eq. (B.7) and Eq. (B.11),

$$R_{cc}(\xi,\chi,\psi) = \int_{w=o}^{2\pi} \int_{\beta=o}^{\pi} d\omega\, d\beta\, \sin\theta\, F_{ij}(\beta,\omega)\, \frac{1}{E^2 A^4}\, \frac{\pi}{2} \cdot$$

$$\{[A_{11}|A| + A_{12}\,\frac{1}{2}\,|A|^3\,(1 + |\frac{R}{A}|)$$

$$+ A_{13}\,\frac{1}{2^3}\,|A|^5\,(3 + 3\,|\frac{R}{A}| + \frac{R^2}{A^2})]\,\exp[-|\frac{R}{A}|]$$

$$+ A_2\,|\frac{E}{\rho_1 B}|\,\exp[-|\frac{R\,\rho_1 B}{E}|]\}\,G_i G_j\,\sigma_f^2\,\ell_3^2 \qquad (5.34)$$

where the different quantities: A_{11}, A_{12}, A_{13}, A_2, A,E,R,B are functions of ω,β and are defined in Appendix B. The integral in Eq. (5.34) is evaluated first over angle β using the Romberg integration technique and then with a simple trapezoidal rule over ω.

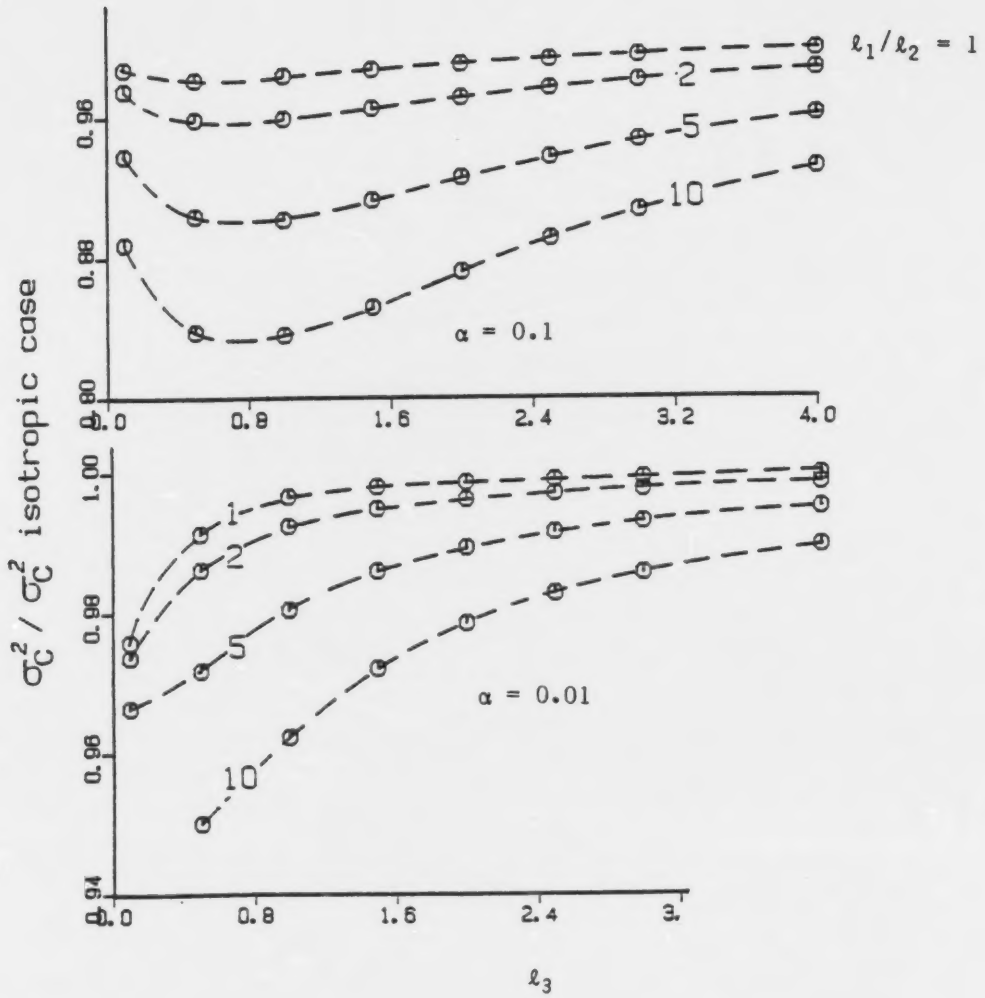

Figure 5.4 Comparison of the variance for an anisotropic aquifer (correlation scales ℓ_1, ℓ_2, ℓ_3) and an equivalent isotropic (correlation scale $\ell = (\ell_1, \ell_2, \ell_3)^{1/3}$)

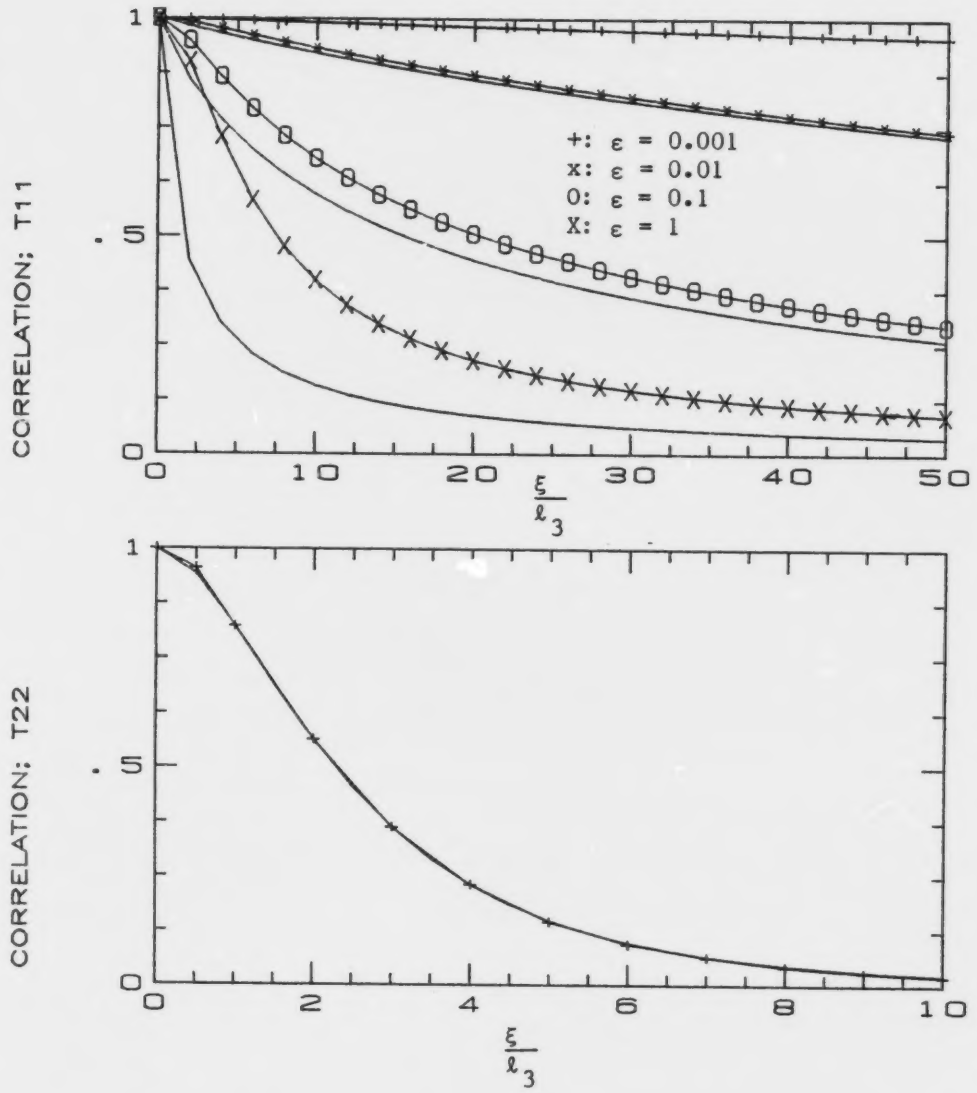

Figure 5.5 Comparison of the approximate analytical expressions and the numerical results for the T_{ij} coefficients
(a) $T_{11}(\cdot)$ along the x direction for different ε
(b) $T_{22}(\cdot)$ along the x direction

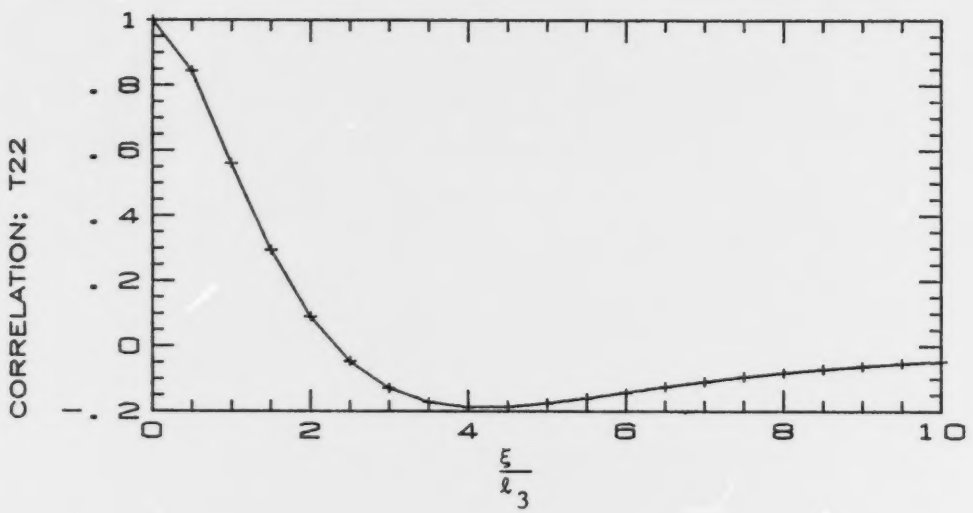

Figure 5.5(c) Comparison of the approximate analytical expressions and the numerical results for the T_{ij} coefficients
$T_{22}(\cdot)$ along the y direction

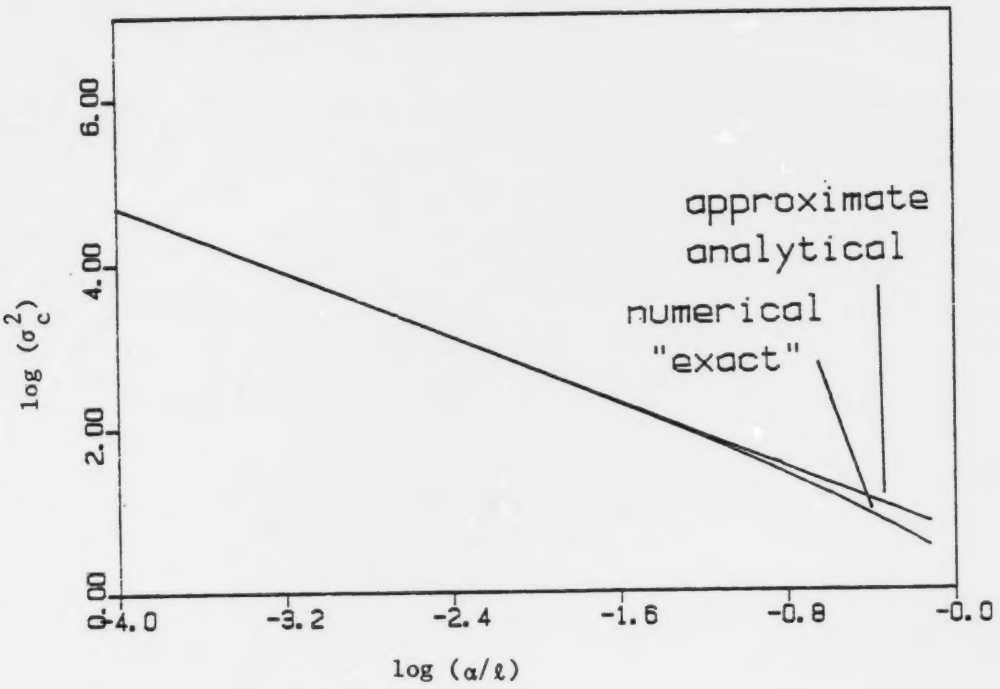

Figure 5.6 Test of the validity of the approximate result for the variance $T_{11}(1,1,\varepsilon,1;0)$ with respect to the ε values

The approximate analytical expressions in Table 5.1 are evaluated by comparison with the numerical integration. A comparison of the numerical results and the approximate analytical is shown in Figure 5.5. The agreement is very good for small values of $\varepsilon\kappa = \alpha_T/\ell$. Figure (5.6) compares the expression for the variance. The analytical approximation gives identical results with the numerical for values of $\varepsilon\kappa = \alpha_T/\ell$ up to 0.10.

Table 5.2 shows the effects of the angles of orientation of the stratification on the variance. For the chosen correlation scales the effect of the vertical inclination seems to be stronger. In most cases the values remain of the same order of magnitude. A notable case is T_{13}, the coefficient that multiplies $(-\partial\bar{c}/\partial x_1)(-\partial c/\partial x_3)$. Its magnitude increases up to an order of magnitude less than the value of T_{11}. Since the longitudinal gradients are very much milder than the vertical ones, such an increase could equalize the effects of the longitudinal and vertical gradients in the estimation of the variance. Table 5.2 demonstrates the complicated interaction of the correlation scales, the local dispersion coefficient and the orientation of the stratification. Further investigation of these relationships is required.

Figure 6.3, in the next section, shows the results of the numerical integration for the covariance of an isotropic hydraulic conductivity field. The presented curves are directly proportional to T_{11}. Very high correlation scales along the flow direction are observed.

Table 5.2

EFFECT OF THE STRATIFICATION ORIENTATION ON THE CONCENTRATION VARIANCE

(a) $\rho_1 = 0.02$, $\rho_2 = 0.2$, $\varepsilon = 0.1$, $\kappa = 1$

ϕ	θ	T_{11}	T_{22}	T_{33}	T_{12}	T_{13}	T_{23}
0	0	518.5	0.72	0.76	0	0	0
0	5	592.96	1.69	3.51	0	30.05	0
0	10	653.14	4.57	11.59	0	64.58	0
0	15	716.22	8.83	24.08	0	102.0	0
5	0	547.74	0.77	0.81	-2.27	0	0
5	5	598.41	1.7	3.62	-1.92	30.87	-0.08
5	10	656.95	4.48	11.82	-1.81	65.05	-0.07
5	15	723.73	8.73	24.57	-1.41	102.06	-0.01
10	0	583.84	0.89	0.92	-5.83	0	0
10	5	612.45	1.77	3.77	-5.24	32.01	-0.27
10	10	658.47	4.32	11.87	-4.19	65.79	-0.26
10	15	725.5	8.34	24.44	-2.5	101.97	-0.05
15	0	607.27	1.09	1.07	-10.07	0	0
15	5	625.75	1.88	3.79	-9.35	32.47	-0.47
15	10	668.91	4.22	11.75	-7.65	65.99	-0.62
15	15	726.47	7.87	23.68	-4.	101.31	-0.23

Table 5.2 (continued)

(b) $\rho_1 = 0.05$, $\rho_2 = 0.2$, $\varepsilon = 0.1$, $\kappa = 1$

ϕ	θ	T_{11}	T_{22}	T_{33}	T_{12}	T_{13}	T_{23}
0	0	228.45	0.52	0.61	0	0	0
0	5	241.45	0.9	1.66	0	12.4	0
0	10	264.17	2.01	4.68	0	25.62	0
0	15	291.39	3.73	9.34	0	39.89	0
5	0	230.72	0.54	0.62	-1.07	0	0
5	5	242.84	0.9	1.67	-0.97	12.44	-0.05
5	10	264.75	2.	4.67	-0.74	25.63	-0.06
5	15	291.74	3.7	9.3	-0.34	39.83	-0.01
10	0	236.25	0.57	0.66	-2.29	0	0
10	5	246.19	0.92	1.68	-2.04	12.51	-0.11
10	10	266.09	1.97	4.64	-1.57	25.62	-0.14
10	15	292.59	3.6	9.18	-0.73	39.62	-0.04
15	0	242.9	0.62	0.71	-3.49	0	0
15	5	250.97	0.95	1.71	-3.23	12.53	-0.17
15	10	268.94	1.93	4.57	-2.50	25.51	-0.22
15	15	294.08	3.46	8.94	-1.21	39.2	-0.09

Table 5.2 (continued)

(c) $\rho_1 = 0.05$, $\rho_2 = 0.2$, $\varepsilon = 0.01$, $\kappa = 1$

ϕ	θ	T_{11}	T_{22}	T_{33}	T_{12}	T_{13}	T_{23}
0	0	2510.15	0.57	0.75	0	0	0
0	5	2587.02	4.23	11.54	0	135.	0
0	10	2740.71	14.75	42.66	0	275.08	0
0	15	2987.12	30.86	90.41	0	421.07	0
5	0	2519.89	0.72	0.81	-15.39	0	0
5	5	2592.82	4.32	11.52	-14.74	134.76	-0.76
5	10	2745.17	14.71	42.39	-12.14	274.3	-1.18
5	15	2989.86	30.64	89.77	- 7.37	419.7	-0.97
10	0	2545.33	1.14	0.98	-30.74	0	0
10	5	2609.93	4.61	11.45	-29.29	133.95	-1.5
10	10	2758.45	14.61	41.6	-24.08	272.14	-2.33
10	15	2998.03	29.99	87.8	-14.6	415.73	-1.93
15	0	2581.12	1.8	1.24	-45.66	0	0
15	5	2637.65	5.04	11.29	-43.34	132.39	-2.17
15	10	2780.19	14.42	40.26	-35.54	268.3	-3.38
15	15	3011.38	28.96	84.69	-21.52	408.9	-2.81

Table 5.2 (continued)

(d) $\rho_1 = \rho_2 = 0.25$, $\varepsilon = 0.02$, $\kappa = 1$

θ	T_{11}	T_{22}	T_{33}	T_{12}	T_{13}	T_{23}
0	259.92	0.28	0.37	0	0	0
5	263.06	0.39	0.78	0	8.43	0
10	272.34	0.79	1.97	0	16.92	0
15	287.58	1.41	3.79	0	25.42	0

SECTION 6

APPLICATION EXAMPLES

Two hypothetical examples will show the applicability of the results developed in Section 5. The examples focus on the estimation of the concentration variances.

The Continuous Concentration Input

If solute mass is injected at a constant rate at the origin (x=y=z=0) in a three-dimensional aquifer with constant mean groundwater flow velocity, the resulting steady mean concentration distribution is approximated by the following form when x>> y,z:

$$\bar{c}(\underline{x}) = \frac{m}{4\pi n\sqrt{A_{22}A_{33}}\,xV} \exp-\left[\frac{y^2}{4A_{22}x} + \frac{z^2}{4A_{33}x}\right] \tag{6.1}$$

where A_{22}, A_{33} = lateral macrodispersivities along y, z
n = porosity
m = rate of mass injection
V = mean pore velocity (assumed along x) = q/n
$\underline{x}$ = (x,y,z) location vector

The components of the gradient of the concentration are given from,

$$\begin{aligned}
\frac{\partial \bar{c}}{\partial x} &= \bar{c}\,\frac{1}{x}\left[-1 + \left(\frac{y^2}{4A_{22}} + \frac{z^2}{4A_{33}}\right)\frac{1}{x}\right] \\
\frac{\partial \bar{c}}{\partial y} &= \bar{c}\,\frac{-y}{2A_{22}x} \\
\frac{\partial \bar{c}}{\partial z} &= \bar{c}\,\frac{-z}{2A_{33}x}
\end{aligned} \tag{6.2}$$

The concentration variance is then given from the form in eq. (5.33c),

$$\sigma_c^2 = \sigma_f^2 \ell_3^2\, T_{ij}\,\frac{\partial \bar{c}}{\partial x_i}\,\frac{\partial \bar{c}}{\partial x_j} \tag{6.3}$$

where the T_{ij}'s will be computed from the approximate analytical expressions in Table 5.1. The following parameters are used [$x_1=x_2$, $x_2=y$, $x_3=z$],

A_{11} = 1.0 m.
A_{22} = A_{33} = 0.01 m.
α = 0.01 m.
$\ell_1=\ell_2=\ell_3$ = 1 m.
σ_f^2 = 1

The concentration is normalized by the quantity $c_s = m/[nA_{22}A_{33}V]$.

Figure 6.1 shows a cross-section of the plume at x=50 m. and z=0 m. plotting the mean concentration plus and minus a standard deviation. It is a

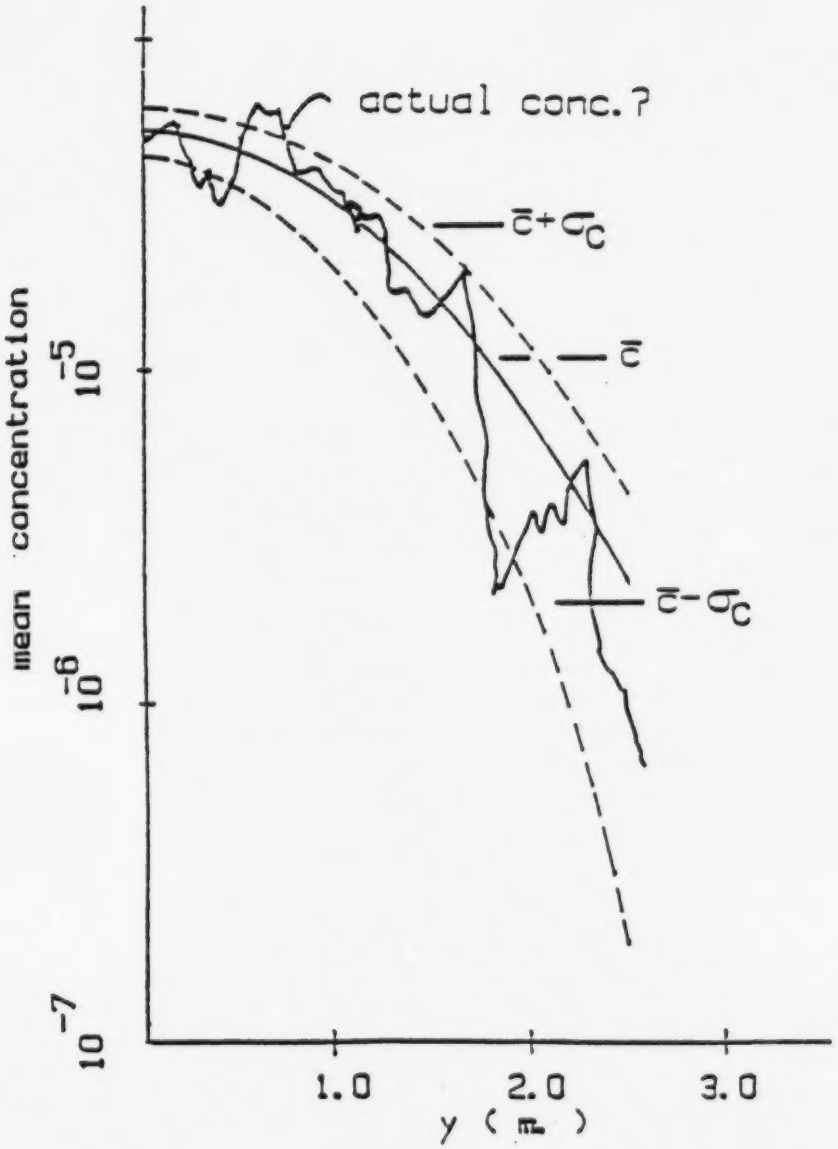

Figure 6.1 Normalized mean concentration and standard deviation at x = 50 m, z = 0 m

logarithmic plot which enables one to observe the increase of the coefficient of variation at the tails of the plume. The fluctuating line is a sketch to illustrate a possible concentration realization. At locations y=z=0 m. due to symmetry the gradients $(\partial\bar{c}/\partial y)$, $(\partial\bar{c}/\partial z) = 0$; however, $(\partial\bar{c}/\partial\bar{x}) \neq 0$, and it is responsible for the approximately 0.25 coefficient of variation observed at this location. Figure 6.2 shows the isoconcentration lines and the standard deviations in a horizontal plane located at z=0 m. This form of plot allows one to visualize how much the contoured configuration of a plume may vary. Figure 6.3 shows the correlation function of the concentration for points located at the longitudinal axis of symmetry of the plume. Along the flow directions extremely high correlation scales are observed.

Along the center line of the plume, the coefficient of variation can be written as

$$\frac{\sigma_c}{\bar{c}} = \frac{\sigma_f \ell}{\gamma x} \left(\frac{2\ell}{3\alpha}\right)^{0.5} \tag{6.4}$$

and for the parameters chosen with the isotropic relationship $\gamma=\exp(\sigma_f^2/6)$

$$\frac{\sigma_c}{\bar{c}} = \frac{7}{x} \quad , \text{ x in m.} \tag{6.5}$$

Thus for distances higher than 100 correlation scales the coefficient of variation will be a few percent. Figure 6.1 shows that this should be viewed as the minimum concentration variability at a given longitudinal distance from the source. The implied near source behavior with very large coefficient of variation must be viewed as only a qualitative feature since the perturbation approach used to develop the coefficients T_{ij} (Section 5) was based on the assumption that the concentration variations were relatively small.

The Pulse Injection

As in the previous case, the form of the mean equation is assumed known, with effective parameters resulting from the aquifer heterogeneity. The mean concentration distribution for an instantaneous point injection at the origin is

$$\bar{c}(\underline{x},t) = \frac{M}{n(4\pi tV)^{3/2}(A_{11}A_{22}A_{33})^{1/2}} \exp-\left[\frac{(x-Vt)^2}{4A_{11}Vt} + \frac{y^2}{4A_{22}Vt} + \frac{z^2}{4A_{33}Vt}\right] \tag{6.6}$$

where M = mass injected

A_{11}, A_{22}, A_{33} = macrodispersivities along x, y, z axes respectively

V = mean pore velocity

$\underline{x} = (x,y,z) = (x_1,x_2,x_3)$

Denote $Vt = x_c$, the location of the center of mass of the plume at any time. The concentration gradients are given from

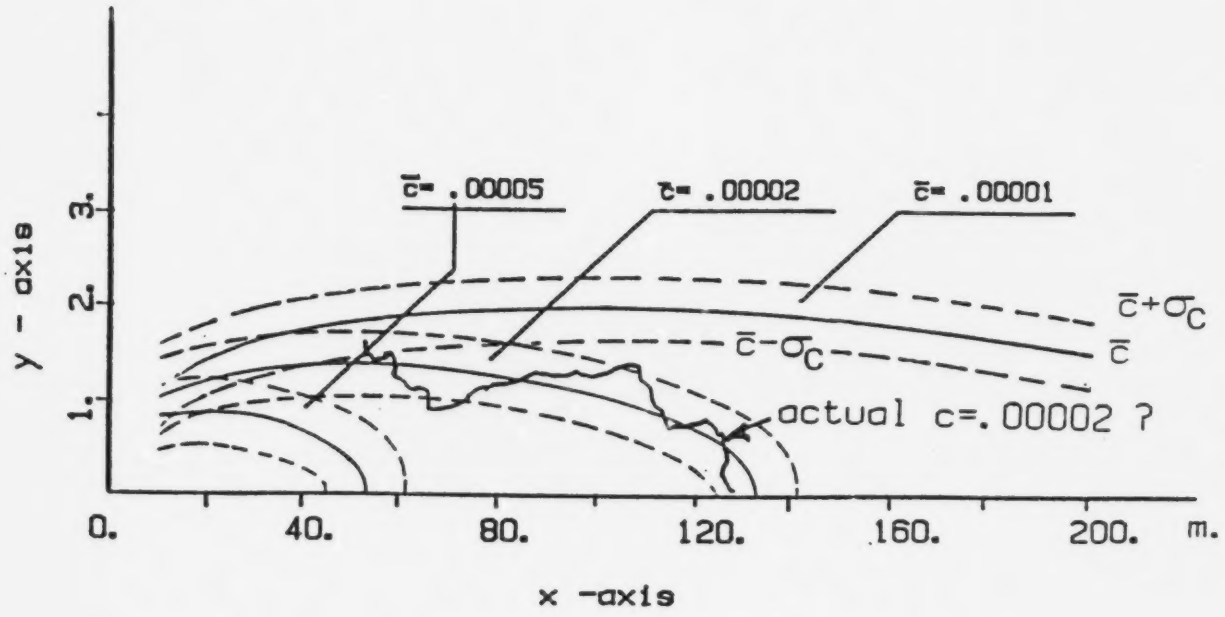

Figure 6.2 Isoconcentration lines and standard deviations at z = 0 m

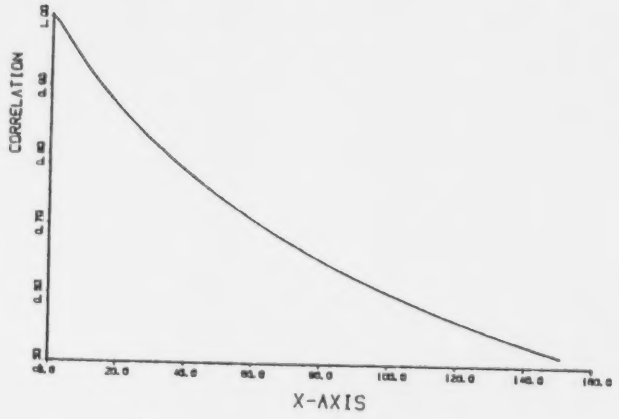

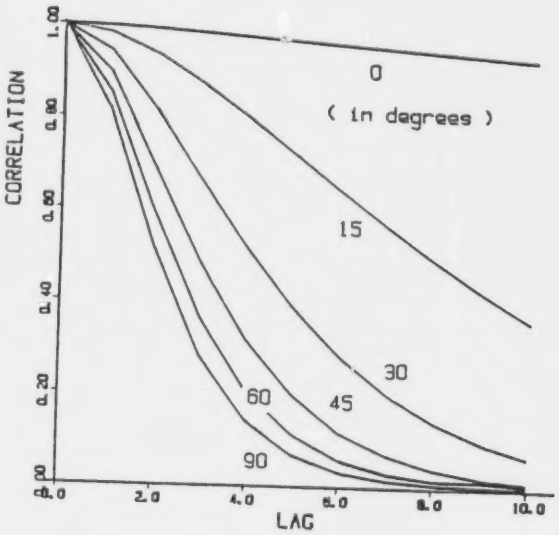

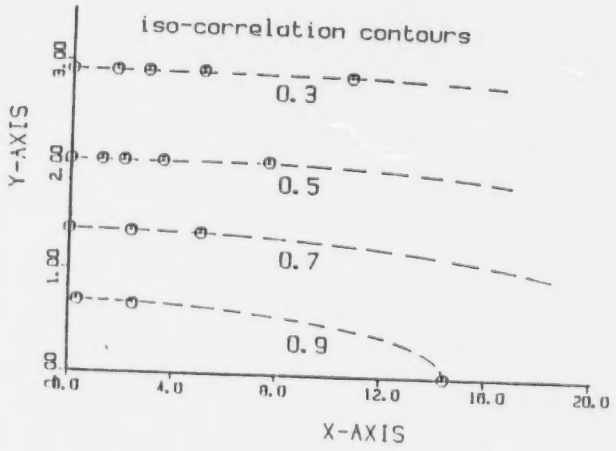

Figure 6.3 Correlation function for a point at y = z = 0
(a) Correlation along x
(b) Correlation along lines in the (x,y) plane at various angles with x
(c) Lag-correlation contours in the (x,y) plane

$$\frac{\partial \bar{c}}{\partial x} = \bar{c}\,\frac{x-x_c}{2A_{11}x_c}$$

$$\frac{\partial \bar{c}}{\partial y} = \bar{c}\,\frac{y}{2A_{22}x_c} \qquad (6.7)$$

$$\frac{\partial \bar{c}}{\partial z} = \bar{c}\,\frac{z}{2A_{33}x_c}$$

The concentration variances were calculated using the numerical evaluation for an anisotropic heterogeneous aquifer with parameters,

$$\ell_1 = 3m\ ,\ \ell_2 = 1m\ ,\ \ell_3 = 0.15m\ ,\ \sigma_f^2 = 0.5\ ,\ \alpha = 0.01m$$

The macrodispersivities are

$$A_{11} = 0.3m\ ,\ A_{22} = A_{33} = 0.01m$$

and the values for T_{11}, T_{22}, and T_{33} are taken from Table 7.4.

The concentration is normalized by

$$c_p = M/[(4\pi)^3 n A_{11}A_{22}A_{33}]$$

Figure 6.4 and 6.5 show the mean plus and minus, a standard deviation for a longitudinal and vertical section respectively along the axes of symmetry of the plume. Note that at the maximum concentration $\sigma_c = 0$. This is because the concentration gradient is zero at this location. The analysis was developed assuming that the concentration gradient is constant. This is clearly not true around the concentration peak, so it is not expected that the results hold at this region.

Figure (6.6) shows the concentration variance in a vertical section 5 m. away from the concentration peak in the x direction and 1 m. in the lateral. The minimum coefficient of variation (at the peak) is not zero anymore.

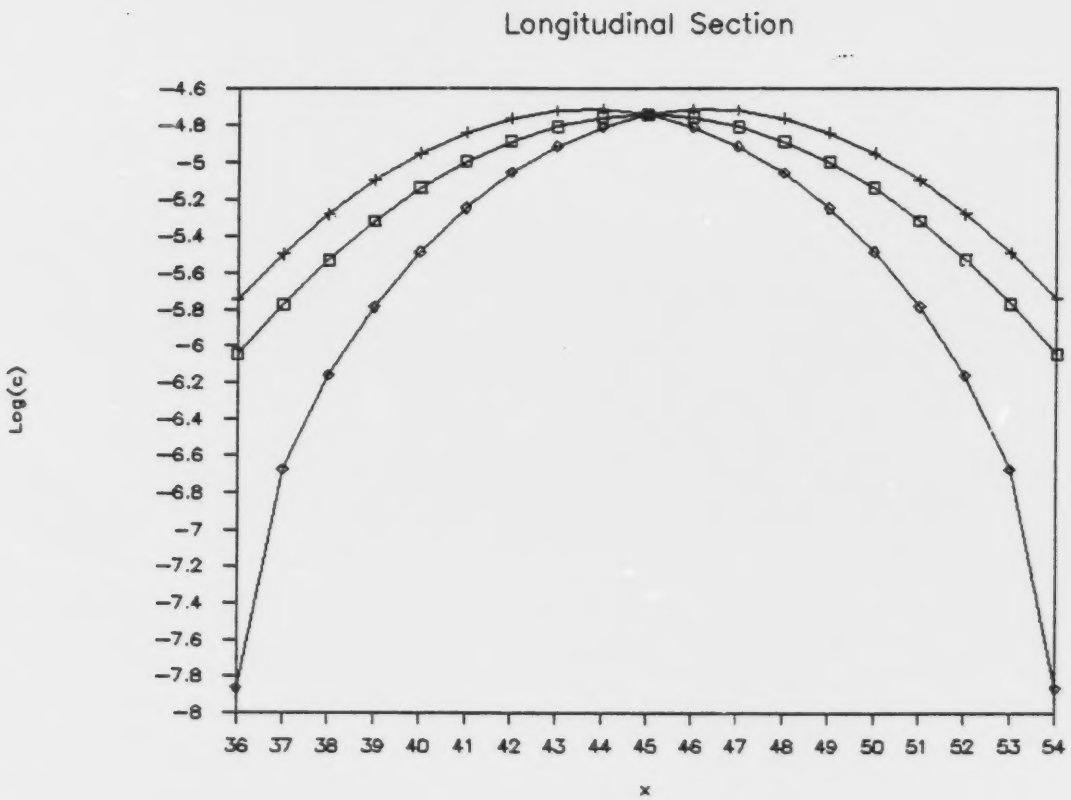

Figure 6.4 Normalized concentration and one standard deviation interval along a longitudinal section (line coordinates y = z = 0)

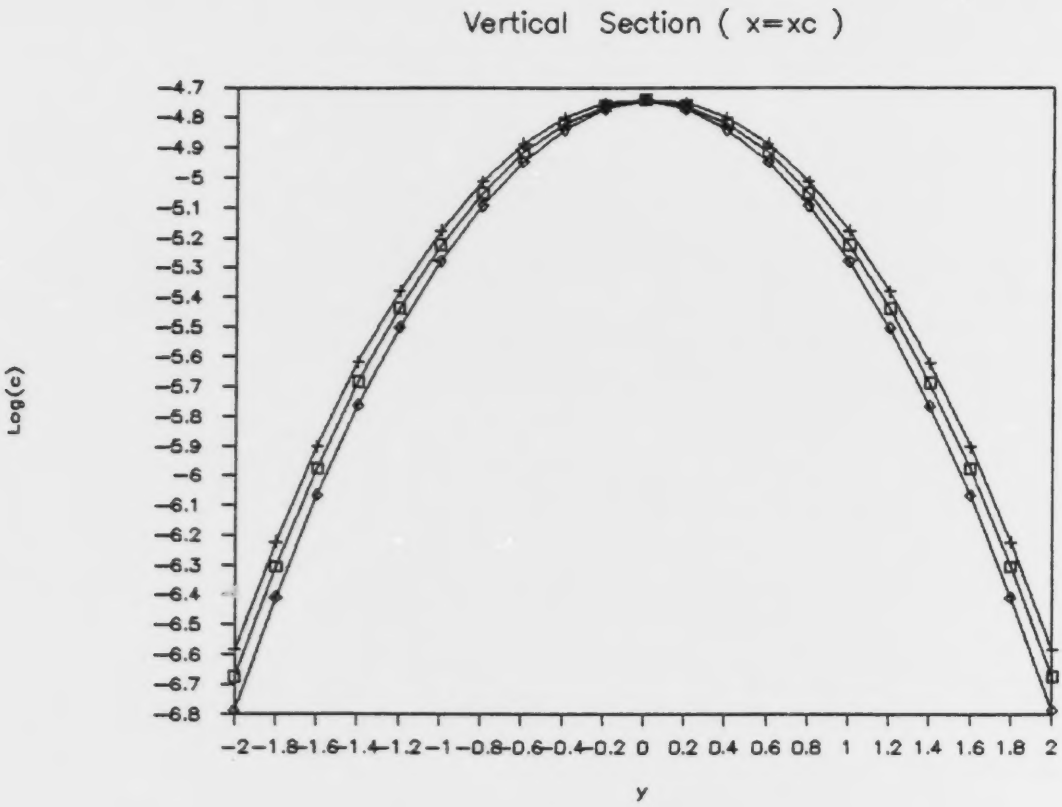

Figure 6.5 Normalized concentration and one standard deviation interval along a vertical section (line coordinates $x = x_c$ - center of mass of plume, $y = 0$)

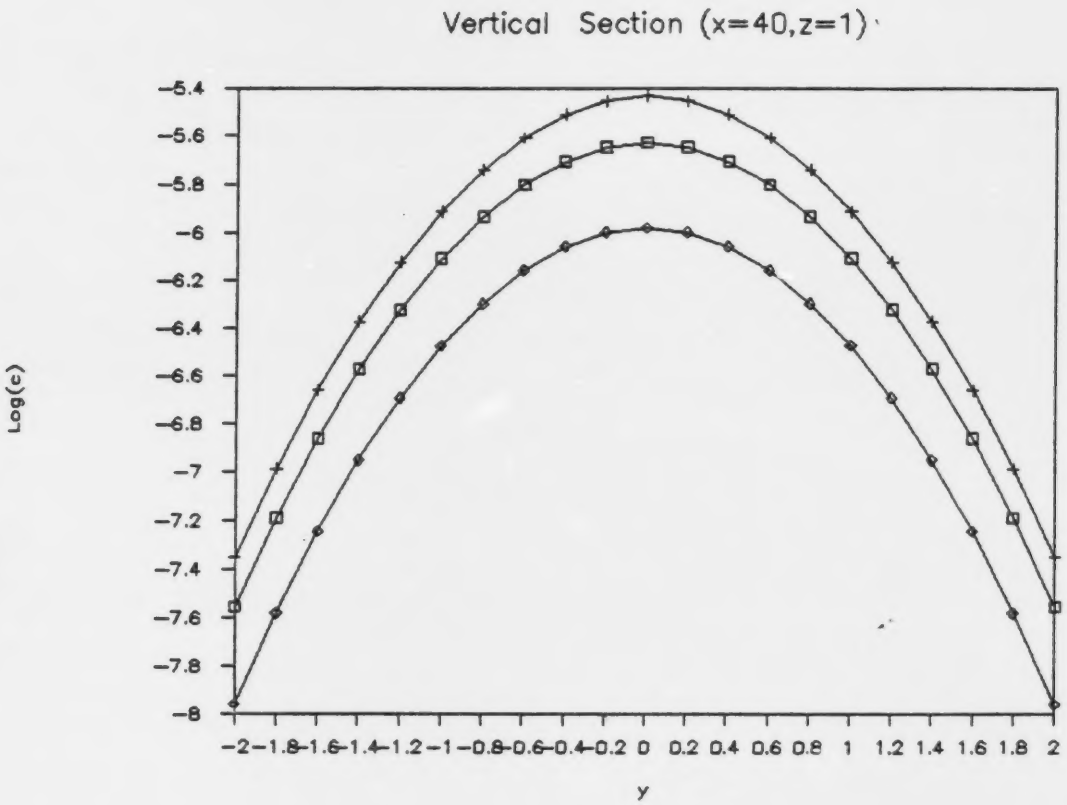

Figure 6.6 Normalized concentration and two standard deviation interval along another vertical section (line coordinates $x = x_c - 5$ m, $z = 1$ m)

SECTION 7

FIELD DATA ANALYSIS: THE CFB BORDEN SITE

The results from the stochastic theory will be applied in the controlled field scale experiment at Canadian Forces Base, Borden, Ontario. This is a preliminary application since the available data represent two sampling dates only, namely, October 25, 1982 and November 28, 1983 (Freyberg, 1984, personal communication). The tracer site is located in a sand quarry down-gradient from an abandoned landfill (Sudicky, 1985). The tracer injection occured on August 23, 1982, and comprised of 10.7 kg of chloride solution injected at an average concentration of 892 mg/l from a zone between 2.0 m and 3.6 m below ground surface (Figure 7.1). Table 7.1 summarizes part of the existing information about the site.

The stochastic theory can be applied to produce estimates of:
(i) effective hydraulic conductivities;
(ii) macrodispersivities; and
(iii) variance and covariance of the concentration deviations.

The input data set required must include:
(a) the mean log-hydraulic conductivity, F, and its standard deviation, σ_f.
(b) correlation scales of the log-hydraulic conductivity field, ℓnK;
(c) direction of its principal axes; and
(d) local dispersivities.

Prior to analyzing the data a preliminary investigation of their information content is required.

Table 7.1

EXISTING INFORMATION ON THE BORDEN SITE PARAMETERS

$\sigma_f^2 \simeq 0.3 - 0.5$

$\ell_1 \simeq 2 - 5$ m; $\ell_2 \simeq 2 - 5$ m; $\ell_3 \simeq 0.10$ m

$A_{11} \simeq 0.30$ m; $A_{22} \simeq 0.034$ m; $A_{33} - << 1^*$ m

$\ell nK = F = K_G = 7.15 \times 10^{-3}$ cm/s

$\psi = -5°$

* Approximately zero was assumed by Sudicky (1985) without actual analysis of the vertical spreading; quantitative analysis of data from an earlier test at the Borden site (Gelhar et al. 1985) shows that vertical spreading is greater than molecular diffusion (A_{33} = 1 to 2 mm).

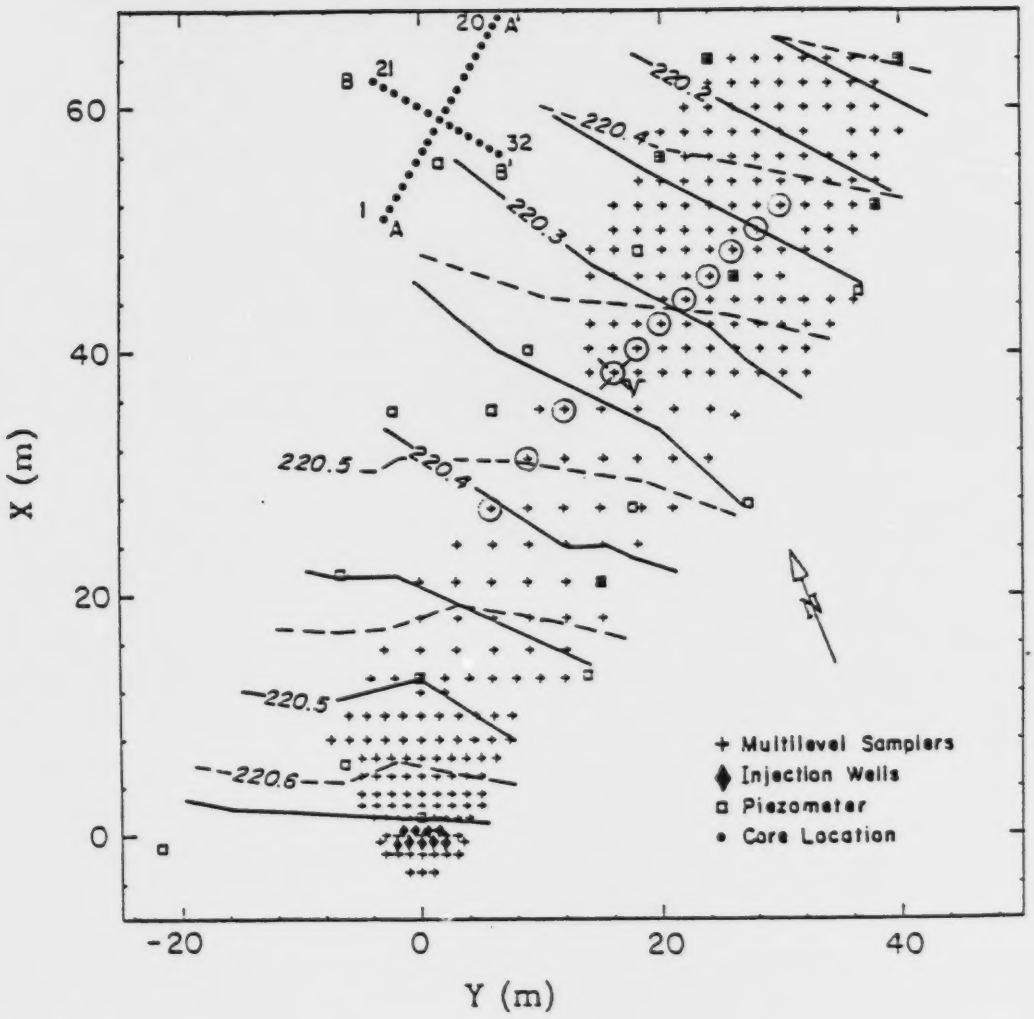

Figure 7.1 Instrumentation, location of cores and hydraulic head distribution on August 10, 1984 (solid line) and November 15, 1984 (dashed line) at the tracer-test site (after Sudicky, 1985b). The circled samplers show the locations of the wells used in this analysis. V denotes the well used for the vertical section analysis.

MAX 319
MIN 0

CONTOURS

1	2.5
2	10
3	60
4	100
5	200
6	280

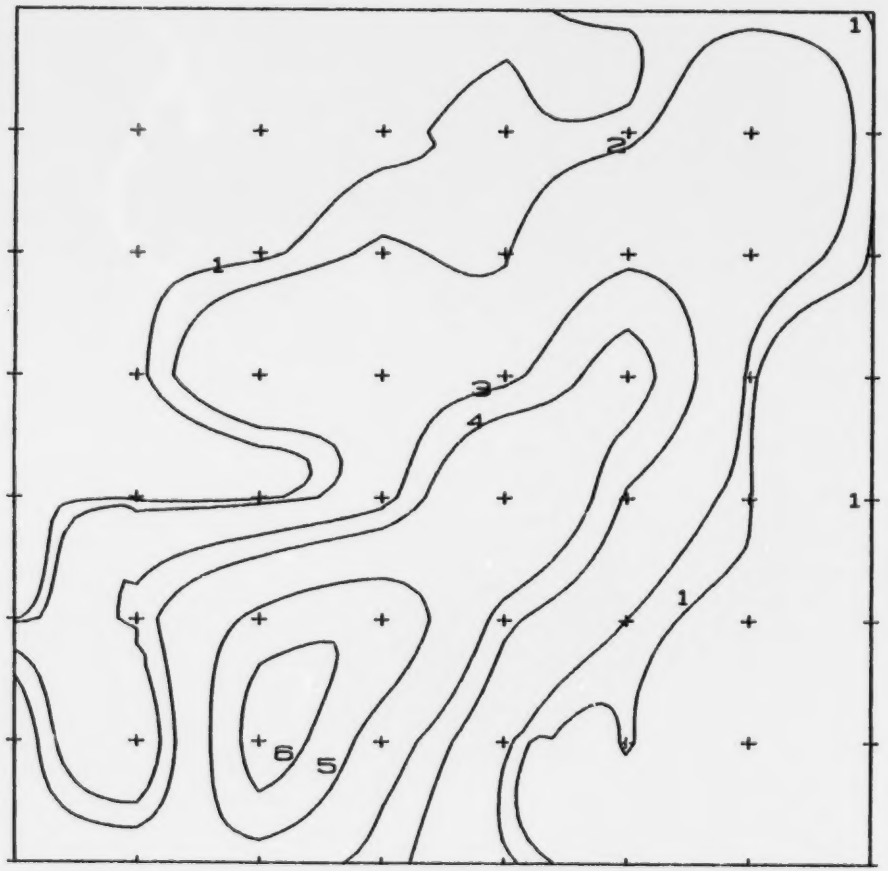

Figure 7.2 Isoconcentration contours at depth z = -5.31m, from the Borden site data (original data from D. Freyberg, personal communication)

Averaging Effects in Sampling

The theory developed assumes point values of all the processes, where as it is traditional in groundwater studies, a "point" is defined in a Representative Elementary Volume (REV) sense, or, at the same scale that the convective-dispersive equation for the mass transport holds. However, the data collected are directly affected by the resolution of the sampling method. For the hydraulic conductivity data at the Borden site, the values were determined from cores 0.05 m. in height and 0.05 m. in diameter. Even at this scale the sampling method introduces an averaging of the true process which results in reduced variances and increased correlation scales (Vanmarke, 1983). A similar analysis was performed at the hydrothermal test site Aefligen, in Switzerland (Hufschmied, 1985). The so-called "variance function", $\chi(a)$, describes the variance reduction in terms of the correlation scale. For a one-dimensional case the measured process is given by,

$$\bar{f}(\bar{z}) = \frac{1}{\Delta z} \int_{\bar{z} - \Delta z/2}^{\bar{z} + \Delta z/2} f(z)\, dz \tag{7.1}$$

and its variance is:

$$\sigma_{\bar{f}}^2 = \sigma_f^2 \; \chi(\Delta z)$$

$$\chi(\Delta z) = \frac{2}{\Delta z} \int_0^{\Delta z} \left(1 - \frac{x}{\Delta z}\right) \rho_{ff}(x)\, dx \tag{7.2}$$

With the exponential model proposed by Sudicky (1985a) for the vertical correlation and with $\ell = 0.1$ m, $\Delta z = 0.05$ m (the height of the sample), $\chi(0.05) \simeq 0.85$. Therefore, the variance of the point values of the log-hydraulic conductivity should be increased by 15%.

The Spectrum of lnK

The estimation of the concentration variance requires a spectrum that enforces stationarity on the underlying process. Such a spectrum has a zero integral scale in three dimensions (Section 5). The exponential covariance function does not possess this property, and this is the reason that a "hole-type" covariance function was used in the theoretical development. The difference between these two covariance functions (see Figure 5.3) is so small as to be practically indistinguishable in terms of statistical inference and, as will be shown in the following, the shape of the spectrum has minimal effects on the estimation of the effective hydraulic conductivities and the macrodispersivities.

The important parameter is the correlation scale which is defined by the lag corresponding to the e^{-1} level of the correlation function. In the isotropic case the correlation function used is,

$$\rho(s) = (1 - \frac{1}{3} s)\, e^{-s} , \quad s = \frac{\xi}{\ell} \tag{7.3}$$

and the e^{-1} level is given by s = 0.723,

$$\rho(0.723) = e^{-1} , \quad \xi_e = \ell(0.723) \tag{7.4}$$

Notice that the correlation scale of the above function is different than the length scale dividing the lag. The opposite holds for the exponential correlation function. It is easy to verify, since the exponential correlation function is given from

$$\rho_E (s') = e^{-s'} , \; s' = \frac{\xi}{\lambda} , \tag{7.5}$$

that

$$\rho_E(1) = e^{-1}, \; \xi_e = \lambda. \tag{7.6}$$

Consequently, the correlation scales determined by Sudicky (1985b) correspond to the λ's (in the notation used here), and the correlation scale for the hole type correlation function, which is used in this analysis, is given from,

$$\ell = \frac{\lambda}{0.723} \tag{7.7}$$

The above relationship can be expanded to the anisotropic case also, where the following will hold:

$$\ell_i = \frac{\lambda_i}{0.723} , \quad i = 1,2,3 \tag{7.8}$$

Therefore, the values given in Sudicky (1985) $\lambda_1=\lambda_2=2$ m, $\lambda_3=0.1$ m, would correspond to

$$\ell_1 = \ell_2 = 2.76 \text{ m}, \; \ell_3 = 0.14 \text{ m} \tag{7.9}$$

With these preliminary remarks, required because of the sampling technique used and the covariance model fitted, the stochastic theory can now be applied to estimate the quantities mentioned in the introduction.

Effective Hydraulic Conductivities

Gelhar and Axness (1983) have developed the general equations for the effective hydraulic conductivities in terms of the spectrum of the log-hydraulic conductivity. The analysis evolved around a linearized version of the flow equation and was heuristically generalized for the case of $\sigma_f^2 > 1$. The effective hydraulic conductivities along the principal axes of flow are given from

$$\bar{K}_{ii} = K_\ell \exp\left[\sigma_f^2 \left(\frac{1}{2} - g_{ii}\right)\right], \quad i = 1,2,3 \tag{7.10}$$

(no summation over repeated indices), where $K_\ell = \exp\left[E(\ln K)\right]$, and the g_{ij}'s can be calculated from

$$g_{ij} = \int_k \frac{k_i' k_j'}{k'^2 \sigma_f^2} S_{ff}(\underline{k}')\, d\underline{k}' \tag{7.11}$$

The primed system of axes is aligned with the principal axes of the hydraulic conductivity. Freyberg (1985) has observed an approximate 5° clockwise horizontal inclination of the principal axes of the plume with respect to the mean flow. This is an indication of horizontal anisotropy in the hydraulic conductivities, in contrast with the reported values of the correlation scale, and a counterclockwise alignment of the principal axes of the plume with respect to the mean flow, or, plume trajectory. Table 7.2 summarizes a series of calculations where the input parameters were the first seven columns, i.e. σ_f^2, ℓ_1, ℓ_2, ℓ_3, α = local dispersivity, ϕ = horizontal angle of x_1' and x, θ = vertical angle of x_1' and x (where x_1' = major principal axis of hydraulic conductivities, x = mean flow direction). In columns 8, 9, 10 the estimated values of $\bar{K}_{11}/K_\ell$, $\bar{K}_{22}/K_\ell$, and $\bar{K}_{33}/K_\ell$ do not show significant variations and compare quite well with the values of 1.18 and 0.85 reported by Sudicky (1985). The high values correspond to variances not considered by Sudicky (1985), i.e., $\sigma_f^2 = 1.5$, and $\sigma_f^2 = 1.0$. It can also be observed that the anisotropy in the effective hydraulic conductivities both in the horizontal as well as the vertical plane is very mild even for aspect ratios of the original field of $\ell_1/\ell_3 = 5/0.5 = 10$.

Note that the coefficients g_{ij}, Eq. (7.11), needed for the estimation of the effective hydraulic conductivities in Table 7.2 were evaluated numerically for the hole type covariances function, Eq. (5.32). No significant difference from the values shown in Gelhar and Axness (1983) was observed.

Asymptotic Macroscopic Dispersion

Gelhar and Axness (1983) have developed expressions for the asymptotic macrodispersivities for the general case of arbitrary orientation of stratification. These expressions are quite complicated to be evaluated analytically except for the case of:

- hydraulic conductivity isotropy in the horizontal or vertical plane,
- negligible local dispersivity,
- exponential log-hydraulic conductivity covariance, where approximate solutions can be obtained.

Table 7.2

EFFECT OF THE INPUT PARAMETERS ON EFFECTIVE CONDUCTIVITIES

σ_f^2	ℓ_1 (m.)	ℓ_2 (m.)	ℓ_3 (m.)	α (m.)	ϕ	θ_{33}	$\bar{K}_{11}/K_\ell$	$\bar{K}_{22}/K_\ell$	$\bar{K}_{33}/K_\ell$
0.4	5	0.5	0.1	0.01	0	5	1.22	1.14	0.87
1	5	0.5	0.1	0.01	5	5	1.64	1.4	0.72
1	2	0.5	0.1	0.01	10	0	1.61	1.41	0.72
1	2	2	0.1	0.01	5	10	1.59	1.59	0.65
0.5	2	0.5	0.1	0.01	0	0	1.27	1.18	0.85
0.5	2	0.5	0.1	0.01	5	0	1.27	1.18	0.85
0.5	2	0.5	0.1	0.01	0	5	1.27	1.18	0.85
0.5	2	0.5	0.1	0.01	0	10	1.27	1.18	0.85
1.5	2.5	0.5	0.1	0.01	20	0	2.07	1.66	0.61
1.5	2.5	0.5	0.1	0.001	20	0	2.07	1.66	0.61
1.5	5	0.5	0.1	0.01	20	0	2.1	1.65	0.61
1.5	5	0.5	0.1	0.001	20	0	2.1	1.65	0.61
0.5	2	0.5	0.1	0.01	20	0	1.27	1.18	0.85
0.5	2	0.5	0.1	0.001	20	0	1.27	1.18	0.85
0.5	2	0.5	0.1	0.01	45	0	1.27	1.18	0.85
0.5	2	0.5	0.1	0.001	30	0	1.27	1.18	0.85
0.5	5	0.5	0.1	0.001	25	0	1.28	1.18	0.85
1	2.5	0.5	0.1	0.001	25	0	1.62	1.4	0.72
1	5	0.5	0.1	0.001	20	0	1.64	1.39	0.72
1	2	1	0.1	0.001	45	0	1.6	1.52	0.67
1	2	1	0.1	0.001	20	0	1.6	1.52	0.67

Using the same set of input parameters as in Table 7.2, a numerical evaluation of the asymptotic macrodispersivities was performed assuming the covariance function of the ℓnK is the hole type, and results are shown on Table 7.3. Recall from Table 7.1 that the estimated longitudinal dispersivity for the side is 30 cm., and that there is a clockwise rotation of the plume with respect to the mean flow. These two characteristics will be the calibration targets for the selection of the correlation scales.

Table 7.3 shows the different combinations of input parameters that produce a longitudinal macrodispersivity of the same order of magnitude as the observed ones. It is more difficult to match the 5° clockwise rotation; Note that most of the input combinations produce angles between 1° and 3°. The predicted asymptotic lateral macrodispersivities are smaller by 2 to 3 orders of magnitude. In that case the local dispersivity, which is additive, will be the prevailing value. Gelhar (1986) in an analysis of the developing macrodispersivities has shown that the lateral dispersivities attain a maximum value and then drop to their asymptotic magnitude. Dagan (1984) derived a similar result following another approach. A plausible speculation, therefore, is that the measured field value for A_{22} of about 3 cm, 38 m downstream from the injection point, is still influenced by the developing transverse dispersion process and, hence, is much larger than its asymptotic value, which is the one that the spectral theory estimates.

With the information presented in Tables 7.1, 7.2 and 7.3, it is considered that a representative set of values for the parameters of the CFB Borden is as in Table 7.4. The correlation scales have been adjusted for the hole type covariance. The variance is slightly increased to account for sampling averaging, and anisotropic behavior is included to produce the longitudinal macrodispersivity.

Variance of the Concentration Field

The theoretical analysis of Section 5 has developed the following form for the concentration covariance,

$$R_{cc}(\underline{\xi}) = \sigma_f^2 \ell_3^2 T_{ij}(\rho_1,\rho_2,\varepsilon,\kappa,\phi,\theta;\underline{\xi}) G_i G_j \qquad (7.12)$$

The analysis has shown that the controlling local dispersivity is α_T ($\kappa\varepsilon = \alpha_T/\ell_3$) and that the effect of ϕ, θ is minimal. Therefore as a first approximation the variance of the concentration field will be calculated from:

$$\sigma_c^2 = \sigma_f^2 \ell_3^2 T_{ii}(\rho_1,\rho_2,\varepsilon,1,0,0;\underline{0}) G_i G_i \qquad (7.13)$$

Table 7.3

EFFECT OF THE INPUT PARAMETERS ON MACRODISPERSIVITIES

σ_f^2	ℓ_1(m)	ℓ_2(m)	ℓ_3(m)	α(m)	ϕ	θ	A_{11}(m)	A^1_{22}	A^1_{33}	A^1_{12}	A^1_{13}	A^{*1}_{11}(m)	A^{*1}_{22}	A^{*1}_{33}	ψ	η
0.4	5	0.5	0.1	0.01	0	5	0.211	0.27	0.62	0	4.3	0.211	0.27	0.53	0	1.2
1	5	0.5	0.1	0.01	5	5	0.276	0.88	1.5	-3.1	14	0.276	0.63	0.88	-0.66	3.1
1	2	0.5	0.1	0.01	10	0	0.209	0.38	0.79	-2.4	0	0.209	3.6	0.79	-0.66	0
1	2	2	0.1	0.01	5	10	0.187	0.72	0.27	0.13	6.6	0.187	0.72	2.5	0.04	2.1
0.5	2	0.5	0.1	0.01	0	0	0.187	0.24	0.54	0	0	0.187	0.24	0.54	0	0
0.5	2	0.5	0.1	0.01	5	0	0.182	0.25	0.56	-0.56	0	0.182	0.25	0.56	0	0
0.5	2	0.5	0.1	0.01	0	5	0.167	0.32	0.77	0	2.9	0.167	0.32	0.72	0	1
0.5	2	0.5	0.1	0.01	0	10	0.126	0.48	0.12	0	5.9	0.126	0.48	0.92	0	2.7
1.5	2.5	0.5	0.1	0.01	20	0	0.175	0.91	1.1	-8.8	0	0.175	0.46	1.1	-2.9	0
1.5	2.5	0.5	0.1	0.001	20	0	0.28	1.3	0.34	-18	0	0.28	0.13	3.4	-3.8	0
1.5	5	0.5	0.1	0.01	20	0	0.185	1.1	1.1	-1.1	0	0.186	0.49	1.1	-3.4	0
1.5	5	0.5	0.1	0.001	20	0	0.31	1.9	0.33	-2.4	0	0.312	0.12	0.33	-4.4	0
0.5	2	0.5	0.1	0.01	20	0	0.14	0.31	0.76	-0.94	0	0.141	0.3	0.76	-3.8	0
0.5	2	0.5	0.1	0.001	20	0	0.224	0.12	0.19	-4	0	0.224	0.049	0.19	-1	0
0.5	2	0.5	0.1	0.01	45	0	0.099	0.27	1	-2	0	0.099	0.23	1.1	-1.2	0
0.5	2	0.5	0.1	0.001	30	0	0.181	0.16	0.21	-4.7	0	0.181	0.045	0.21	-1.5	0
0.5	5	0.5	0.1	0.001	25	0	0.236	0.24	0.2	-6.7	0	0.236	0.047	0.2	-1.6	0
1	2.5	0.5	0.1	0.001	25	0	0.264	0.79	0.31	-13	0	0.265	0.092	0.31	-2.9	0
1	5	0.5	0.1	0.001	20	0	0.316	0.84	0.3	-15	0	0.317	0.09	0.3	-2.8	0
1	2	1	0.1	0.001	45	0	0.306	0.19	0.27	-7	0	0.307	0.028	0.28	-1.3	0
1	2	1	0.1	0.001	20	0	0.383	0.11	0.24	-5.6	0	0.384	0.032	0.24	-0.85	0

[1] Units are in mm.

Table 7.4

PARAMETERS USED IN THE VARIANCE ESTIMATION

$\sigma_f^2 = 0.5$

$\ell_1 = 3.0$ m; $\ell_2 = 1.0$ m; $\ell_3 = 0.15$ m

$\alpha_T = \alpha_L = \alpha = 0.01$ m.

$T_{11} = 776.09$; $T_{22} = 1.03$; $T_{33} = 0.88$

Table 7.5

CONCENTRATION GRADIENTS IN THE VERTICAL SECTION
AT (x,y) = (38.3 m., 16.08 m.)

z (m.)	$\frac{\partial \bar{c}}{\partial x}$	$\frac{\partial \bar{c}}{\partial y}$	R*
-3.51	0.185	-.707	0.3788
-3.81	0.981	-4.14	0.579
-4.11	4.824	-5.61	0.627
-4.41	1.25	-7.77	0.641
-4.71	6.838	3.64	0.411
-5.01	6.64	-4.92	0.205
-5.31	18.21	-1.75	0.208
-5.61	1.7	1.934	0.087
-5.91	2.16	9.731	0.508
-6.21	-13.79	20.78	0.735
-6.51	-2.83	20.48	0.825

* R = coefficient of multiple determination, which is equivalent to the correlation coefficient in univariate regression analysis (Neter and Wasserman, 1974).

The values for the coefficients T_{ii} are shown in Table 7.4. They were calculated using the numerical integration programs developed under the general name TIJ_ND (where I, J = 1,2,3). The next task in the calculation of the variance of concentration is the estimation of the mean gradient. Two sections will be shown, an approximate longitudinal one and a vertical one (Figure 7.1). The approximate longitudinal section, follows a line at $z = -5.31$ m and is rotated at an angle of about 15° clockwise from the principal axes of the computed macrodispersivities. Although at this depth the choice of this direction appears justified (Figure 7.2), it was mainly necessitated by the location of the sampling wells, the objective being to use the original raw concentration data. Consequently, this direction will be considered as the x direction for the calculation of the gradients. The vertical gradient was estimated through analytical curves, of a Gaussian type, that were fitted to the data at each well along x. The gradient along y was estimated roughly from the plotted contours. For the vertical section, at $(x,y) = (38.3\text{ m}, 16.08\text{ m})$, the same Gaussian curve fitting as before was used to estimate the vertical gradient, while the gradients along x and y (Table 7.5) were estimated by fitting a regression plane through that point and its eight surrounding ones (Neter and Wasserman, 1974). These procedures are summarized in Figure 7.3.

The longitudinal section with the fitted mean is shown on Figure 7.4. The series of Figures 7.5(a) through (i) show the fitted curves in the vertical direction along the wells. Appendix D describes the parameters for each curve. Finally, Figure 7.2 is used to estimate the gradients along the y direction. All this information is collected in Table 7.6 and with the T_{ii}'s presented at Table 7.4 the variance of the concentration can easily be estimated. Figure 7.4 shows the $(\bar{c}_c + \sigma_c , \bar{c}_c - \sigma_c)$ interval which will include approximately 67% of all measurements if concentration is normally distributed.

Table 7.7 shows the data used for the vertical section at (38.3, 16.08). The gradients $\partial\bar{c}/\partial x$, $\partial\bar{c}/\partial y$ are calculated from the linear regression as described above. The $\bar{c} \pm \sigma_c$ interval is plotted in Figure 7.6. The effects of the vertical gradients on the variance are quite strong in this case. A three-order of magnitude difference in the coefficients T_{11} and T_{33} is balanced by a four-orders of magnitude difference in the squared gradients (Table 7.7). The lateral horizontal gradient has a minimal contribution. The logarithmic version of the previous plot shows the increase of the coefficient of variation at the tails (Figure 7.7).

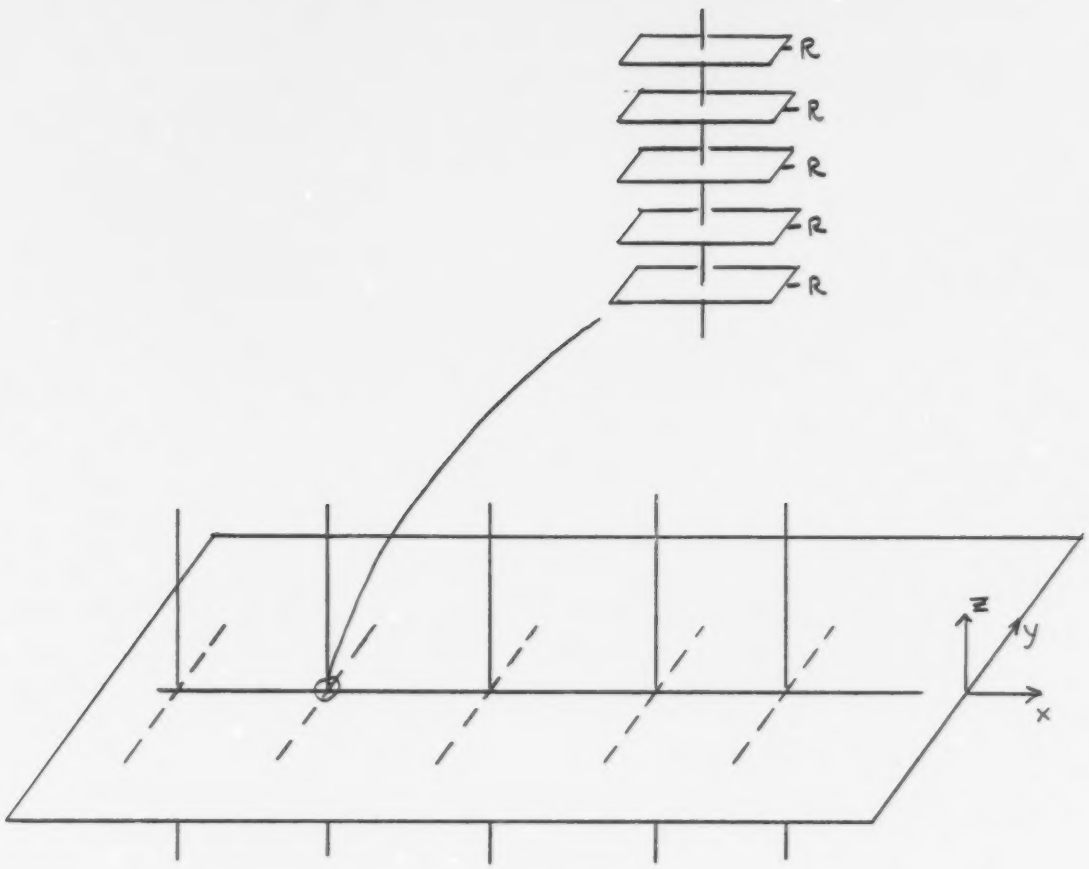

——: gradient along this direction was estimated by a continuous curve fit

---: gradient along this direction was estimated from contour plotting

-R : gradients on this plane were estimated from linear regression

Figure 7.3 Schematic presentation of the methods used for the estimation of the mean concentration

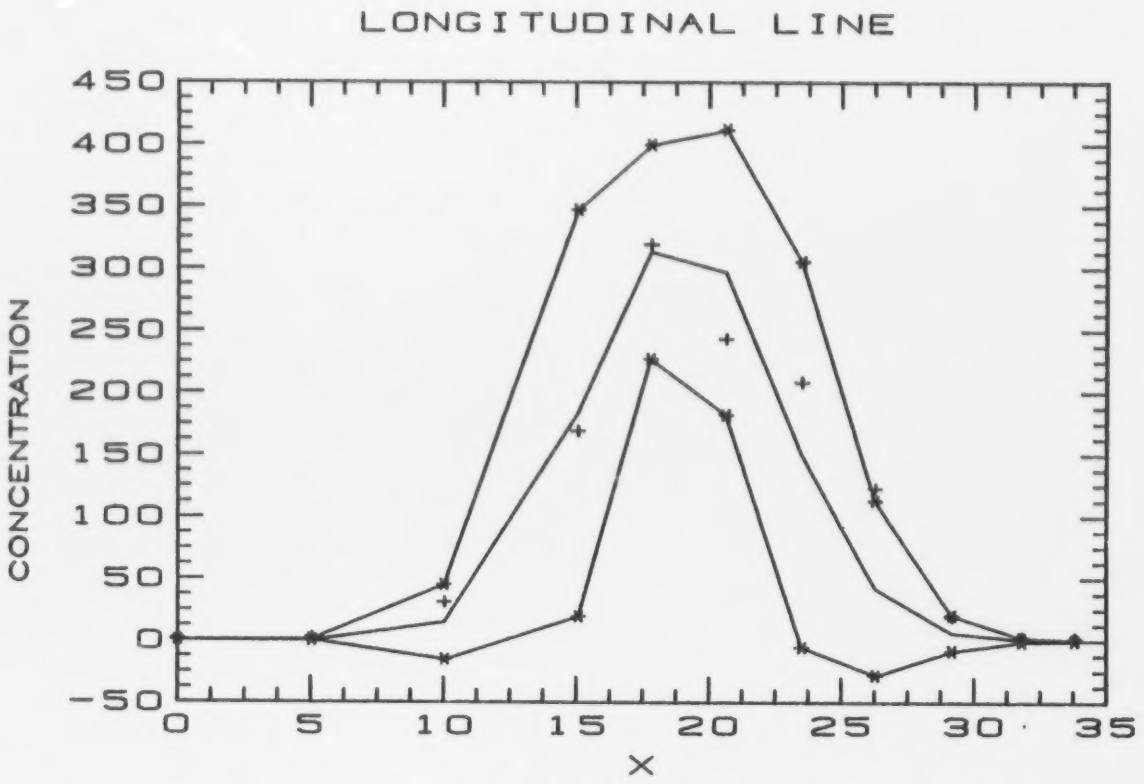

Figure 7.4 The measured, fitted and plus-minus one standard deviation concentration profiles along the longitudinal section at z = -5.31m

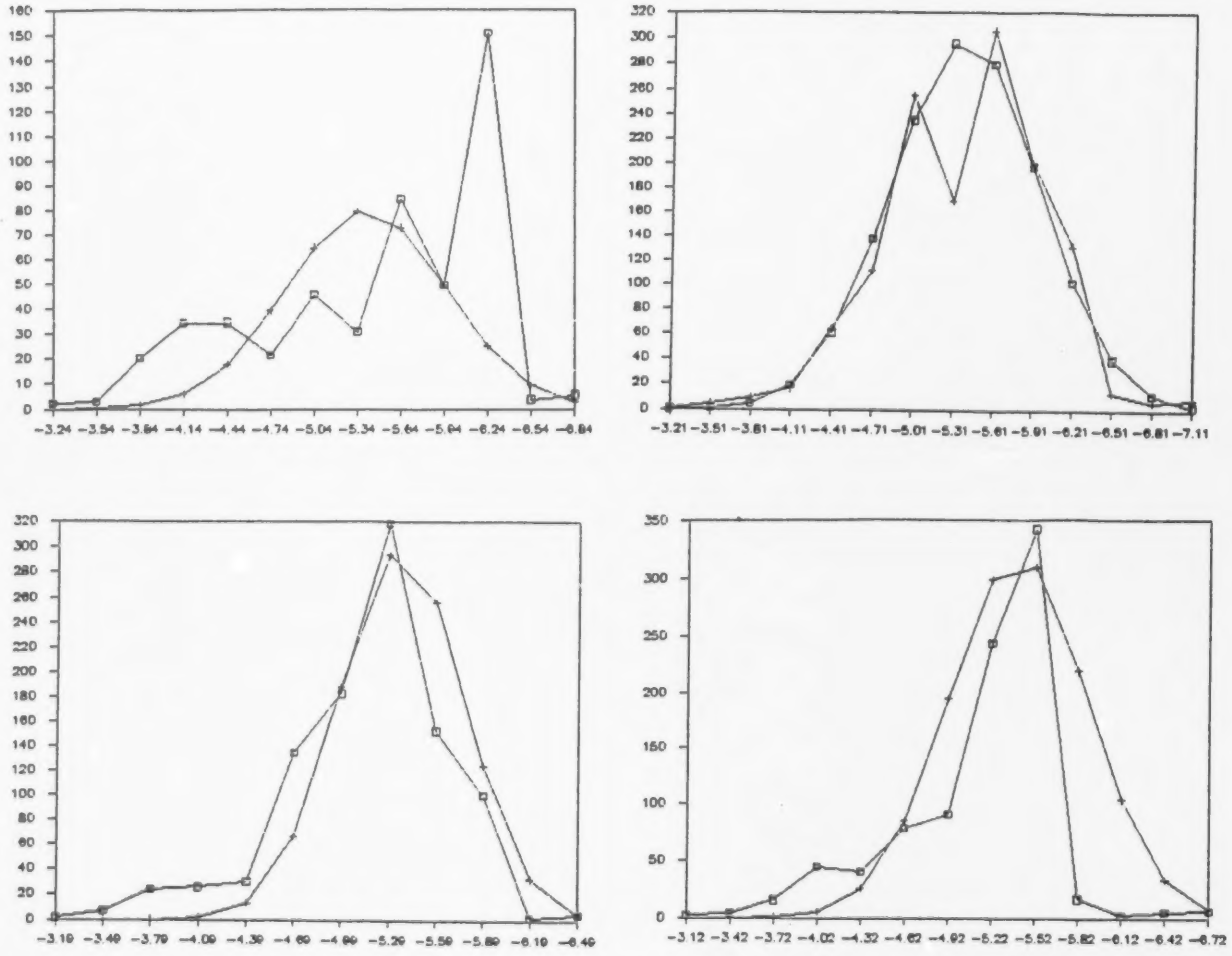

Figure 7.5 The mean concentration curves fitted at the wells on the longitudinal section (c in the vertical vs. z) +=fitted, □ =measured

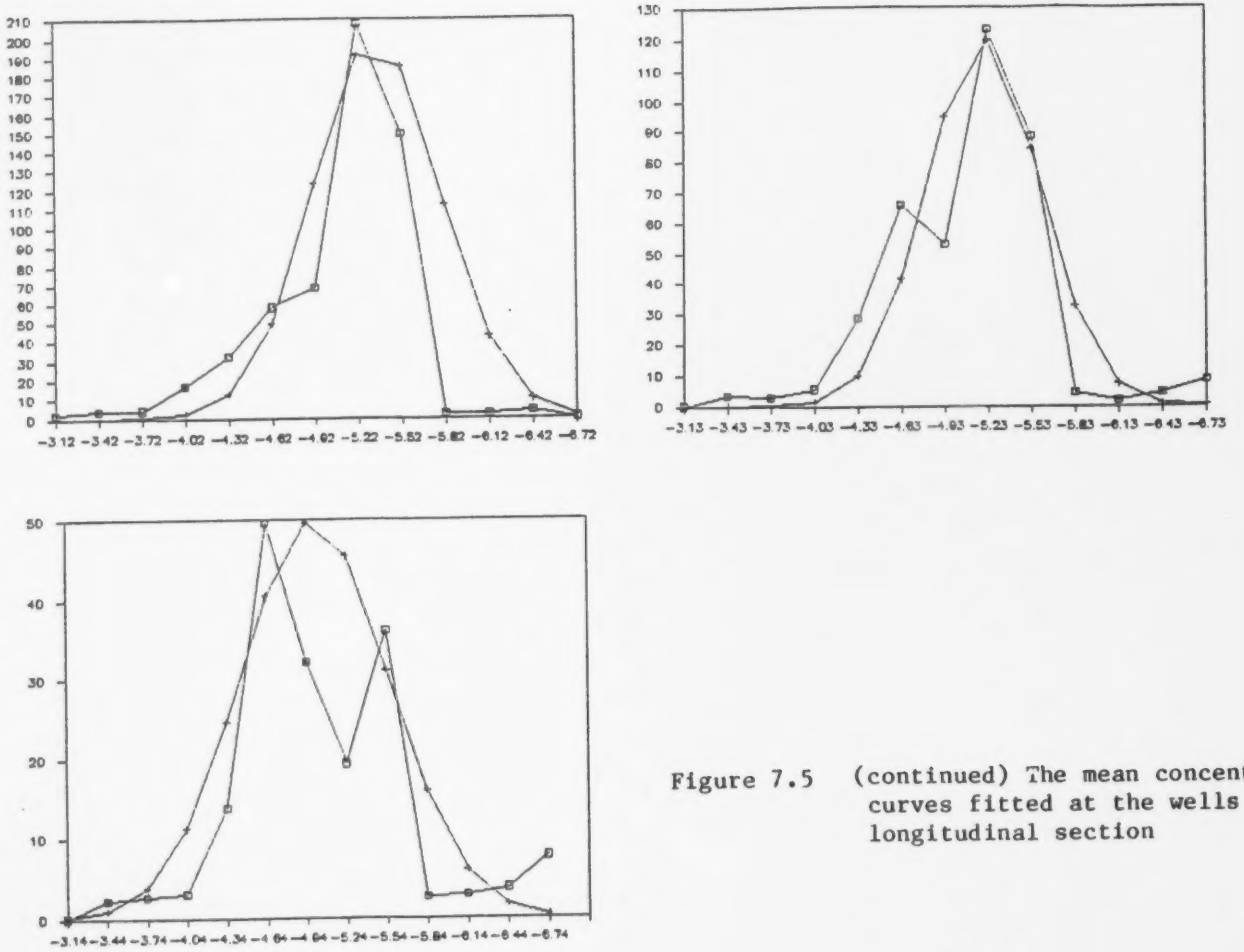

Figure 7.5 (continued) The mean concentration curves fitted at the wells on the longitudinal section

Table 7.6

ESTIMATION OF THE RANGE OF VARIATIONS
IN THE LONGITUDINAL SECTION

x (m.)	y (m.)	z (m.)	c (mg/ℓ) (meas.)	$\bar{c}$ (mg/ℓ) (fitted)	$\partial\bar{c}/\partial x$	$\partial\bar{c}/\partial y$	$\partial\bar{c}/\partial z$	σ_c	$\bar{c}+\sigma_c$	$\bar{c}-\sigma_c$
27.25	6	-5.39	1.6	2.82E-4	0.0004	0	0	0.001	0.001	-0.0094
31.3	9	-5.31	2.3	0.17	0.18	0	0	0.55	0.73	-0.38
35.3	12	-5.34	31.1	14.76	10.23	0	15.57	30.29	45.06	-15.5
38.3	16.08	-5.31	169	183.18	55.29	0	86.96	163.62	346.80	19.55
40.3	17.94	-5.29	319	312.97	28.34	7	207.06	86.26	399.23	226.70
42.3	19.95	-5.22	243	296.61	-38.11	0	233.59	115.00	411.62	181.61
44.3	22	-5.22	208	149.67	-52.36	0	129.9	155.26	304.93	-5.59
46.22	24	-5.23	123	42.20	-23.81	0	23.43	70.39	112.59	-28.19
48.35	25.95	-5.24	19.3	5.98	-4.71	9.3	35.65	14.40	20.38	-8.42
50	28	-5.3	3	0.57	-0.57	0	0	1.68	0.29	-1.11
52	30	-5.3	2	0.06	-0.07	0	0	0.23	0.29	-0.16

Table 7.7

ESTIMATION OF THE RANGE OF VARIATIONS
IN THE VERTICAL SECTION

z(m.)	c(mg/ℓ) (measured)	$\bar{c}$(mg/ℓ) (fitted)	$\partial\bar{c}/\partial z$	$\partial\bar{c}/\partial x$	$\partial\bar{c}/\partial z$	σ_c	$\bar{c} + \sigma_c$	$\bar{c} - \sigma_c$
-3.21	0.4	0.12	0.85	0	0	0.08	0.20	0.03
-3.51	4.2	0.88	5.44	0.18	-0.70	0.77	1.65	0.10
-3.81	9.2	4.84	25.1	0.98	-4.14	3.86	8.70	0.98
-4.11	16.4	19.85	83.57	4.82	-5.61	16.52	36.37	3.32
-4.41	63.6	60.6	195.82	1.25	-7.77	19.90	80.51	40.69
-4.71	112	137.9	310.64	6.83	3.64	37.00	174.95	100.93
-5.01	254	234.06	297.92	6.64	-4.92	35.62	269.68	198.43
-5.31	169	296.06	86.96	18.21	-1.75	54.50	350.56	241.55
-5.61	306	279.17	-191.33	1.7	1.93	19.74	298.91	259.42
-5.91	200	196.24	-326.63	2.16	9.73	33.23	229.47	163.00
-6.21	132	102.83	-271.85	-13.79	20.78	49.00	151.84	53.82
-6.51	13.1	40.17	-145.53	-2.83	20.48	16.90	57.076	23.26
-6.81	5.6	11.69	-53.86	0	0	5.37	17.071	6.32
-7.11	7.8	2.54	-14.17	0	0	1.41	3.95	1.12

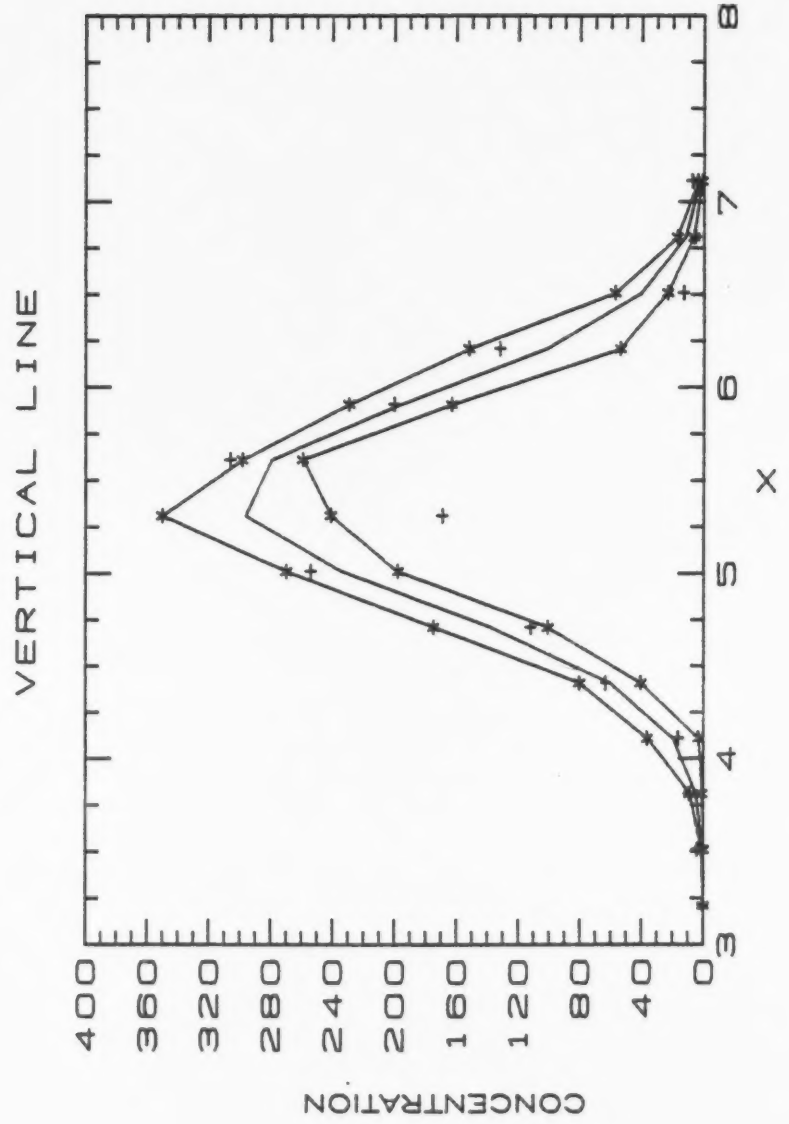

Figure 7.6 The measured, fitted and plus-minus one standard deviation concentration profiles along the vertical section at (x,y) = (38.3, 16.08)

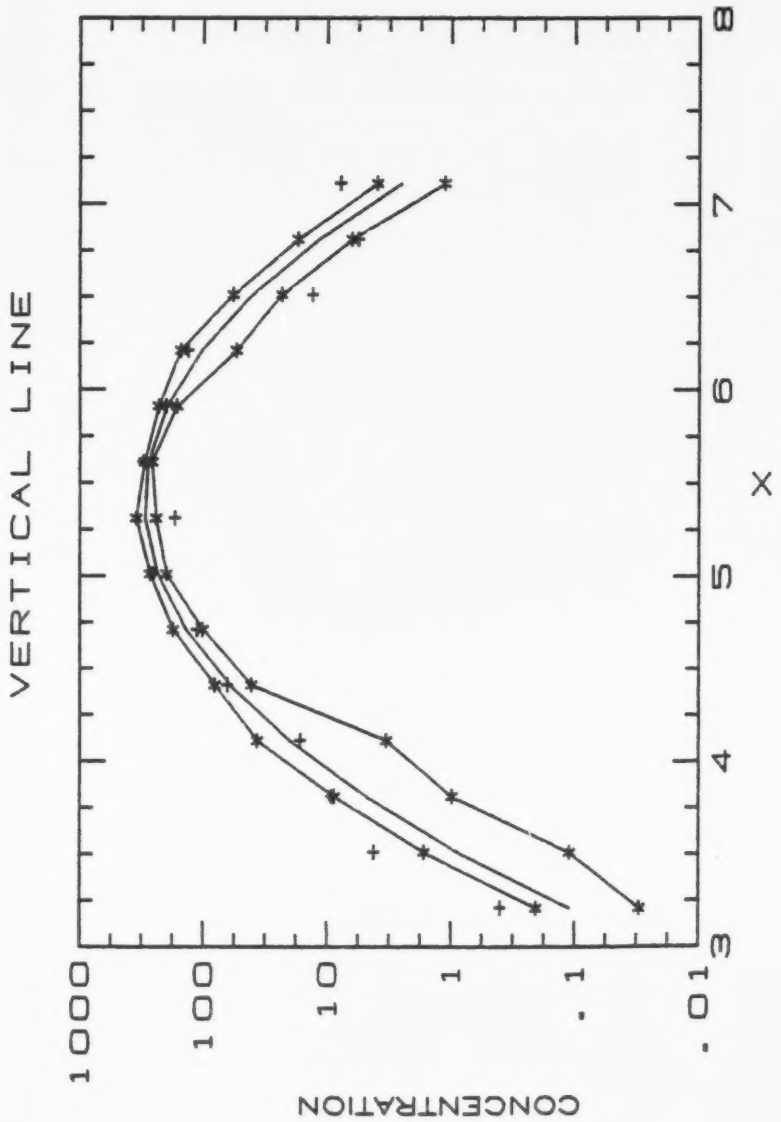

Figure 7.7 The values plotted in Fig. 5.6 in a semi-logarithmic plot

Conclusions

The analysis of the field data demonstrates the validity of the stochastic theory results for the concentration variance. The predicted concentration intervals defined by $\pm \sigma_c$ are consistent with the observed fluctuations of concentration around a smooth mean and capture most of the measured values. The effect of the longitudinal concentration gradient in the calculation of the variance is dominant except when focusing on vertical sections where the vertical concentration gradient is higher by 2 or 3 orders of magnitude.

The estimated effective hydraulic conductivities are quite close to the observed geometric mean of the measured hydraulic conductivities. The estimated longitudinal macrodispersivity is also comparable to the one estimated through the method of moments.

The analysis reveals the need for the development of a formal procedure for the estimation of the mean. Analysis of data from subsequent sampling dates is needed to show the robustness of the results.

SECTION 8

DISCUSSION OF RESULTS

A simple theoretical result was developed to quantify the concentration variability. When measurements of the concentration exist, it can be thought of as giving a measure of the range of expected variation of the concentration around a smooth mean concentration distribution. The theory is also useful as a predictive tool when the solute distribution is extrapolated for distances far downstream using a classical dispersive transport model.

The functional form of the concentration variance is easy to implement. It is a local relationship that involves the mean concentration gradient, the variance and correlation scales of the log-hydraulic conductivity field, and the local dispersivity values. The mean concentration gradient can be estimated either in a predictive context with numerical or analytical models, or through a simple curve fitting with existing plume measurements. The former approach was demonstrated in Section 6 and the later by the analysis of the Borden site data in Section 7.

The variance of the log-hydraulic conductivity can be measured in situ or, as more information for the behavior of different types of aquifer materials is accumulated, it can be estimated from information about geologically similar sites.

The local dispersivities can be also found from a laboratory test of soils from the site or estimated based on the general properties of the soil (Klotz, et al. 1980). It should be noted that the effect of the local dispersivity on the variance is significant and cannot be neglected. This behavior is in contrast to that of the macrodispersivity which is not sensitive to the value of the local dispersivity.

An important factor needed for the variance estimation is the correlation scales. Analyses such as Sudicky's (1985a,b) show ways to estimate their values in situ. It is very encouraging that the estimated correlation scales give a consistent picture for the mean plume when used to estimate the macrodispersivities and the concentration variance as a measure of the variation around the mean plume. Gelhar (1985) presents a collection of the variances and correlation scales for log-hydraulic conductivity or log-transmissivity estimated either from direct analysis of measurements or through inverse modeling procedures (Hoeksema and Kitanidis, 1985).

The predicted concentration variance is an appropriate calibration target for the numerical models. Other sources of error such as measurement errors or discretization errors associated with the numerical scheme should also be considered, but typically those effects are not expected to be the predominant ones. Therefore, if the root mean squared difference between the observed and simulated concentration fields is used as an index of the model error, the calibration of the numerical model could be considered adequate when the model error and the error (standard deviation) predicted from the stochastic theory are of the same magnitude.

Although the results of the comparison with field data are encouraging and indicate the workability of the stochastic theory to predict concentration variance, there are a number of approximations and/or refinements which need to be evaluated before the full range of applicability of the theory can be established. These features are discussed in the following paragraphs.

The development of the unsteady concentration case in Section 5, invokes an expansion of the concentration gradient around the current time t. Although only the first two terms of the expansion have been retained, additional terms could easily be included and evaluated numerically. Since these terms are multiplied by the time derivatives of the mean concentration, it is expected that they will have a minimal effect on the variance except near the concentration peak where $\partial \bar{c}/\partial x_i$, i = 1,2,3 changes rapidly. The effects of these unsteady terms near the peak need to be explicitly evaluated in order to understand their significance.

The $t \to \infty$ assumption for the integration of Eq. (5.22) is not required. Eq. (5.21) could be integrated for any finite time, which would result in an additional factor $[1-\exp(-\theta t)]$ multiplying the complex amplitude in Eq. (5.23). From the form of Eq. (5.21), it is evident that the asymptotic result will overestimate the variance for finite time and consequently will usually be conservative. This finite time effect should be evaluated in future work.

In a heterogeneous aquifer, the local dispersivities are expected to be variable in space. The effect of local variation of dispersivities can be analyzed using an approach similar to that of Naff (1978). This effect may be of significance in determining an effective local dispersivity to be used in the calculation of the concentration variance.

The behavior of the concentration covariance along the mean flow direction is somewhat puzzling from a physical point of view. As is shown in Figure 5.5a, the longitudinal correlation scale of the concentration variation becomes very large. This implies that regions of high or low deviation from the mean concentration will persist over very large longitudinal distances, say up to 10 or 100 times the correlation scale of ℓ_{nk}. Note that the degree of longitudinal persistence increases as $\varepsilon=\alpha/\ell_1$ decreases. Although somewhat similar behavior seems to be indicated by other methods (Dagan 1984), we feel that this behavior is questionable in terms of our intuition about the physical system. Intuitively we expect a smaller degree of longitudinal persistence. This feature requires additional detailed investigation because the concentration covariance function is a very important factor in the design of plume monitoring networks. Preliminary results indicate that the high persistence is caused by the distribution of the spectrum energy at high wave numbers.

REFERENCES

1. Ababou, R., D. McLaughlin, L.W. Gelhar and A.F.B. Tompson. Numerical Simulation of Saturated/Unsaturated Flow Fields in Randomly Heterogeneous Porous Media. Proceedings of International Association of Hydraulic Research Symposium on the Stochastic Approach to Subsurface Flow, Montvillargenne, France, June 1985.

2. Aldama, A.A. Rodriguez. Theory and applications of two-and three-scale filtering approaches for turbulent flow simulation. Ph.D. dissertation, Massachusetts Inst. of Tech., 397 pp., November 1985.

3. Anderson, M.P. Using Models to Simulate the Movement of Contaminants Through Groundwater Flow Systems. Critical Reviews in Environmental Controls, 9(2), pp. 97-156, 1979.

4. Bakr, A.A. Stochastic Analysis of the effect of spatial variations of hydraulic conductivity of groundwater flow. Ph.D. dissertation, New Mexico Institute of Mining and Technology, 244 p, 1976.

5. Bakr, A.A., L.W. Gelhar, A.L. Gutjahr and J.R. MacMillan. Stochastic Analysis of Spatial Variability in Subsurface Flows 1. Comparison of One- and Three-Dimensional Flows, Vol. 14, No. 2, pp 263-271, April 1978.

6. Beran, M.J. Statistical Continuum Theories, Interscience, New York, 1968.

7. Betson, R.P., J.M. Boggs, S.C. Young, and L.W. Gelhar. Design of field experiment to investigate ground water saturated zone transport processes, Electric Power Research Institute, Inc., Interim Report RP 2485-05, 104 pp, 1985.

8. Chirlin, G.R. and G. Dagan. Theoretical head variograms for steady flow in statistically homogeneous aquifers. Water Resources Res. 16(6), pp 1001-1015, 1980.

9. Dagan, G. Models of groundwater flow in statistically homogeneous porous formations, Water Resources Res. 15(1), 47-63, 1979.

10. Dagan, G. Stochastic Modeling of Groundwater Flow by Unconditional and Conditional Probabilities, part 1, Conditional Simulation and the direct problem. Water Resour. Res., 18, pp. 813-833, August 1982a.

11. Dagan, G. Stochastic Modeling of Groundwater Flow by Unconditional and Conditional Probabilities. 2. The Solute Transport. Water Resour. Res., Vol. 18, No. 4., pp. 835-848, August 1982b.

12. Dagan G. Solute Transport in heterogeneous porous formations. J. Fluid Mechanics, 145, pp. 151-177, 1984.

13. Freeze, R.A. A Stochastic-Conceptual Analysis of One-Dimensional Groundwater Flow in Nonuniform Homogeneous Media. Water Resour. Res., Vol. 11, No. 5, pp. 725-741, October 1975.

14. Freyberg, D.L., D.M. Mackay and J.A. Cherry. Advection and Dispersion in an Experimental Groundwater Plume. Proceedings of the Hydraulics Division Specialty Conference in Frontiers in Hydraulics Engineering, A.S.C.E., pp. 36-41, July 1983.

15. Freyberg, D.L. A natural gradient experiment on solute transport in a sand aquifer II. Spatial moments and the advection and dispersion of non-reactive tracers. Water Resourc. Res., (in submittal) 1985.

16. Gelhar, L.W. Stochastic Analysis of Phreatic Aquifers. Water Resour. Res., Vol. 10, No. 3, pp. 539-545, 1974.

17. Gelhar, L.W. Effects of Hydraulic Conductivity Variations on Groundwater Flows. Second International Symposium on Stochastic Hydraulics, Lund, Sweden, in Hydraulic Problems solved by Stochastic Methods, Water Res. Publications, Fort Collins, Colorado, pp. 409-431, 1977.

18. Gelhar, L.W. Stochastic Analysis of Solute Transport in Saturated and Unsaturated Porous Media. (in press 1986).

19. Gelhar, L.W. Stochastic Subsurface Hydrology: from Theory to Applications. Proceedings of International Association of Hydraulic Research Symposium on the Stochastic Approach to Subsurface Flow, Montvillargenne, France, June 1985.

20. Gelhar, L.W. Stochastic Analysis of Flow in Heterogeneous Porous Media, in Fundamentals of Transport Phenomena in Porous Media, J. Bear and M.Y., Corapcioglou, eds., Martinus Nijhoff Publishers, Dordrecht, The Netherlands, 1984.

21. Gelhar, L.W., A.L. Gutjahr and R.L. Naff. Stochastic Analysis of Macrodispersion in a Stratified Aquifer. Water Resour. Res., Vol. 15, No. 6, pp. 1387-1397, Dec. 1979.

22. Gelhar, L.W., A.L. Gutjahr and R.L. Naff. Reply to Comments on Stochastic Analysis of Macrodispersion in a Stratified Aquifer. Water Resour. Res., 17, pp. 1739-1740, 1981.

23. Gelhar, L.W. and A.L. Gutjahr. Stochastic Solution of the One-Dimensional Convective-Dispersive Equation. Report No. H-11, New Mexico Institute of Mining and Technology, pp. 20, 1982.

24. Gelhar, L.W. and C.L. Axness. Three-dimensional stochastic analysis of macrodispersion in aquifers. Water Resour. Res., 19, 161-180, 1983.

25. Gelhar, L.W., A. Mantoglou, C. Welty and K.R. Rehfeldt. A Review of Field Scale Physical Solute Transport Processes in Saturated and Unsaturated Porous Media, Research Project 2485-5, EPRI EA-4190, Electric Power Research Institute, Palo Alto, California, 116 pp., August 1985.

26. Gutjahr, A.L., L.W. Gelhar, A.A. Bakr and J.R. MacMillan. Stochastic Analysis of Spatial Variability in Subsurface Flows 2. Evaluation and Application, Water Resour. Res., Vol. 14, No. 5, pp. 953-959, October 1978.

27. Gutjahr, A.L. and L.W. Gelhar. Stochastic Models of Subsurface Flow: Infinite Versus Finite Domain and Stationarity. Water Resour. Res., Vol. 17, No. 2, pp. 337-350, April 1981.

28. Gutjahr, A.L., E.J. Bonano and R.M. Cranwell. Treatment of Parameter Uncertainties in Modeling Contaminant Transport in Geologic Media: Stochastic Models vs. Deterministic Models with Statistical Parameter Sampling. Proceedings of International Association of Hydraulic Research Symposium on the Stochastic Approach to Subsurface Flow, Montvillargenne, France, June 1985.

29. Gradshteyn, I.S. and I.M. Ryzhik. Table of Integrals, Series and Products, Academic Press, 1980.

30. Hinze, J.O. Turbulence, McGraw-Hill, 1975.

31. Hoeksema, R.J. and P.K. Kitanidis. An Application of the Geostatistical Approach to the Inverse Problem in Two-Dimensional Groundwater Modeling. Water Resour. Res., Vol. 20 (7), pp. 1003-1020, 1984.

32. Hoeksema, R.J. and P.K. Kitanidis. Analysis of the spatial structure of properties of selected aquifiers, Water Resour. Res., 21, 563-572, 1985.

33. Hufschmied, P. Estimation of three-dimensional statistically anisotropic hyraulic conductivity field by means of single well pumping tests combined with flowmeter measurements. Proceedings of International Association of Hydraulic Research Symposium on the Stochastic Approach to Subsurface Flow, Montvillargenne, France, June 1985.

34. Kitanidis, P.K., and E.G. Vomvoris. A Geostatistical Approach to the Inverse Problem in Groundwater Modeling (Steady State) and One-Dimensional Simulations. Water Resour. Res., Vol. 14(3), pp. 677-690, 1983.

35. Klotz, D., K.-P. Seiler, H. Moser and F. Neumaier. Dispersivity and velocity relationship from laboratory and field experiments. Journal of Hydrology, 45, 169-184, 1980.

36. LeBlanc, D.R., Ed., Movement and fate of solutes in a plume of sewage contaminated groundwater, Cape Cod, Massachusetts: U.S. Geological Survey Toxic Waste Groundwater Contamination Program Papers presented at the Toxic Waste Technical Meeting, Tucson, Arizona, March 20-22, 1984, U.S.G.S. Open File Report 84-475, 1984.

37. Lumley, J.L. and H.A. Panofsky. The Structure of Atmospheric Turbulence, John Wiley and Sons, Inc., New York, 1964.

38. Matheron, G. and G. de Marsily. Is transport in porous media always diffusive? A counterexample. Water Resour. Res., 16, pp. 901-917, 1980.

39. McLaughlin, D.B. A Distributed State Space Approach for Evaluating the Accuracy of Groundwater Predictions, Ph.D. Thesis, Dept. of Civil Engineering, Princeton University, Princeton, 1985.

40. Mizell, S.A., A.L. Gutjahr and L.W. Gelhar. Stochastic Analysis of Spatial Variability in Two-Dimensional Steady Groundwater Flow Assuming Stationary and Nonstationary Heads. Water Resour. Res., Vol. 18, No. 4, pp. 1053-1067, August 1982.

41. Moltyaner, G.L. Stochastic versus deterministic: A case study. Proceedings of Intern. Assoc. of Hydr. Res. Symposium on the Stochastic Approach to Subsurface Flow, Montvillargenne, France, June 1985.

42. Naff, R.L. A Continuum Approach to the Study and Determination of Field Longitudinal Dispersion Coefficients. Ph.D. thesis, New Mexico Institute of Mining and Technology, Socorro, New Mexico, pp. 176, 1978.

43. Netter, J. and W. Wasserman. Applied linear statistical models, R. D. Irwin, Inc., Hornewood, Illinois, 842 p., 1974.

44. Schwartz, F.W. Macroscopic Dispersion in Porous Media: The Controlling Factors. Water Resour. Res., Vol. 13, No. 4, pp. 743-752, August 1977.

45. Smith, L., and R.A. Freeze. Stochastic Analysis of Steady State Groundwater Flow in a Bounded Domain. 1. One-Dimensional Simulations. Water Resour. Res., Vol. 15, No. 3, pp. 521-528, June 1979a.

46. Smith, L., and R.A. Freeze. Stochastic Analysis of Steady State Groundwater Flow in a Bounded Domain. 2. Two-Dimensional Simulations. Water Resour. Res., Vol. 15, No. 6, pp. 1543-1559, Dec. 1979b.

47. Smith, L. and F.W. Schwartz. Mass Transport 3. Role of Hydraulic Conductivity Data in Prediction. Water Resour. Res., Vol. 17, No. 5, pp. 1463-1479, October 1981.

48. Sudicky, E.A. Spatial Variability of Hydraulic Conductivity at the Borden Tracer Test Site. Proceedings of Intern. Assoc. of Hydr. Res. Symposium on the Stochastic Approach to Subsurface Flow, Montvillargenne, France, June, 1985a.

49. Sudicky, E.A. A Natural-Gradient Experiment on Solute Transport in a Sand Aquifer: Spatial Variability of Hydraulic Conductivity and its Role in the Dispersion Process. Water Resour. Res., (Submitted, 1985b).

50. Taylor, G.I. Diffusion by Continuous Movements. Proc. of London Math. Soc., Ser. 2, Vol. XX, pp. 196-212, 1921.

51. Vanmarke, E. Random Fields: Analysis and Synthesis. The MIT Press, Cambridge, 1983.

52. Vomvoris, E. Groundwater Parameter Estimation: A Geostatistical Approach. M.S. thesis, Univ. of Iowa, p. 188, July 1982.

53. Vomvoris, E.G. and L.W. Gelhar. Stochastic Analysis of Concentration Variability in Transport in Aquifers. Proceedings of the Intern. Assoc. of Hydr. Res. Symposium on the Stochastic Approach to Subsurface Flow, Montvillargenne, France, June 1985.

APPENDIX A

THE MATHEMATICS OF THE APPROXIMATE ANALYTICAL EVALUATIONS

This appendix describes the mathematical solutions used for the approximate analytical results presented in Table 5.1. The following symbols will be used repeatedly to provide non-dimensional quantities:

$$u_1 = k_1\ell_1,\ u_2 = k_2\ell_2,\ u_3 = k_3\ell_3,\ u^2 = u_1^2 + u_2^2 + u_3^2$$

$$\varepsilon = \frac{\alpha_L}{\ell_3},\ \kappa = \frac{\alpha_T}{\alpha_L},\ \upsilon = \frac{u_1}{\varepsilon},\ \rho_1 = \frac{\ell_3}{\ell_1},\ \rho_2 = \frac{\ell_3}{\ell_2} \qquad \text{(A.1)}$$

$$U^2 = u_2^2 + u_3^2,\quad \hat{U}^2 = \rho_2^2 u_2^2 + u_3^2,\quad \hat{u}^2 = \rho_1^2 u_1^2 + \kappa\hat{U}^2$$

$$\dot{u}^2 = \rho_1^2 u_1^2 + \hat{U}^2$$

$$V^2 = \varepsilon^2\upsilon^2 + U^2,\quad \dot{V}^2 = \rho_1^2\varepsilon^2\upsilon^2 + \hat{U}^2,\quad \hat{V}^2 = \rho_1^2\varepsilon^2\upsilon^2 + \kappa\hat{U}^2$$

$$R^2 = 1 - \rho_1^2$$

$$\zeta = \frac{\xi}{\ell},\ \beta = \kappa\varepsilon\zeta,\ \underline{\xi}' = \left(\frac{\xi_1}{\ell}, \frac{\xi_2}{\ell}, \frac{\xi_3}{\ell}\right)$$

$$E = \frac{\sigma_f^2}{\pi^2}\,\frac{1}{\gamma^2}\,\frac{4}{3}\,\ell_3^2$$

where $\ell_3 = \ell_2 = \ell_1 = \ell$ in the isotropic case.

Variance; anisotropic case - T_{11}

From eqs. (5.33b) and (5.32),

$$T_{11} = E \cdot I_{11} \qquad \text{(A.2)}$$

$$I_{11} = \frac{\ell_1\ell_2}{\ell_3}\int_{-\infty}^{\infty} \frac{\ell_1^2 k_1^2}{(1 + \ell_1^2 k_1^2)^3}\,\frac{(1 - \frac{k_1^2}{k^2})^2}{k_1^2 + [\alpha_L k_1^2 + \alpha_T(k_2^2 + k_3^2)]^2}\,dk_1 dk_2 dk_3$$

Changing the variables with the aid of Eq. (A.1)

$$I_{11} = \int_{-\infty}^{\infty} \frac{u^2}{(1+u^2)^3} \frac{1}{\rho_1^2 u_1^2 + \varepsilon^2 \hat{u}^4} \left(1 - \rho_1^2 \frac{u_1^2}{\hat{u}^2}\right)^2 du_1 du_2 du_3 \tag{A.3}$$

Introducing the variable $\upsilon = u_1/\varepsilon$, Eq. (A.3) can be written as:

(A.4)

$$I_{11} = \int_{-\infty}^{\infty} \frac{V^2}{(1+V^2)^3} \frac{1}{\rho_1^2 \upsilon^2 \varepsilon^2 + \varepsilon^2 \hat{V}^4} \left(1 - \rho_1^2 \frac{\upsilon^2 \varepsilon^2}{\hat{V}^2}\right) \varepsilon \, d\upsilon \, du_2 du_3$$

Taking the limit $\varepsilon \to 0$,

$$V^2 + u_2^2 + u_3^2 = U^2$$

$$\left(1 - \rho_1^2 \frac{\upsilon^2 \varepsilon^2}{\hat{V}^2}\right)^2 \to 1$$

$$\rho_1^2 \upsilon^2 + \hat{V}^4 \to \rho_1^2 \upsilon^2 + \kappa^2 \hat{U}^4$$

and hence, I_{11} takes the form

$$I_{11}\ (\varepsilon \to 0) \simeq \frac{1}{\varepsilon} \int_{-\infty}^{\infty} \frac{U^2}{(1+U^2)^3} \frac{1}{\rho_1^2 \upsilon^2 + \kappa^2 \hat{U}^4} d\upsilon \, du_2 du_3 \tag{A.5}$$

Integrating over υ, after changing variables $x = \rho_1 \upsilon$,

$$\int_{-\infty}^{\infty} \frac{1}{\rho_1^2 \upsilon^2 + \kappa^2 \hat{U}^4} d\upsilon = \frac{1}{\rho_1} 2 \int_{-\infty}^{\infty} \frac{1}{x^2 + \kappa^2 \hat{U}^4} dx = \frac{1}{\rho_1} 2 \frac{\pi}{2} \frac{1}{\kappa \hat{U}^2} = \frac{1}{\rho_1} \frac{\pi}{\kappa \hat{U}^2} \tag{A.6}$$

Hence, Eq. (A.5) becomes the double integral,

$$I_{11}\ (\varepsilon \to 0) \simeq \frac{1}{\varepsilon \kappa} \frac{\pi}{\rho_1} \int_{-\infty}^{\infty} \frac{U^2}{(1+U^2)^3} \frac{1}{\hat{U}^2} du_2 du_3 \tag{A.7}$$

Using polar coordinates, $u_2 = U \cos\phi$, $u_3 = U \sin\phi$,

$$I_{11} \simeq \frac{1}{\varepsilon} \frac{\pi}{\rho_1} \int_0^{\infty} \int_0^{2\pi} \frac{U^2}{(1+U^2)^3} \frac{1}{U^2(\rho_2^2 \cos^2\phi + \sin^2\phi)} U \, dU \, d\phi \tag{A.8}$$

Evaluating separately, for each variable, [Gradshteyn & Ryzhik, 1980, 3.642(3)]

$$\int_0^\infty \frac{U}{(1+U^2)^3}\,dU = \frac{1}{4} \tag{A.9}$$

$$\int_0^{2\pi} \frac{1}{\rho_2^2\cos^2\phi + \sin^2\phi}\,d\phi = \frac{2}{\rho_2}\,\pi$$

which result after substitution in Eq. (A.8) and Eq. (A.2),

$$T_{11} \simeq \frac{\sigma_f^2}{\gamma^2}\,\ell_3^2\,\frac{2}{3}\,\frac{1}{\varepsilon\kappa}\,\frac{1}{\rho_1}\,\frac{1}{\rho_2} \tag{A.10}$$

Variance; vertical isotropy - T_{22}.

$$T_{22} = E\,I_{22}^o$$

$$I_{22}^o = I_{22}\,(\alpha_L = \alpha_T = 0) = \int_{-\infty}^{\infty} \frac{u^2}{(1+u^2)^3}\,\frac{u_2^2}{u^4}\,du_1du_2du_3 \tag{A.11}$$

Changing to spherical coordinates (u, ϕ, θ), with $\rho_2 = 1$,

$$\begin{aligned} u_1 &= u\cos\phi \\ u_2 &= u\sin\phi\cos\theta \\ u_3 &= u\sin\phi\sin\theta \end{aligned} \tag{A.12}$$

$$I_{22}^o = \int_0^\infty \frac{u^2}{(1+u^2)^3}\,du \int_0^\pi \int_0^{2\pi} \frac{\sin^2\phi\cos^2\theta}{(\rho_1^2\cos^2\phi + \sin^2\phi)^2}\sin\phi\,d\phi\,d\theta \tag{A.13}$$

The three integrals can be evaluated separately,

$$\int_0^\infty \frac{u^2}{(1+u^2)^3}\,du = \frac{\pi}{16} \tag{A.14a}$$

$$\int_0^{2\pi} \cos^2\theta\,d\theta = \pi \tag{A.14b}$$

$$\int_0^\pi \frac{\sin^3\phi}{(\rho_1^2\cos^2\phi + \sin^2\phi)^2}\,d\phi = 2\int_0^1 \frac{1-x^2}{(1-R^2x^2)^2}\,dx$$

$$= \frac{1}{2\rho_1^2} + \frac{1}{R^2} + \left(\frac{1}{2} + \frac{1}{R^2}\right) \frac{1}{R} \ell n \frac{R + 2R^2}{R - 2R^2} \qquad \text{(A.14c)}$$

The combination of Eqs. (A.14a), (A.14b) and (A.14c) gives the result presented in Table 5.1. Note that when $\ell_1=\ell_2=\ell_3=\ell$, eq. (A.14c) becomes

$$\int_0^{\pi} \sin^3\phi \, d\phi = \frac{4}{3} \qquad \text{(A.15)}$$

and, then,

$$T_{11} = E \cdot \pi^2 \frac{1}{12} = \frac{\sigma_f^2}{\gamma^2} \ell^2 \frac{1}{9} \qquad \text{(A.16)}$$

For T_{33} the only change occurs at Eq. (14b), which becomes

$$\int_0^{\infty} \sin^3\theta \, d\theta = \pi \qquad \text{(A.16b)}$$

Thus, $T_{22} = T_{33}$ as claimed in Table 5.1.

Covariance; isotropic case - $T_{11}(\xi,0,0)$

From eq. (5.12),

$$R_{cc}(\underline{\xi}) = \int_{-\infty}^{\infty} e^{i\underline{k}\cdot\underline{\xi}} S_{cc}(\underline{k}) \, d\underline{k} \qquad \text{(A.17)}$$

The spectrum $S_{cc}(\underline{k})$ is even with respect to $\underline{k} = (k_1,k_2,k_3)$ for the case considered here. The exponential can be expressed as,

$$e^{i\underline{k}\cdot\underline{\xi}} = \cos(\underline{k}\cdot\underline{\xi}) + i \sin(\underline{k}\cdot\underline{\xi}) \qquad \text{(A.18)}$$

and, since the sin(•) is odd it will cancel out. Therefore, the $T_{11}(\underline{\xi})$ is given from,

$$T_{11}(\underline{\xi}) = \frac{E}{\varepsilon} \int_{-\infty}^{\infty} \cos(\underline{u}\cdot\underline{\xi}') \frac{1}{u_1^2 + \varepsilon^2 \hat{u}^4} \left(1 - \frac{u_1^2}{u^2}\right)^2 S_{ff}(\underline{u}) \, du \qquad \text{(A.19)}$$

Introducing $\upsilon = u_1/\varepsilon$, and taking the limit $\varepsilon \to 0$,

$$\underline{u}\cdot\underline{\xi}' = \varepsilon\upsilon\frac{\xi_1}{\ell} + u_2 \frac{\xi_2}{\ell} + u_3 \frac{\xi_3}{\ell} \qquad \hat{u}^4 \to \kappa^2 U^4$$

$$(1 - \frac{v^2}{u^2}\varepsilon^2)^2 \to 1 \qquad S_{ff}(\underline{u}) \to S_{ff}(0,u_2,u_3) \tag{A.20}$$

The $\underline{u}\cdot\underline{\xi}$ argument in the cosine does not allow for analytical integration unless only one of the ξ_i's, or, equivalently, u_i's, is retained. Hence, for $\underline{\xi} = (\xi,0,0)$, Eqs. (A.19), (A.20) and (5.32) for $S_{ff}(\underline{k})$,

$$T_{11}(\xi,0,0) \simeq E\frac{1}{\varepsilon}\int_{-\infty}^{\infty}\cos(\varepsilon v\zeta)\,\frac{1}{v^2+\kappa^2U^4}\,\frac{U^2}{(1+U^2)^3}\,dv\,du_2du_3 \tag{A.21}$$

Integrating over v first,

$$\int_{-\infty}^{\infty}\cos(\varepsilon v\zeta)\,\frac{1}{v^2+\kappa^2U^4}\,dv = \frac{\pi}{\kappa U^2}\,e^{-\kappa U^2\varepsilon\zeta} \tag{A.22}$$

The remaining integral becomes,

$$T_{11}(\xi,0,0) \simeq E\frac{\pi}{\varepsilon\kappa}\int_{-\infty}^{\infty}e^{-\beta U^2}\,\frac{1}{(1+U^2)^3}\,du_2du_3 \tag{A.23}$$

Converting to polar coordinates, $u_2 = U\cos\phi$, $u_3 = U\sin\phi$

$$T_{11}(\xi,0,0) \simeq E\frac{\pi}{\varepsilon\kappa}\int_0^{2\pi}d\phi\int_0^{\infty}e^{-\beta U^2}\,\frac{U}{(1+U^2)^3}\,dU \tag{A.24}$$

The second integral can be evaluated analytically in terms of the Exponential integral [Gradshteyn and Ryzhik, 3.353(4)]

$$T_{11}(\xi,0,0) \simeq E\frac{2\pi^2}{\varepsilon\kappa}\frac{1}{4}\left[1-\beta-\beta^2e^{\beta}Ei(-\beta)\right] \tag{A.25}$$

Note that the term in the brackets equals 1 when $\beta = 0$, which verifies the variance relationship.

For $\beta \ll 1$,

$$E_i(-\beta) = C + \ln\beta - \beta + \ldots \tag{A.26}$$

$$e^{\beta} = 1 + \beta + \ldots$$

where $C \simeq 0.577215$, Euler's constant [Gradshteyn & Ryzhik, 8.214 (1)] and the term in the brackets becomes

$$\left[1 - \beta - \beta^2(C + \ln\beta) + \ldots\right] \tag{A.27}$$

For $\beta \gg 1$,

$$e^{\beta}Ei(-\beta) = \frac{1}{\beta} + \frac{1}{\beta^2} - \frac{2}{\beta^3} + \ldots. \tag{A.28}$$

[Gradshteyn & Ryzhik, 8.215] and the term in the brackets becomes

$$\left[\frac{2}{\beta} \right] \tag{A.29}$$

Covariance; isotropic case - $T_{11}(0,\xi,0)$

In this case Eqs. (A.17) through (A.20) are the same. With $\underline{\xi} = (0,\xi,0)$, Eq. (A.21) becomes

$$T_{11}(0,\xi,0) = E \frac{1}{\varepsilon} \int_{-\infty}^{\infty} \cos(u_2\zeta) \frac{1}{\upsilon^2 + \kappa^2 U^4} \frac{U^2}{(1+U^2)^3} \, d\upsilon \, du_2 \, du_3 \tag{A.30}$$

From Eq. (A.22) the integral over υ, for $\beta = 0$, is known. Changing to polar coordinates,

$$T_{11}(0,\xi,0) = E \frac{\pi}{\varepsilon\kappa} \int_0^{\infty} \int_0^{2\pi} \frac{\cos(U\cos\phi\zeta)}{(1+U^2)^3} \, U \, dU \, d\phi \tag{A.31}$$

The integral over ϕ is given in Gradshteyn & Ryzhik, [3.715(18)],

$$\int_0^{2\pi} \cos(\cos\phi U\zeta) \, d\phi = 2\pi \, J_o(U\zeta) \tag{A.32}$$

and, finally,

$$\int_0^{\infty} J_o(U\zeta) \frac{U}{(1+U^2)^3} \, dU = \frac{1}{8} \zeta^2 K_2(\zeta) \tag{A.33}$$

from [Gradshteyn & Ryzhik 6.565(4), 8.486(16)] where $J_o(.)$ and $K_2(.)$ are a Bessel function of first kind, zero order and a modified Bessel function of second kind, second order, respectively. The coefficient $T_{22}(0,\xi,0)$ is given from,

$$T_{11}(0,\xi,0) = \frac{\sigma_f^2}{\gamma^2} \ell^2 \frac{1}{\varepsilon\kappa} \frac{1}{3} \zeta^2 K_2(\zeta) \tag{A.34}$$

Note that $\zeta^2 K(\zeta) = 2$, at $\zeta = 0$, verifying the variance result.

For the case $\underline{\xi} = (0,0,\xi)$ the only change is in eq. (A.32) which becomes,

$$\int_0^{2\pi} \cos(U\zeta \sin\phi) \, d\phi = 2\pi \, J_o(\zeta U) \tag{A.35}$$

[Gradshteyn & Ryzhik, 3.715(9)], therefore,

$$T_{11}(0,\xi,0) = T_{11}(0,0,\xi) \tag{A.36}$$

Covariance; isotropic case - $T_{22}(\xi,0,0)$

As in the variance case, the coefficient T_{22} can be evaluated when $\varepsilon = 0$. The same arguments for the exponential, Eq. (A.18), hold. Therefore, for $\varepsilon = 0$ and a combination of Eqs. (A.11), (A.17) and (A.18);

$$T_{22}(\underline{\xi}) = E \int_{-\infty}^{\infty} \cos(\underline{u}\ \underline{\xi}') \frac{1}{(1+u^2)^3} \frac{u_2^2}{u^2} du_1 du_2 du_3 \tag{A.37}$$

Changing to spherical coordinates and for $\underline{\xi} = (\xi,0,0)$

$$T_{22}(\underline{\xi}) = E \int_0^{\infty}\int_0^{\pi}\int_0^{2\pi} \cos(u\zeta\cos\phi) \frac{u}{(1+u^2)^3} \sin^3\phi\cos^2\theta\ d\theta\ d\phi\ du \tag{A.38}$$

The integral over u equals,

$$\int_0^{\infty} \cos(u\zeta\cos\phi) \frac{u^2}{(1+u^2)^3} du = \frac{\pi}{16} e^{-|a|}[1 + |a| - a^2] \tag{A.39}$$

where $a = \zeta\cos\theta$. In addition, the integral over θ equals π, from Eq. (A.14b). Hence

$$T_{22}(\xi,0,0) = E \frac{\pi^2}{16} \int_0^{\pi} e^{-|a|}[1 + |a| - a^2] \sin^3\phi\ d\phi \tag{A.40}$$

Changing variables to $\cos\phi = x$, and using the following equalities,

$$\begin{aligned}
\int_0^1 e^{bx}(1-x^2)\,dx &= e^b\left(\frac{2}{b^2} - \frac{2}{b^3}\right) - \left(\frac{1}{b} - \frac{2}{b^3}\right) \\
\int_0^1 e^{bx}(1-x^2)x\,dx &= e^b\left(\frac{2}{b^2} - \frac{6}{b^3} + \frac{6}{b^4}\right) + \left(\frac{1}{b^2} - \frac{6}{b^4}\right) \\
\int_0^1 e^{bx}(1-x^2)x^2dx &= e^b\left(\frac{2}{b^2} - \frac{10}{b^3} + \frac{24}{b^4} - \frac{24}{b^5}\right) + \left(\frac{-2}{b^3} + \frac{24}{b^5}\right)
\end{aligned} \tag{A.41}$$

the expression for $T_{22}(\xi,0,0,)$ becomes,

$$T_{22}(\xi,0,0) = \frac{\sigma_f^2}{\gamma^2} \ell^2 \frac{4}{3}\left[\frac{2}{\zeta^3} - e^{-\zeta}\left(\frac{2}{\zeta^3} + \frac{2}{\zeta^2} + \frac{1}{\zeta} + \frac{1}{4}\right)\right] \tag{A.42}$$

Expanding, $e^{-\zeta} = 1 - \zeta + \frac{\zeta^2}{2!} - \frac{\zeta^3}{3!} + \ldots$, shows that the term in the brackets becomes for $\zeta = 0$,

$$\left[\frac{1}{12}\right] \tag{A.43}$$

verifying the variance result.

Covariance; isotropic case - $T_{22}(0,\zeta,0)$

The general Eq. (A.37) is the same. The conversion to spherical coordinates is introduced in the following way,

$$\begin{aligned} u_2 &= u\cos\phi \\ u_1 &= u\sin\phi\cos\theta \\ u_3 &= u\sin\phi\sin\theta; \qquad \phi: 0\text{-}\pi;\ \theta: 0\text{-}2\pi \end{aligned} \tag{A.44}$$

The coefficient $T_{22}(0,\zeta,0)$ is given from,

$$T_{22}(0,\xi,0) = E\,\frac{1}{\ell}\int_0^{\infty}\int_0^{\pi}\int_0^{2\pi} \cos(u\zeta\cos\phi)\,\cos^2\phi\,\frac{u^2}{(1+u^2)^3}\,\sin\phi\;du\;d\phi\;d\theta \tag{A.45}$$

The integral over θ equals 2π, and the one over u is given in Eq. (A.39). Introducing these results into Eq. (A.45) and changing variables to $x = \cos\phi$,

$$T_{22}(0,\xi,0) = E\,\frac{1}{\ell}\,\frac{\pi^2}{4}\int_0^1 x^2(1 + a - a^2)\,e^{-a}\,dx \tag{A.46}$$

where $a = \zeta x$. Using the following evaluations,

$$\begin{aligned} \int_0^1 x^2 e^{-\beta x}\,dx &= \frac{2}{\beta^3}\left[1 - e^{-\beta}\left(\frac{\beta^2}{2} + \beta + 1\right)\right] \\ \int_0^1 x^3 e^{-\beta x}\,dx &= \frac{6}{\beta^4}\left[1 - e^{-\beta}\left(\frac{\beta^3}{6} + \frac{\beta^2}{2} + \beta + 1\right)\right] \\ \int_0^1 x^4 e^{-\beta x}\,dx &= \frac{24}{\beta^5}\left[1 - e^{-\beta}\left(\frac{\beta^4}{24} + \frac{\beta^3}{6} + \frac{\beta^2}{2} + \beta + 1\right)\right] \end{aligned} \tag{A.47}$$

the final equation for $T_{22}(0,\xi,0)$ is

$$T_{22}(0,\xi,0) = \frac{\sigma_f^2}{\gamma^2}\,\ell^2\,\frac{1}{3}\,\frac{1}{\zeta^3}\left[e^{-\zeta}\left(16 + 16\zeta + 8\zeta^2 + 3\zeta^3 + \zeta^4\right) - 16\right] \tag{A.48}$$

It can be shown that the term in brackets as $\zeta \to 0$, approaches the value $1/3\,\zeta^3$, verifying thus the asymptotic result for the variance.

Covariance; isotropic case - $T_{33}(0,0,\xi)$

The general Eq. (A.37) is the same. If the following conversion to spherical coordinates is introduced,

$$\begin{aligned} u_3 &= u\cos\phi \\ u_1 &= u\sin\phi\cos\theta \\ u_2 &= u\sin\phi\sin\theta \end{aligned} \tag{A.49}$$

the expression for $T_{22}(0,0,\xi)$ becomes,

$$T_{22}(0,0,\xi) = E\int_0^{\infty}\int_0^{\pi}\int_0^{2\pi} \cos(u\zeta\cos\phi)\,\frac{u^2}{(1+u^2)^3}\sin^3\phi\sin^2\theta\; d\theta d\phi du \tag{A.50}$$

Since

$$\int_0^{2\pi}\sin^2\theta\, d\theta = \int_0^{2\pi}\cos^2\theta\, d\theta = \pi \tag{A.51}$$

It can be easily seen that

$$T_{22}(0,0,\xi) = T_{22}(\xi,0,0) \tag{A.52}$$

Covariance; isotropic case - $T_{33}(\xi,0,0)$

The general equation is:

$$T_{33}(\xi,0,0) = \frac{E}{\ell}\int_{-\infty}^{\infty}\cos(u_1\zeta)\,\frac{1}{(1+u^2)^3}\,\frac{u_3^2}{u^2}\,du_1du_2du_3 \tag{A.53}$$

Changing to spherical coordinates,

$$\begin{aligned} u_1 &= u\cos\theta \\ u_2 &= u\sin\phi\cos\theta \\ u_3 &= u\sin\phi\sin\theta \end{aligned} \tag{A.54}$$

Eq. (A.53) becomes identical to Eq. (A.50). Hence,

$$T_{33}(\xi,0,0) = T_{22}(\xi,0,0) \tag{A.55}$$

Covariance; isotropic case - $T_{33}(0,\xi,0)$

The general equation is,

$$T_{33}(0,\xi,0) = \frac{E}{\ell}\int_{-\infty}^{\infty}\cos(u_2\zeta)\,\frac{1}{(1+u^2)^3}\,\frac{u_3^2}{u^2}\,du_1du_2du_3 \tag{A.56}$$

Changing to spherical coordinates as in Eq. (A.44), it can be seen that

$$T_{33}(0,\xi,0) = T_{33}(\xi,0,0) \tag{A.57}$$

Covariance; isotropic case - $T_{33}(0,0,\xi)$

The general equation is,

$$T_{33}(0,0,\xi) = \frac{E}{\ell} \int_{-\infty}^{\infty} \cos(u_3\zeta) \frac{1}{(1+u^2)^3} \frac{u_3^2}{u^2} du_1 du_2 du_3 \tag{A.58}$$

Changing the spherical coordinates as in Eq. (A.49),

$$T_{33}(0,0,\xi) = \frac{E}{\ell} \int_{0}^{\infty} \int_{0}^{\pi} \int_{0}^{2\pi} \cos(u\zeta\cos\phi) \frac{u^2}{2\ 3} \cos^2\phi \sin\phi d\theta d\phi du \tag{A.59}$$

APPENDIX B

THE INTEGRATION OVER WAVE-NUMBER

The spectrum of the concentration can be written as follows, Eq. (5.10) and (5.11),

$$S_{cc}(\underline{k}) = E \frac{k_j^2 \ell_j^2}{(1+k_j^2 \ell_j^2)^3} \frac{S_{ff}(\underline{k})}{k_1+a^2k^4} [G_j G_\ell J_m J_n (\delta_{jm} - \frac{k_j k_m}{k^2})(\delta_{\ell n} - \frac{k_\ell k_n}{k^2})] \qquad (B.1)$$

where $E = \frac{1}{\gamma^2} \frac{4}{3} \frac{\ell_1 \ell_2 \ell_3}{\pi^2}$, and summation over j,ℓ,m,n in the branches is assumed.

Note that introduction of spherical coordinates makes the terms inside the brackets independent of k. Hence, when one evaluates the covariance,

$$R_{cc}(\underline{\xi}) = \int_{-\infty}^{\infty} \exp(i\underline{k}\cdot\underline{\xi})\, S_{cc}(\underline{k})\, d\underline{k} \qquad (B.2)$$

transforming to spherical coordinates and evaluating the integral over wave number k, results in the following:

$$R_{cc}(\underline{\xi}) = \int_0^{\pi} \int_0^{2\pi} I(\beta,\omega) \int_0^{\infty} \exp(ik\cos\beta) \frac{k^2A^2}{(1+k^2A^2)^3} \frac{1}{B^2+a^2k^2} \, dk d\beta d\omega \qquad (B.3)$$

where A, B depend on the angular coordinates from the used transformation and $I(\theta,\omega)$ contains the remaining terms in Eq. (B.2).

Note that due to symmetry of $S_{cc}(\underline{k})$, i.e.,

$$S_{cc}(k_1,k_2,k_3) = S_{cc}(-k_1,-k_2,-k_3)$$

expanding the exponent, $\exp(iD) = \cos D + i\sin D$, in the integral Eq. (B.2) cancels the imaginary part.

The spherical coordinate transformation is chosen so that $\underline{k}\cdot\underline{\xi} = k\,\xi\,\cos\beta$, i.e., depends only in two parameters of integration k,β. Appendix C describes the details of the used transformation which is similar to the one used by Bakr et al. (1978) to obtain analytical results for the head field covariance.

Denote,

$$\begin{aligned} B &= \alpha_x\cos\theta + \alpha_y\sin\theta\cos\omega + \alpha_z\sin\theta\sin\omega \\ C &= \beta_x\cos\theta + \beta_y\sin\theta\cos\omega + \beta_z\sin\theta\sin\omega \\ D &= \gamma_x\cos\theta + \gamma_y\sin\theta\cos\omega + \gamma_z\sin\theta\sin\omega \end{aligned} \qquad (B.4)$$

where $\alpha_\cdot$, $\beta_\cdot$, $\gamma_\cdot$ are defined in Appendix C.

The integrals can be nondimensionalized using the parameters

$$\rho_1 = \frac{\ell_3}{\ell_1}\ ,\ \rho_2 = \frac{\ell_3}{\ell_2}\ ,\ (\rho_3 = 1),\quad \varepsilon = \frac{\alpha_L}{\ell_3}\ ,\quad \kappa = \frac{\alpha_T}{\alpha_L}\ ,\quad u_i = k_i \ell_i \tag{B.5}$$

Then converting to spherical coordinates and denoting

$$E^2 = \varepsilon^2 \left[\rho_1^2 B^2 + \kappa(\rho_2^2 C^2 + D^2)\right]^2 \tag{B.6a}$$

$$A^2 = \frac{1}{\rho_1^2}\left[a_{1j}\rho_j u_j\right]^2 + \frac{1}{\rho_2^2}\left[a_{2j}\rho_j u_j\right]^2 + \left[a_{3j}\rho_j u_j\right]^2 \tag{B.6b}$$

$[a_{ij}]$ = Transformation matrix between the hydraulic conductivity principal axes and the axes aligned to the mean flow direction

$$R = \rho_1 B\xi_1' + \rho_2 C\xi_2' + D\xi_3',\quad \xi_i' = \xi_i/\ell_3 \tag{B.6c}$$

$$P = \frac{1}{\gamma^2}\ \frac{4}{3}\ \frac{1}{\pi^2} \tag{B.6d}$$

the integrals become

$$R_{cc}(\xi,\chi,\psi) = \sigma_f^2 \ell_3^2 \int_0^{\pi}\int_0^{2\pi} PF_{ij}(\beta,\omega;\chi,\psi)\sin\beta M\, d\beta d\omega\ G_i G_j \tag{B.7a}$$

$$M = \int_0^{\infty} \cos(Ru)\ \frac{A^2u^2}{(1+A^2u^2)^3}\ \frac{1}{\rho_1^2 B^2 + u^2 E^2}\, du \tag{B.7b}$$

Eq. (B.7) is the same as Eq. (5.33c) if one denotes the three-dimensional integral as $T_{ij}(.)$. The coefficient $F_{ij}(.)$ in the integrand is given from:

$$F_{ij}(\beta,\omega;\chi,\psi) = \left[J_k(\delta_{ik} - \rho_i\rho_k B_i B_k/L)\right]\left[J_m(\delta_{jm} - \rho_j\rho_m B_j B_m/L)\right]/J_1^2$$
$$L = \rho_1^2 B^2 + \rho_2^2 C^2 + D^2 \tag{B.8}$$

The integral over u in Eq. (B.7b) can be estimated analytically.

From partial fraction expansion, for $A^2 \neq 0$, $E^2 \neq \rho_1^2 A^2 B^2$, $B \neq 0$,

$$\frac{k^2A^2}{(1+k^2A^2)^3}\ \frac{1}{\rho_1^2B^2+E^2k^2} = \frac{1}{E^2A^4}\left[A_{11}\frac{1}{k^2-p_1} + A_{12}\frac{1}{(k^2-p_1)^2} + A_{13}\frac{1}{(k^2-p_1)^3}\right.$$

$$\left. + A_2\frac{1}{k^2-p_2}\right] \qquad \text{(B.9a)}$$

$$p_1 = \frac{-1}{A^2}\ ,\quad p_2 = -\rho_1^2\frac{B^2}{E^2} \qquad \text{(B.9b)}$$

$$A_{11} = \frac{p_2}{(p_1-p_2)^3}\ ,\quad A_{12} = \frac{-p_2}{(p_1-p_2)^2}\ ,\quad A_{13} = \frac{p_1}{p_1-p_2}\ ,\quad A_2 = \frac{-p_2}{(p_1-p_2)^3}$$

with the aid of the following integration formulas [Gradshteyn and Ryzhik, 1980, 3.737]

$$\int_0^\infty \frac{\cos(ax)}{(b^2+x^2)^3}\,dx = \frac{\pi}{16|b|^5}\left[a^2b^2+3|ab|+3\right]e^{-|ab|}$$

$$\int_0^\infty \frac{\cos(ax)}{(b^2+x^2)^3}\,dx = \frac{\pi}{4|b|^3}\left[1+|ab|\right]e^{-|ab|} \qquad \text{(B.10)}$$

$$\int_0^\infty \frac{\cos(ax)}{(b^2+x^2)^3}\,dx = \frac{\pi}{2|b|}e^{-|ab|}$$

Eq. (7b) becomes:

Case 1: $A^2 \neq 0$, $E^2 \neq A^2B^2\rho_1^2$, $B \neq 0$.

$$M = \frac{1}{E^2A^4}\ \frac{\pi}{2}\left\{\left[A_{11}|A| + A_{12}\left(\tfrac{1}{2}|A|^3\right)\left(1+\left|\frac{R}{A}\right|\right)\right.\right.$$

$$\left. + A_{13}\frac{1}{8}|A|^5\left(\frac{R^2}{A^2}+3\left|\frac{R}{A}\right|+3\right)\right]\cdot\exp\left[-\left|\frac{R}{A}\right|\right] \qquad \text{(B.11)}$$

$$\left.\left. + A_2\frac{E}{\rho_1|B|}\exp\left[-\left|\frac{R\rho_1B}{E}\right|\right]\right]\right\}$$

If B = 0, Eq. (B.6) becomes,

$$M = \left|\frac{A}{E^2}\right| \frac{\pi}{16} \left(\frac{R^2}{A^2} + 3\left|\frac{R}{A}\right| + 3\right) \exp\left[-\left|\frac{R}{A}\right|\right] \tag{B.12}$$

If $E^2 = \rho_1{}^2 A^2 B^2$, Eq. (B.6) becomes

$$M = \int_0^\infty \cos(kR) \frac{1}{E^2 A^4} \frac{k^2}{\left(\frac{1}{A^2} + k^2\right)^4} dk$$

$$= \frac{\pi}{E^2} \left|\frac{A}{32}\right| \left(-\frac{1}{3}\left|\frac{R}{A}\right|^3 + \left|\frac{R}{A}\right| + 1\right) \exp\left[-\left|\frac{R}{A}\right|\right] \tag{B.13}$$

Finally, if A = 0,

$$M = 0 \tag{B.14}$$

The remaining eq. (B.7a) is solved numerically using a Romberg integration scheme for the integration over β and the trapezoidal rule for the resulting one-dimensional integral.

APPENDIX C

TRANSFORMATION TO POLAR COORDINATES

The coordinate system (x^o, y^o, z^o) in Figure C-1 represents the original coordinate system to which (x_1,x_2,x_3) or (k_1,k_2,k_3) are aligned. The objective of the transformation to the polar coordinates is to express the dot product $\underline{k} \cdot \underline{\xi}$ in the exponential in Eq. (5.12) in terms of k and β, i.e., two parameters only. The transformation will be performed in three steps.

Step 1 Create a Cartesian system of axes, $(\vec{\xi}_1,\vec{\varepsilon},\vec{\ell})$, where $\vec{\varepsilon}$ belongs to the plane (x_o,y_o) and $\vec{\xi}_1$ is on vector $\vec{\xi}$.

The vectors $\vec{\xi}_1,\vec{\varepsilon},\vec{\ell}$ can be expressed in terms of the angles χ,ψ (Figure C-1).

$\vec{\xi}_1 = [\cos\chi, \sin\chi\cos\psi, \sin\chi\sin\psi]^T$, where the superscript "T" stands for transpose and $\vec{\xi}_1$ has unit length.

$\vec{\varepsilon} = [\varepsilon_x, \varepsilon_y, 0]$, since it belongs in (x_o,y_o). Invoking its orthogonality with respect to $\vec{\xi}$, $\vec{\varepsilon} \cdot \vec{\xi} = 0$, or,

$$\vec{\varepsilon} = [-\sin\chi\sin\psi, \cos\chi, 0]^T \cdot \frac{1}{(1 - \sin^2\chi\cos^2\psi)^{1/2}}$$

Finally, for $\vec{\ell}$, from orthogonality

$$\vec{\ell} \cdot \vec{\varepsilon} = 0 \quad \text{and} \quad \vec{\ell} \cdot \vec{\xi} = 0$$

and the following expression can be obtained:

$$\vec{\ell} = \begin{vmatrix} \cos\chi\sin\chi\cos\psi \\ \sin^2\chi\sin\psi\cos\psi \\ 1 - \sin^2\chi\cos^2\psi \end{vmatrix} \frac{1}{(1 - \sin^2\chi\cos^2\psi)^{1/2}}$$

Note, as a verification, that when $\vec{\xi} \parallel x_o$, i.e., $\chi = 0$,

$$[\vec{\xi},\vec{\varepsilon},\vec{\ell}] = \begin{vmatrix} 1 & 0 & 0 \\ 0 & 1 & 0 \\ 0 & 0 & 1 \end{vmatrix}$$

For notation purposes, denote,

$$[\xi,\varepsilon,\ell] = \begin{vmatrix} \alpha_x & \alpha_y & \alpha_z \\ \beta_x & \beta_y & \beta_z \\ \gamma_x & \gamma_y & \gamma_z \end{vmatrix}$$

Step 2 Express $\vec{k}$, in terms of polar coordinates (k,β,ω) in the system $(\vec{\xi},\vec{\varepsilon},\vec{\ell})$

$$\vec{k} = [k\cos\beta,\ k\sin\beta\cos\omega,\ k\sin\beta\sin\omega]^T = [k_1',k_2',k_3']^T$$

where, for the integration purposes, $\beta:0\to\pi$, $\omega:0\to2\pi$, $k:0\to\infty$.

Step 3 Express $[k_1',k_2',k_3']^T$ in terms of $[k_1,k_2,k_3]$. This operation is given from:

$$\begin{vmatrix} k_1 \\ k_2 \\ k_3 \end{vmatrix} = \begin{vmatrix} \alpha_x & \alpha_y & \alpha_z \\ \beta_x & \beta_y & \beta_z \\ \gamma_x & \gamma_y & \gamma_z \end{vmatrix} \begin{vmatrix} k_1' \\ k_2' \\ k_3' \end{vmatrix}$$

It can be easily verified that $\underline{k} \cdot \underline{\xi} = k\xi\cos\beta$.

$$\underline{k} \cdot \underline{\xi} = \underline{k}^T \underline{\xi} = \underline{k}'^T [\underline{\xi}_1,\underline{\varepsilon},\underline{\ell}]^T \underline{\xi} = \underline{k}'^T \begin{vmatrix} \xi \\ 0 \\ 0 \end{vmatrix} = k\xi\cos\beta$$

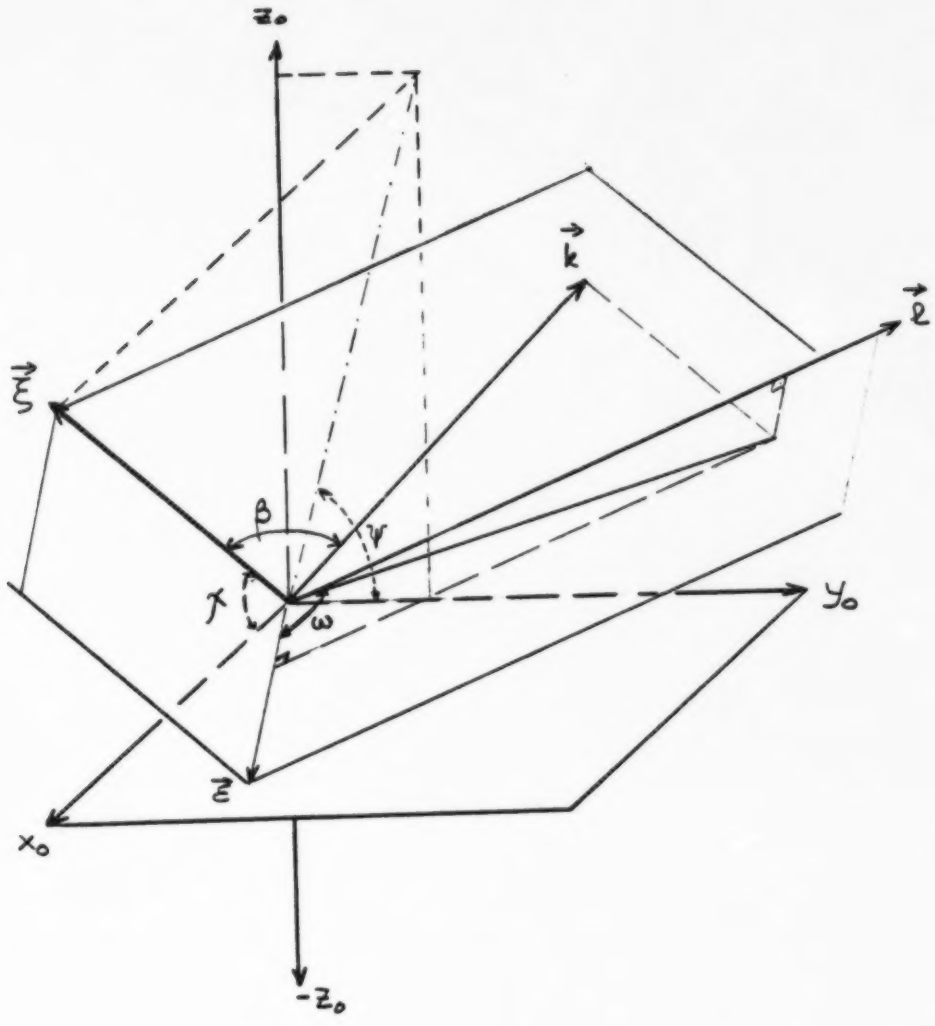

Figure C.1 Schematic graph of the coordinate transformation geometry

APPENDIX D

MEAN CONCENTRATIONS FITTED AT THE BORDEN SITE DATA

For the longitudinal section the fitted curve had the following form,

$$\bar{c}(x) = K \cdot \exp\left[- \frac{(x - \bar{x})^2}{4A_L \bar{x}} \right] \qquad (D.1)$$

Through a manual trial and error adjustment of the parameters, the values selected for Figure 7.5 are:

$K = 319$ mg/ℓ
$A_L = 0.34$ m
$\bar{x} = 17.83$ m

For the vertical sections the fitted curves had the following form:

$$\bar{c}(z) = K_v \exp\left[- \frac{(z - z_o)^2}{4A_v(38.3)} \right] \qquad (D.2)$$

where 38.3 m = $\bar{x}$, the longitudinal coordinate of the center of mass of the plume, as given in Sudicky (1985). Through a similar manual trial and error adjustment of the parameters, the values selected for Figures 7.6(a) through 7.6(i) are shown in Table D.1.

TABLE D.1

PARAMETERS USED TO FIT MEAN CONCENTRATION AT THE WELLS

x (m)	y (m)	K_v (mg/ℓ)	z_o(m)	A_v (m)
35	12	80	-5.4	0.004
38.3	16	300	-5.4	0.004
40.3	17.94	300	-5.4	0.002
42.3	20	320	-5.4	0.003
44.3	22	200	-5.35	0.0025
46.22	24	120	-5.2	0.002
48.3	25.95	50	-5.0	0.004

This is 22-004

Efficiency® GRAPH PADS

STOCK NO.	DESCRIPTION	STOCK NO.	DESCRIPTION
QUADRILLE RULED 50 SHEETS 8¼ x 11" 20 SUB			
22-000	4 x 4	22-005	8 x 8
22-001	4 x 4 3 HOLES	22-006	10 x 10
22-002	5 x 5	22-007	4 x 4 8½ x 14
22-003	5 x 5 3 HOLES	22-008	5 x 5 8½ x 14
22-004	6 x 6		
QUADRILLE RULED 50 SHEETS 8½ x 11" 10 SUB			
22-030	4 x 4	22-035	8 x 8
22-031	4 x 4 3 HOLES	22-036	10 x 10
22-032	5 x 5	22-037	4 x 4 17 x 11
22-033	5 x 5 3 HOLES	22-038	5 x 5 17 x 11
22-034	6 x 6		
METRIC QUADRILLE RULED 50 SHEETS 8¼ x 11 20 SUB			
22-170	1CM (10MM)		
22-171	5MM		
CROSS SECTION RULED 40 SHEETS 8½ x 11" 20 SUB			
22-020	4 x 4	22-026	10 x 10
22-022	5 x 5	22-027	8 x 8 8½ x 14
22-024	6 x 6	22-028	10 x 10 8½ x 14
22-025	8 x 8		
CROSS SECTION RULED 40 SHEETS 8½ x 11 10 SUB			
22-040	4 x 4	22-046	8 x 8
22-042	5 x 5	22-048	10 x 10
22-044	6 x 6		
CROSS SECTION LITHOGRAPHED 30 SHEETS 8½ x 11 10 SUB			
22-100	4 x 4	22-105	8 x 8
22-102	5 x 5	22-106	10 x 10
22-104	6 x 6	22-107	20 x 20

American Pad and Paper Co. Holyoke, Massachusetts 01040